การวิเคราะห์เชิงอุณหพลศาสตร์ของการผลิตไฮโดรเจนจากการสลายตัวของมีเทนสำหรับเซลล์เชื้อเพลิงแบบต่างๆ

นายวัชรพงษ์ ขาวดี

วิทยานิพนธ์นี้เป็นส่วนหนึ่งของการศึกษาตามหลักสูตรปริญญาวิศวกรรมศาสตรดุษฎีบัณฑิต
สาขาวิชาวิศวกรรมเคมี ภาควิชาวิศวกรรมเคมี
คณะวิศวกรรมศาสตร์ จุฬาลงกรณ์มหาวิทยาลัย
ปีการศึกษา 2555

THERMODYNAMIC ANALYSIS OF HYDROGEN PRODUCTION FROM DECOMPOSITION OF METHANE FOR DIFFERENT FUEL CELLS

Mr. Watcharapong Khaodee

A Dissertation Submitted in Partial Fulfillment of the Requirements
for the Degree of Doctor of Engineering Program in Chemical Engineering
Department of Chemical Engineering
Faculty of Engineering
Chulalongkorn University
Academic Year 2012

Thesis Title	THERMODYNAMIC ANALYSIS OF HYDROGEN PRODUCTION FROM DECOMPOSITION OF METHANE FOR DIFFERENT FUEL CELLS
By	Mr. Watcharapong Khaodee
Field of Study	Chemical Engineering
Thesis Advisor	Professor Suttichai Assabumrungrat, Ph.D.

Accepted by the Faculty of Engineering, Chulalongkorn University in Partial Fulfillment of the Requirements for the Doctoral Degree

.....Dean of the Faculty of Engineering
(Associate Professor Boonsom Lerdhirunwong, Dr.Ing.)

THESIS COMMITTEE

.....Chairman
(Associate Professor Muenduen Phisalaphong, Ph.D.)

.....Thesis Advisor
(Professor Suttichai Assabumrungrat, Ph.D.)

.....Examiner
(Assistant Professor Apinan Soottitantawat, Ph.D.)

.....Examiner
(Assistant Professor Amornchai Arpornwichanop, D.Eng.)

.....External Examiner
(Assistant Professor Ratanawan Kiattikomol, Ph.D.)

วัชรพงษ์ ขาวดี : การวิเคราะห์เชิงอุณหพลศาสตร์ของการผลิตไฮโดรเจนจากการสลายตัวของมีเทนสำหรับเซลล์เชื้อเพลิงแบบต่างๆ (THERMODYNAMIC ANALYSIS OF HYDROGEN PRODUCTION FROM DECOMPOSITION OF METHANE FOR DIFFERENT FUEL CELLS) อ. ที่ปรึกษาวิทยานิพนธ์หลัก: ศ.ดร.สุทธิชัย อัสสะบำรุงรัตน์, 127 หน้า.

งานวิทยานิพนธ์นี้ศึกษาการวิเคราะห์เชิงอุณหพลศาสตร์ของการผลิตไฮโดรเจนสำหรับเซลล์เชื้อเพลิงต่างๆ ได้แก่ เซลล์เชื้อเพลิงชนิดเยื่อแลกเปลี่ยนโปรตอนและเซลล์เชื้อเพลิงชนิดออกไซด์แข็ง โดยเริ่มจากทำการศึกษาการผลิตไฮโดรเจนจากกระบวนการสลายตัวและรีฟอร์มมิงด้วยไอน้ำซึ่งป้อนด้วยเชื้อเพลิงต่างๆ เช่น ไฮโดรคาร์บอนเบา (มีเทน, อีเทน และโพรเพน) และ แอลกอฮอล์ (เมทานอล, เอทานอล และกลีเซอรอล) และทำการเปรียบเทียบสมรรถนะของปฏิกิริยาระหว่างทั้งสองกระบวนการภายใต้การดำเนินการที่พลังงานสุทธิของระบบเป็นศูนย์ โดยการแบ่งสายป้อนหรือสายผลิตภัณฑ์ไปเผาเพื่อให้ความร้อนแก่ระบบ จากการศึกษาพบว่าระบบที่แบ่งสายป้อนจะให้ไฮโดรเจนมากกว่าเมื่อเทียบกับระบบที่แบ่งสายผลิตภัณฑ์ ในขณะที่ระบบแบบหลังจะให้คาร์บอนมากกว่าและปลดปล่อยคาร์บอนไดออกไซด์น้อยกว่าแบบแรก แม้ว่ากระบวนการรีฟอร์มมิงด้วยไอน้ำส่วนใหญ่จะให้ไฮโดรเจนมากกว่ากระบวนการสลายตัว แต่กระบวนการสลายตัวนั้นน่าสนใจมากกว่าในแง่ของการพิจารณาด้านสิ่งแวดล้อม และยังพบอีกว่าการสลายตัวของไฮโดรเจนเบาที่อุณหภูมิสูงนั้นเหมาะกับเซลล์เชื้อเพลิงชนิดเยื่อแลกเปลี่ยนโปรตอนและเซลล์เชื้อเพลิงชนิดออกไซด์แข็ง อย่างไรก็ตามการสลายตัวของแอลกอฮอล์สามารถใช้ได้กับเซลล์เชื้อเพลิงชนิดออกไซด์แข็ง จากการพิจารณากระบวนการทั้งหมดที่ศึกษาพบว่าการสลายตัวของมีเทนเป็นตัวเลือกที่น่าสนใจภายใต้การพิจารณาด้านสิ่งแวดล้อม ยิ่งไปกว่านั้นแก๊สชีวภาพที่ประกอบด้วยแก๊สเรือนกระจก นั่นคือมีเทนและคาร์บอนไดออกไซด์ นั้นถูกนำมาศึกษาในกระบวนการสลายตัว เมื่อพิจารณาแก๊สชีวภาพที่มีอัตราส่วนของคาร์บอนไดออกไซด์ต่อมีเทนเป็น 40 ต่อ 60 นั้น จะต้องมีการแยกคาร์บอนไดออกไซด์ออกก่อนที่จะป้อนเข้าหน่วยสลายตัวเพื่อให้ได้สมรรถนะของปฏิกิริยาที่สูงขึ้น ถึงกระนั้น กระบวนการสลายตัวที่ป้อนด้วยแก๊สชีวภาพประกอบกับการจับคาร์บอนไดออกไซด์ภายใต้สภาวะที่พลังงานสุทธิของระบบเป็นศูนย์นั้นไม่เหมาะกับเซลล์เชื้อเพลิงชนิดเยื่อแลกเปลี่ยนโปรตอน เนื่องจากความเข้มข้นของคาร์บอนมอนอกไซด์นั้นยังมากกว่า 10 ส่วนในล้านส่วน สำหรับเซลล์เชื้อเพลิงชนิดออกไซด์แข็ง กระบวนการสลายตัวที่ป้อนด้วยแก๊สชีวภาพแบบแบ่งสายป้อนนั้นจะดำเนินการที่ 1275 เคลวินเพื่อให้ได้ไฮโดรเจนและคาร์บอนมอนอกไซด์มากที่สุด ในขณะที่กระบวนการแบบแบ่งสายผลิตภัณฑ์นั้นจะดำเนินการที่ 1300 เคลวิน เพื่อให้ได้คาร์บอนมากที่สุดและการปล่อยคาร์บอนไดออกไซด์จากเตาเผาน้อยที่สุด

ภาควิชา วิศวกรรมเคมี ลายมือชื่อนิสิต .....

สาขาวิชา วิศวกรรมเคมี ลายมือชื่อ อ.ที่ปรึกษาวิทยานิพนธ์หลัก .....

ปีการศึกษา 2555

4971827321 : MAJOR CHEMICAL ENGINEERING
KEYWORDS : THERMODYNAMIC ANALYSIS / DECOMPOSITION / GIBBS FREE ENERGY MINIMIZATION / METHANE / BIOGAS

WATCHARAPONG KHAODEE : THERMODYNAMIC ANALYSIS OF HYDROGEN PRODUCTION FROM DECOMPOSITION OF METHANE FOR DIFFERENT FUEL CELLS. ADVISOR : PROF. SUTTICHAI ASSABUMRUNGRAT, Ph.D., 127 pp.

This dissertation studies thermodynamic analysis of hydrogen production for different fuel cells including polymer electrolyte membrane fuel cell (PEMFC) and solid oxide fuel cell (SOFC). Firstly, hydrogen production from decomposition and steam reforming processes fed by different primary fuels; i.e. light hydrocarbons (methane, ethane, and propane) and alcohols (methanol, ethanol, and glycerol) was investigated and comparison of reaction performances between both processes under energy self-sustained operation by splitting feed or product gas stream to combust for heating the system was then carried out. From the study, it was found that the system with splitting feed can give higher hydrogen production, compared to that with splitting product stream, while the latter can provide higher carbon yield but lower CO_2 emission than the former. Although most of the steam reforming processes could gain higher hydrogen production than the decomposition processes, the decomposition ones were more interesting in term of the environmental concern. It was further revealed that the decomposition of light hydrocarbons at high temperature is suitable for PEMFC and SOFC. However, the decomposition of alcohols could be employed with SOFC. Among all processes, methane decomposition was an attractive choice under the environmental concern. In addition, biogas consisting of greenhouse gases i.e. methane and carbon dioxide was tested in the decomposition process. Considering biogas with the CO_2/CH_4 ratio of 40:60, it was necessary to separate carbon dioxide before supplying to the decomposition unit in order to achieve higher reaction performance. Nonetheless, the decomposition process fed by biogas with CO_2 capture under thermally self-sustained condition was not compatible with PEMFC due to the presence of carbon monoxide concentration higher than 10 ppm. For SOFC, the decomposition process fed by biogas with splitting feed was operated at 1275 K to obtain the highest hydrogen and carbon monoxide production, while that with splitting product stream was carried out at 1300 K to gain the highest carbon yield and the lowest CO_2 emission from the burner.

Department : Chemical Engineering Student's Signature .....

Field of Study : Chemical Engineering Advisor's Signature .....

Academic Year : 2012 .....

ACKNOWLEDGEMENTS

The author would like to show his high appreciation to Professor Suttichai Assabumrungrat, his advisor for his invaluable suggestion and guidance in both research study and life attitude throughout his research study. In addition, the author wishes to thank Assistant Professor Worapon Kiatkittipong and Dr. Suwimol Wongsakulphasatch for their collaboration in the accomplished paper. I would also grateful to thank to Associate Professor Muenduen Phisalaphong as the chairman, Assistant Professor Apinan Soottitantawat, Assistant Professor Amornchai Arpornwichanop and Assistant Professor Ratanawan Kiattikomol as the members of the thesis committee for their kind cooperation.

Best regards are expressed to many friends in Center of Excellence in Catalysis and Catalytic Reaction Engineering who always provide the encouragement and cooperation along the dissertation study.

Moreover, the author would like to thank the Chulalongkorn University Graduate Scholarship commemoratory the 72nd Anniversary of H.M. Rama IX as well as the Graduate School of Chulalongkorn University, The Thailand Research Fund and Center of Excellence in Catalysis and Catalytic Reaction Engineering for their financial support. Finally, he also would like to dedicate this dissertation to his parents for their worthy support and encouragement at all times.

CONTENTS

PAGE

PAGE

LIST OF TABLES

PAGE

LIST OF FIGURES

PAGE

PAGE

PAGE

PAGE

LIST OF ABBREVIATIONS

A_j	total number of atoms of *j*-th element in the reaction mixture [-]
a_{ij}	number of atoms of the *j*-th element present in each molecule of *i*-th species [-]
f_i^0	standard-state fugacity of the *i*-th species [-]
$\hat{f}_i$	fugacity of the *i*-th species [-]
G^t	total Gibbs free energy [J mol^{-1}]
G_i^0	standard-state Gibbs free energy of the *i*-th species [J mol^{-1}]
$\Delta G_{f_i}^0$	standard Gibbs function of formation of the *i*-th species [J mol^{-1}]
$G_{C_{(s)}}$	molar Gibbs free energy of solid carbon [J mol^{-1}]
H_i	enthalpy of the *i*-th species [J mol^{-1}]
K_{eq}	equilibrium constant
N	total species [-]
n_i	mole of the *i*-th species [mol]
Q_c	heat energy of the burner [kJ mol^{-1}]

Q_r	heat energy of the reactor [kJ mol^{-1}]
R	ideal gas constant, 8.314472 [J $mol^{-1}K^{-1}$]
T, T_r	operating temperature [K]
y_i	mole fraction of each substance in gas products [-]

Greek letters

δ_{ij}	interaction coefficient
α_C	carbon activity
λ_j	Lagrange multiplier [-]
μ_i	chemical potential of species i [J mol^{-1}]
$\hat{\phi}_i$	fugacity coefficient of species i [-]
ω	acentric factor

Subscripts

i, j, k	component identifications
in	inlet stream to the process
out	outlet stream to the process
SOFC	solid oxide fuel cell

CHAPTER I
INTRODUCTION

1.1 Rationale

Hydrogen is an important feedstock for various applications such as fuel cell, hydrotreating hydrogenation, and production of ammonia or methanol [1]. One of the promising hydrogen utilization is as a fuel for fuel cell, an electrical power generation technology with high efficiency. In addition, fuel cell has been known as an environmental friendly device due to low greenhouse gases emission. There are several types of fuel cells that are commonly used, including polymeric electrolyte membrane fuel cell (PEMFC) and solid oxide fuel cell (SOFC). Classifying the fuel cell by the operating temperature, low temperature (PEMFC) and high temperature types (SOFC) are suitable for fuel cell applications such as moving vehicles and stationary power plants, respectively. Considering the possible fuel fed to the fuel cell, it relies on the fuel cell category as summarized in Table 1.1. For PEMFC, the hydrogen supplied is typically limited under condition of high purity of hydrogen with considerably low concentration of carbon monoxide (CO). An acceptable value at which the active sites on the anode of PEMFC can be tolerable and unharmed from poisonous gaseous CO is around 10-50 ppm [2-4]. On the other hand, CO can be performed as another fuel source in SOFC.

Numerous alternative methods to produce hydrogen have been carried out such as steam reforming, partial oxidation, autothermal reforming, coal gasification, electrolysis, or decomposition [5]. Among these methods, steam reforming is a conventional process that is carried out in a number of industries due to high capability of hydrogen production and energy efficiency [5]. However, it has been revealed that the steam reforming process generates larger amount of greenhouse gas such as carbon dioxide (CO_2) compared to other processes [6]. Currently, the global warming issue caused by greenhouse gases is enormously concerned. According to

the environmental concern, the decomposition of hydrocarbon has been recently attracted a great attention in hydrogen production as it gives pure hydrogen without any CO_x exhausts and yields valuable and marketable by-product, carbon, in different forms, such as carbon nanofiber (CNF) [7-9] or carbon nanotube (CNT) [10-12], depending on the type of catalyst used in the reaction. The CNF and CNT have been widely used in electronic applications, gas storage materials, composite materials, and catalyst supports [13-17], etc. However, the steam reforming as widely used in many industries is typically processed by providing an excess of steam in order to prevent carbon formation on the catalyst. Although higher hydrogen is yielded from the condition of excess steam, higher CO_2 emission is gained. Conversely, the decomposition is focused on obtaining the carbon as the valuable by-product. More importantly, carbon capture by means of decomposition process is certainly beneficial to surroundings as a result of an ability to suppress the CO_2 emission to atmosphere.

Table 1.1 Summary of major fuel constituent for different fuel cell types [2].

Gas species	Fuel cell type	
	PEMFC	SOFC
H_2	Fuel	Fuel
CO	Poison (<50 ppm)	Fuel
CH_4	Diluent	Fuel
CO_2 and H_2O	Diluent	Diluent

The comparison between the decomposition and steam reforming processes has been proposed by several researchers [18-21]. In case of using methane as a fuel, it was obviously found that the decomposition requires significantly lower energy input per mole of hydrogen produced (37.8 kJ mol^{-1} H_2), compared to the steam reforming (63.3 kJ mol^{-1} H_2). In addition, the amount of CO_2 emission of the latter was greatly higher than that of the former (0.43 and 0.05 mol CO_2 mol^{-1} H_2) [20]. As reported by Steinberg [18], it was revealed that the decomposition of methane is more effective than the steam reforming especially in term of the easiness of separating the stable solid carbon from the decomposition process compared to sequestering CO_2

produced as a reactive gas or low temperature liquid from the steam reforming. Among hydrogen production from thermal and autocatalytic decomposition of methane and the steam reforming with and without CO_2 capture and storage, the autocatalytic decomposition exhibited the lowest total environmental impact and CO_2 emissions. Although lower CO_2 emissions could be achieved by the steam reforming with CO_2 capture and storage, its total environmental impact was higher than the conventional one [19].

At the present, hydrocarbons, such as methane (CH_4), ethane (C_2H_6), ethylene (C_2H_4), propane (C_3H_8), butane (C_4H_{10}) and alcohols, including methanol (CH_3OH), ethanol (C_2H_5OH) and glycerol ($C_3H_8O_3$), have been generally employed in steam reforming processes as primary fuels [22-26]. All these fuels give hydrogen-containing products which are typically supplied as a fuel in SOFC. However, it could be supplied to PEMFC after reducing the CO concentration via the secondary reactors i.e. water gas shift or preferential oxidation units. However, those hydrocarbons and alcohols can be also employed in the decomposition process. Related to the decomposition system, methane has been the most preferable primary fuel in various investigations [27-30]. Besides the use of pure methane as gaseous fuel, biogas has been another interesting fuel source since it is available and being renewable energy sources derived from biomass, which mainly composes of methane and high concentration of carbon dioxide. Methane content in biogas varies in the range of 40-65%, relying on the source of biogas and the fermentation process [31]. In addition, both compositions of biogas have been known as the greenhouse gases. Hence, it is useful for reducing the greenhouse gases to the environment in order to relieve the global warming problem.

As considered the biogas as the primary fuel for the decomposition process, methane and carbon dioxide would be preferably converted to hydrogen and carbon monoxide via the dry reforming reaction. However, it is possible to form the carbon in this system. Several researchers [7, 32-34] have experimented the decomposition process fed by biogas for hydrogen or synthesis gas production. Under the study of carbon prevention [35], the oxygen was supplied to reduce the carbon formation for

this process. However, nanostructured carbonaceous material such as carbon nanofiber as a valuable carbon by-product with hydrogen-rich fuel gas or synthesis gas could be obtained [7, 32]. Therefore, the decomposition process fed by biogas is another promising alternative for producing hydrogen-rich gas accompanied with the useful carbon by-product. According to the biogas decomposition process, since the dilute methane with carbon dioxide, the concentration of hydrogen produced should be reduced. Therefore, the increase in hydrogen purity can be achieved when carbon dioxide is sequestered from biogas before feeding to the decomposition unit. There are various types of CO_2 sequestration technologies as generally used, for instance, absorption [36], adsorption [37], membrane technology [38], etc. Thus, the decomposition process of biogas with CO_2 capture would be another issue for further investigations.

However, the methane decomposition is not currently used in industrial process due to the problem of separating the valuable carbon by-product from the catalyst. Several researchers [11, 39] have attempted to resolve this problem, but there is no practical way to handle. Since the CO_2 emission topic is importantly concerned, the methane decomposition is possible to industrially operate in near future. Therefore, the decomposition process should be paid attention and the development of the system and catalyst is needed to further investigate.

In this research, the hydrogen production is focused on supplying to the different fuel cell types. Firstly, thermodynamic study of the decomposition system fed by hydrocarbons and alcohols as primary fuels is considered. In addition, it is compared to the conventional steam reforming process in order to determine the suitable system. Nevertheless, the decomposition process as this process gives high hydrogen purity and is environmental friendly is mainly focused on. Methane and methane-containing gases i.e. biogas are properly selected as primary fuels for the decomposition process. The system configurations with CO_2 separation based on thermodynamic analysis are proposed and the suitable operating mode is examined in order to match the different fuel cells.

1.2 Objectives

- To determine the suitable operation of hydrogen production for different fuel cell grades and to investigate the capability of the methane decomposition from the comparative study of the reaction performance based on thermodynamic calculation between the decomposition process and the steam reforming process fed by different primary fuels i.e. light hydrocarbons and alcohols.

- To examine the appropriate system configuration of the decomposition process fed by biogas to match each fuel cell type by using thermodynamic analysis.

1.3 Scope of Work

1. Based on thermodynamic analysis, the effect of operating temperature on the reaction performances in terms of the equilibrium conversion, the selectivity of product (H_2) and of by-products (CH_4, CO, and CO_2), processing by the decomposition and steam reforming processes fed by different primary fuels i.e. light hydrocarbons (methane, ethane, and propane) and alcohols (methanol, ethanol, and glycerol) is investigated.

2. The major reaction performances obtained from the decomposition and steam reforming systems fed by different primary fuels under the thermally self-sustained operations such as hydrogen production, purity of hydrogen, mole fraction of carbon monoxide in product stream, and carbon yield are considered.

3. The suitable operating mode and operating condition under energy self-sustained condition of the decomposition and steam reforming systems fed by different primary fuels to match each fuel cell type are determined, based on the criteria of maximum hydrogen production or carbon capture and CO_2 emission.

4. The system configurations of the decomposition process fed by biogas equipped with CO_2 separation technologies are taken into account by thermodynamic analysis.

5. Under thermally self-sustained operation, the appropriate operating condition of the decomposition system fed by biogas for different fuel cell grades is selected.

CHAPTER II
THEORY

Since this research focuses on hydrogen production for different fuel cells, the basic principle of fuel cell is firstly mentioned in this chapter (Section 2.1). For the hydrogen production technologies, the information of the decomposition and the conventional steam reforming processes fed by different primary fuels such as light hydrocarbons and alcohols, including the occurrence of the possible reactions is provided in Section 2.2. Furthermore, the use of CO_2 capture technology with hydrogen production process is described in Section 2.3 and the examples of CO_2 separation methods such as absorption and membrane techniques are also presented.

2.1 Basic Principle of Fuel Cell

As known, fuel cells are energy conversion devices that galvanically convert chemical energy to electrical energy. A fuel cell configuration is shown in Figure 2.1. As seen in Figure 2.1, a fuel cell consists of an electrolyte sandwiched between two electrodes; i.e. anode and cathode. Typically, fuel is fed to anode and an oxidant is fed to cathode. The electrochemical reactions take place at both electrodes. Then, ionic-electronic charges transport between those electrodes, leading to producing the electricity. A fuel cell operates like a battery. However, a fuel cell can produce electrical energy as long as fuel and oxidant are supplied, but the electrical energy produced from battery decreases when those reactants are consumed.

At present, various types of fuel cells are currently used in many applications. These types can be classified by several criteria such as electrolyte, operating temperature, charge carrier, etc. Classification of fuel cells is by type of electrolyte as follows:

1. Polymer electrolyte membrane fuel cell (PEMFC)
2. Direct methanol fuel cell (DMFC)

3. Alkaline fuel cell (AFC)
4. Phosphoric acid fuel cell (PAFC)
5. Molten carbonate fuel cell (MCFC)
6. Solid oxide fuel cell (SOFC)

Other details of all types of fuel cell are illustrated in Table 2.1.

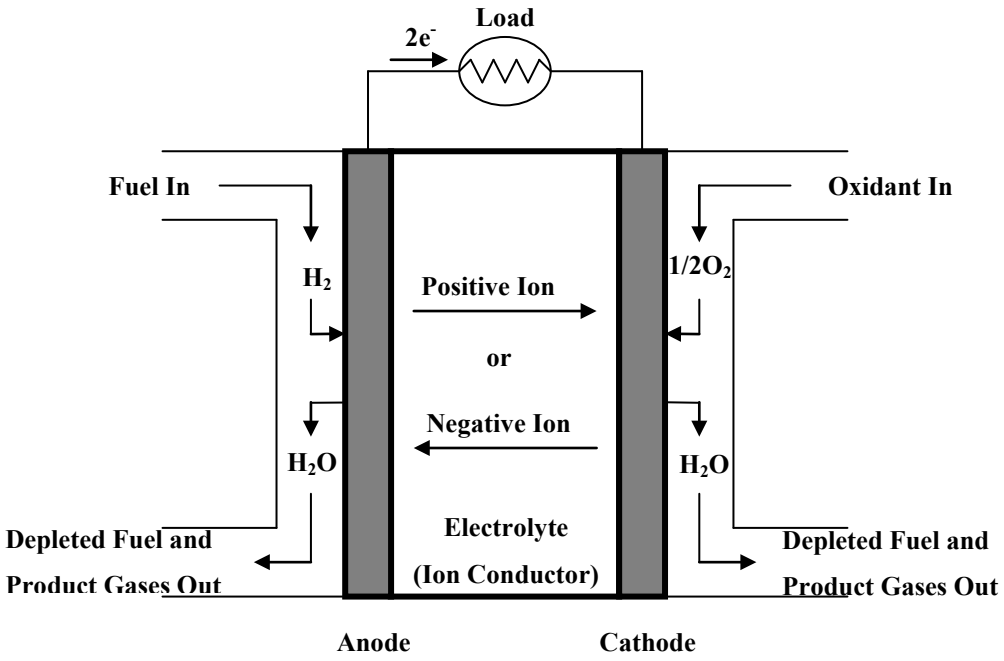

Figure 2.1 Schematic of an individual fuel cell [40].

From the different types of fuel cells as shown in Table 2.1, the operating temperature increases with fuel cells from left to right, ranging from 80^{o}C for PEMFC to 1000^{o}C for SOFC. The low temperature fuel cells (PEMFC, DMFC, AFC, and PAFC) with aqueous electrolyte use hydrogen or methanol as fuel. For high temperature fuel cells (MCFC and SOFC), natural gas can be used as a fuel because it can be internally reformed to hydrogen and carbon monoxide and then can be further oxidized to produce electrical energy and heat. The uses of low temperature fuel cells as power sources are in small-scale applications such as cars and computer notebooks. For high temperature fuel cells (MCFC and SOFC), they are promising technologies to use as power generation such as stationary electric power plant.

Table 2.1 Types of fuel cells [40].

Item	Type of fuel cell					
	PEMFC	DMFC	AFC	PAFC	MCFC	SOFC
Electrolyte	Ion exchange membrane	Ion exchange membrane	Alkaline	Phosphoric acid	Alkali Carbonate mixtures	Stabilized zirconia (ZrO_2)
Operating Temp. (^oC)	50-85	50-100	50-250	160-220	630-650	800-1000
Charge Carrier	H^+	H^+	OH^-	H^+	CO_3^{2-}	O^{2-}
Electrolyte State	Solid	Solid	Liquid	Immobilized Liquid	Immobilized Liquid	Solid
Corrosiveness	None	None	High	High	High	None
Fuel	H_2	CH_3OH	H_2	H_2	Synthesis gas, CH_4	Synthesis gas, CH_4
Cathode Catalyst	Pt, Pt/Ru	Pt, Pt/Ru	Pt/Au, Pt, Ag	Pt/Cr/Co. Pt/Ni	Li/NiO	$LaSrMnO_3$
Anode Catalyst	Pt	Pt	Pt/Au, Pt, Ag	Pt	Ni, Ni/Cr	Ni/ZrO_2
Cogeneration Heat	None	None	None	Low quality	High	High
Size (MW)	0.25	0.30	Very small	11	2	1-2
Application	Transport, small appliances	Buses, cars, small appliances	Small power in aerospace	Power generation, CHP	Power generation, CHP	Power generation, CHP
Efficiency (%)	<40	40-50	>60	40-45	50-60	50-60

2.2 Related Reactions of Decomposition and Steam Reforming Processes

According to hydrogen production from the decomposition and the steam reforming processes, hydrogen can be produced from various types of primary fuels. In this research, the studied primary fuels are light hydrocarbons (C_1-C_3) i.e. methane, ethane, and propane, and alcohols i.e. methanol, ethanol, and glycerol. A number of possible reactions would take place in both processes. However, main reactions can be summarized as follows:

Decomposition:

Methane cracking:

$$CH_4 \rightleftharpoons C(s) + 2H_2 \qquad \Delta H^0 = 74.9 \text{ kJ mol}^{-1} \qquad (2\text{-}1)$$

Ethane cracking:

$$C_2H_6 \rightleftharpoons 2C(s) + 3H_2 \qquad \Delta H^0 = 83.9 \text{ kJ mol}^{-1} \qquad (2\text{-}2)$$

Propane cracking:

$$C_3H_8 \rightleftharpoons 3C(s) + 4H_2 \qquad \Delta H^0 = 104.7 \text{ kJ mol}^{-1} \qquad (2\text{-}3)$$

Methanol decomposition:

$$CH_3OH \rightleftharpoons CO + 2H_2 \qquad \Delta H^0 = 90.5 \text{ kJ mol}^{-1} \qquad (2\text{-}4)$$

Ethanol decomposition to CO:

$$C_2H_5OH \rightleftharpoons CO + CH_4 + H_2 \qquad \Delta H^0 = 49.9 \text{ kJ mol}^{-1} \qquad (2\text{-}5)$$

Ethanol decomposition to CO_2:

$$C_2H_5OH \rightleftharpoons \tfrac{1}{2}CO_2 + \tfrac{3}{2}CH_4 \qquad \Delta H^0 = -73.8 \text{ kJ mol}^{-1} \qquad (2\text{-}6)$$

Glycerol decomposition:

$C_3H_8O_3 \rightleftharpoons 3CO + 4H_2$ $\Delta H^0 = 246.3$ kJ mol^{-1} (2-7)

Steam reforming:

Methane steam reforming (MSR):

$CH_4 + H_2O \rightleftharpoons CO + 3H_2$ $\Delta H^0 = 206.2$ kJ mol^{-1} (2-8)

Methane steam reforming (overall):

$CH_4 + 2H_2O \rightleftharpoons CO_2 + 4H_2$ $\Delta H^0 = 165.0$ kJ mol^{-1} (2-9)

Ethane steam reforming (overall):

$C_2H_6 + 4H_2O \rightleftharpoons 2CO_2 + 7H_2$ $\Delta H^0 = 264.2$ kJ mol^{-1} (2-10)

Propane steam reforming (overall):

$C_3H_8 + 6H_2O \rightleftharpoons 3CO_2 + 10H_2$ $\Delta H^0 = 375.2$ kJ mol^{-1} (2-11)

Methanol steam reforming (overall):

$CH_3OH + H_2O \rightleftharpoons CO_2 + 3H_2$ $\Delta H^0 = 49.3$ kJ mol^{-1} (2-12)

Ethanol steam reforming (overall):

$C_2H_5OH + 3H_2O \rightleftharpoons 2CO_2 + 6H_2$ $\Delta H^0 = 173.8$ kJ mol^{-1} (2-13)

Glycerol steam reforming (overall):

$C_3H_8O_3 + 3H_2O \rightleftharpoons 3CO_2 + 7H_2$ $\Delta H^0 = 122.9$ kJ mol^{-1} (2-14)

As shown in the decomposition process, C_1-C_3 hydrocarbons can be converted to the desired gaseous hydrogen and solid carbon [reactions (2-1)-(2-3)], whereas alcohols typically decompose to hydrogen and other gases such as CH_4, CO and CO_2

[reactions (2-5)-(2-7)], which can lead to more carbon formation according to the following reactions, as well as the methane cracking [reaction (2-1)].

Boudouard reaction:

$$2CO \rightleftharpoons C + CO_2 \qquad \Delta H^0 = \text{-}172.5 \text{ kJ mol}^{-1} \qquad (2\text{-}15)$$

Reverse gasification of C to CO:

$$CO + H_2 \rightleftharpoons H_2O + C \qquad \Delta H^0 = \text{-}131.3 \text{ kJ mol}^{-1} \qquad (2\text{-}16)$$

Reverse gasification of C to CO_2:

$$CO_2 + 2H_2 \rightleftharpoons 2H_2O + C \qquad \Delta H^0 = \text{-}90.2 \text{ kJ mol}^{-1} \qquad (2\text{-}17)$$

In addition, side reactions as shown below need to be taken into account when by-products appeared.

Water gas shift (WGS):

$$CO + H_2O \rightleftharpoons CO_2 + H_2 \qquad \Delta H^0 = \text{-}41.2 \text{ kJ mol}^{-1} \qquad (2\text{-}18)$$

Dry reforming (DR):

$$CH_4 + CO_2 \rightleftharpoons 2CO + 2H_2 \qquad \Delta H^0 = 247.3 \text{ kJ mol}^{-1} \qquad (2\text{-}19)$$

In case of steam reforming process, CO and CO_2 are major by-products which can be possibly involved in the reactions (2-15)-(2-19).

However, in case of biogas as a primary fuel fed to the decomposition unit, the highly endothermic dry reforming reaction [reaction (2-17)] is preferably occurred since high CO_2 content presented in CH_4 feeding gas. In addition, the reactions (2-15)-(2-18) can be also occurred as a result of the intermediate CO generation and the carbon can be possibly yielded.

2.3 CO_2 Capture Systems

The main application of CO_2 capture is likely to be at large point sources: fossil fuel power plants, fuel processing plants and other industrial plants, particularly for the manufacture of iron, steel, cement and bulk chemicals.

There are four basic systems for capturing CO_2 from use of fossil fuels and/or biomass:

1. Capture from industrial process streams
2. Post-combustion capture
3. Oxy-fuel combustion capture
4. Pre-combustion capture

These systems are shown in simplified form in Figure 2.2.

2.3.1 Capture from Industrial Process Streams

CO_2 has been captured from industrial process streams for 80 years [41], although most of the CO_2 that is captured is vented to the atmosphere because there is no incentive or requirement to store it. Current examples of CO_2 capture from process streams are purification of natural gas and production of hydrogen-containing synthesis gas for the manufacture of ammonia, alcohols and synthetic liquid fuels. Most of the techniques employed for CO_2 capture in the examples mentioned are also similar to those used in pre-combustion capture. Other industrial process streams which are a source of CO_2 that is not captured include cement and steel production, and fermentation processes for food and drink production. CO_2 could be captured from these streams using techniques that are common to post-combustion capture, oxy-fuel combustion capture and pre-combustion capture.

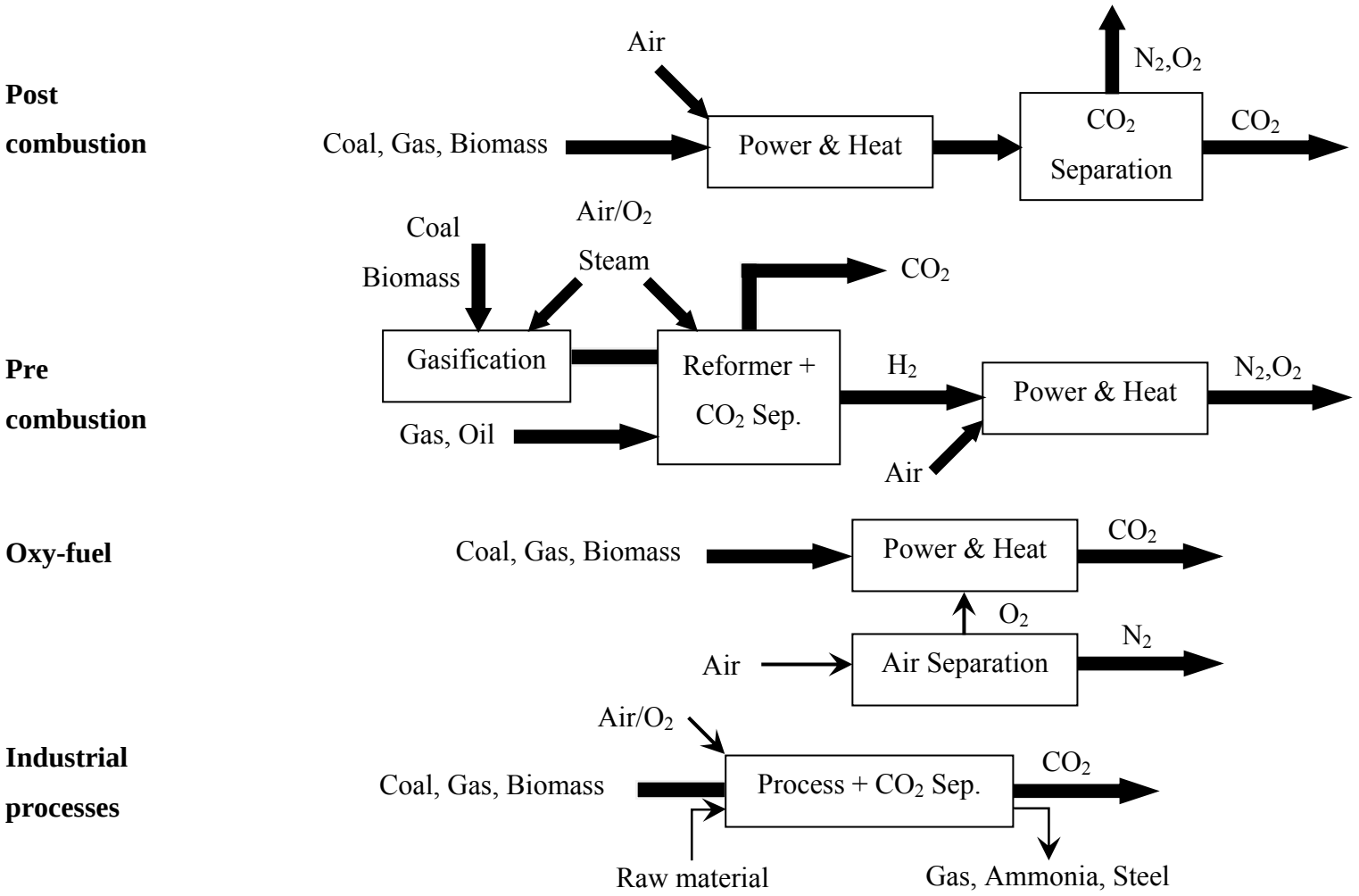

Figure 2.2 CO_2 capture system [42].

2.3.2 Post-Combustion Capture

Capture of CO_2 from flue gases produced by combustion of fossil fuels and biomass in air is referred to as post-combustion capture. Instead of being discharged directly to the atmosphere, flue gas is passed through equipment which separates most of the CO_2. The CO_2 is fed to a storage reservoir and the remaining flue gas is discharged to the atmosphere. A chemical sorbent process as described in Section 2.4.1 would normally be used for CO_2 separation. Other techniques are also being considered but these are not at such an advanced stage of development.

2.3.3 Oxy-Fuel Combustion Capture

In oxy-fuel combustion, nearly pure oxygen is used for combustion instead of air, resulting in flue gas that is mainly CO_2 and H_2O. If fuel is burnt in pure oxygen, the flame temperature is excessively high, but CO_2 and/or H_2O-rich flue gas can be recycled to the combustor to moderate this. Oxygen is usually produced by low temperature (cryogenic) air separation and novel techniques to supply oxygen to the fuel, such as membranes and chemical looping cycles are being developed.

2.3.4 Pre-Combustion Capture

Pre-combustion capture involves reacting a fuel with oxygen or air and/or steam to give mainly a synthesis gas (syngas) or fuel gas composed of carbon monoxide and hydrogen. The carbon monoxide is reacted with steam in a catalytic reactor, called a shift converter, to give CO_2 and more hydrogen. CO_2 is then separated, usually by a physical or chemical absorption process, resulting in a hydrogen-rich fuel which can be used in many applications, such as boilers, furnaces, gas turbines, engines and fuel cells.

2.4 Types of CO_2 Capture Technologies

CO_2 capture systems use many of the known technologies for gas separation which are integrated into the basic systems. A summary of these separation methods is given below.

2.4.1 Absorption

Even though there are several methods to sequester the gaseous CO_2, the chemical absorption process is the most commonly used in refineries, petrochemical plants, natural gas processing plants and other industries. In order to remove CO_2, the aqueous solutions of various amines such as alkanolamines are mostly used. Typically, there are several different alkanolamines which can be divided into three groups as follows:

(1) Primary amines such as monoethanolamine (MEA) and diglycolamine (DGA)
(2) Secondary amines such as diethanolamine (DEA) and di-isopropylamine (DIPA)
(3) Tertiary amines such as triethanolamine (TEA) and methyl-diethanolamine (MDEA)

The different amines can refer to the difference in their absorption equilibrium in the separation process.

In general, the amine absorption process or it is called the amine gas treating process comprises of an absorber unit and a regenerator unit as illustrated in Figure 2.3. Firstly, the gas stream with CO_2 enters at the bottom of the absorber whereas the liquid amine solution is fed at the top. The CO_2-rich gas and the liquid amine solution flow up and down, respectively, and both reactants are subsequently contacted. The gaseous CO_2 from the gas stream is then absorbed by the amine solvent and it flows out at the bottom whereas the remaining gas leaves at the top. The amine solution containing the gaseous CO_2 is then entered the regeneration unit in order to separate

CO_2 from the reusable amine solution by using condition of high temperature and low pressure.

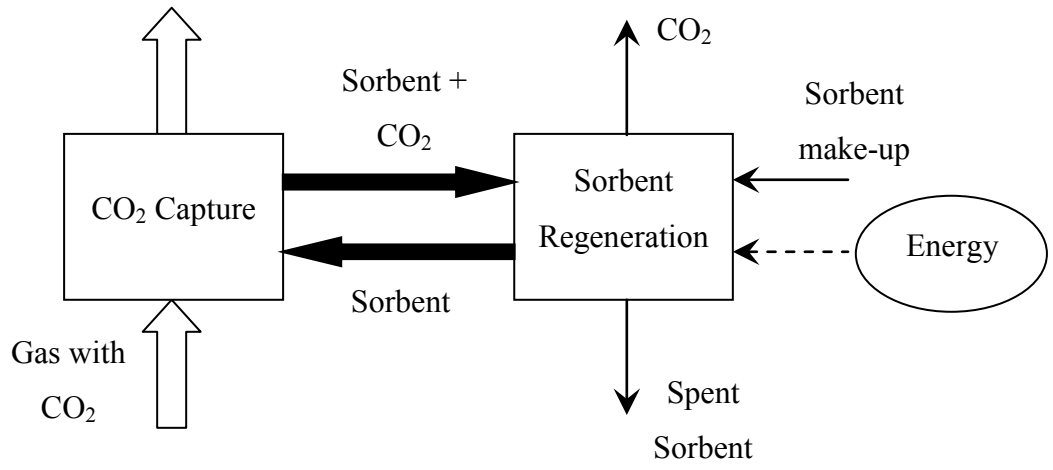

Figure 2.3 System configuration of CO_2 separation by absorption.

For example of the CO_2 absorption process by using MEA as amine, the related chemical reactions are listed as the following equations.

$$2H_2O \rightleftharpoons H_3O^+ + OH^- \quad (2\text{-}20)$$

$$CO_2 + 2H_2O \rightleftharpoons H_3O^+ + HCO_3^- \quad (2\text{-}21)$$

$$HCO_3^- + H_2O \rightleftharpoons H_3O^+ + CO_3^{2-} \quad (2\text{-}22)$$

$$2MEA^+ + CO_2 \rightleftharpoons MEAH^+ + MEACOO^- \quad (2\text{-}23)$$

$$MEAH^+ + H_2O \rightleftharpoons MEA + H_3O^+ \quad (2\text{-}24)$$

$$MEACOO^- + H_2O \rightleftharpoons MEA + HCO_3^- \quad (2\text{-}25)$$

The amines among various alkanolamines that has been the most generally used in industrial plants are MEA, DEA, and MDEA. However, MEA is the mostly used amine for CO_2 absorption process among the primary amines due to the availability and low cost. Since MEA has the lowest molecular weight, the highest theoretical CO_2 absorption capacity is provided. In addition, MEA has the highest

vapour pressure among alkanolamines; hence, high reusable solvent can be obtained from the regeneration step. However, in order to operate the CO_2 absorption process, the amine concentration is an important parameter. For instance, the MEA concentration used in the commercial process up to 30 wt.% has been successfully employed to remove 80%-90% of the CO_2 from the feed stream [43]. Currently, the amine gas treating has been attracted a great attention to remove CO_2 from the flue gases emitted by fossil fuel power plants. In addition, this CO_2 absorption process is one of the commonly used processes for removing the excess CO_2 in the final hydrogen purification step from the steam reforming processes of hydrocarbons.

2.4.2 Membrane Separation

The membrane is a layer of material that allows selective permeation of a certain gas. There are several types of membranes that can indicate the type of permeate gas. Membranes can be typically divided into three types i.e. inorganic, polymeric and biological membranes. These three types of membranes are classified by their structure and functionality. Various membrane configurations such as hollow fiber arranged in shell-and-tube and flat sheet packed in spiral-wound module are usually used in gas separation system. The membrane technology has been widely used in many applications such as hydrogen recovery from purge gases in ammonia synthesis, refinery and natural gas dehydration, sour gas removal from natural gas, and nitrogen production from air. The membrane technology has advantages over other CO_2 separation technologies such as no requirement of separating agent or solvent, leading to eliminating the regeneration unit. Since this membrane technology is compact, relatively inexpensive and simple to use, it is an interesting technique for employing in separation process.

At present, several commercial polymer membranes that are mostly derived from cellulose acetate, polysulfone, and polyimide are available for CO_2 separation. The separation of CO_2 from CH_4/CO_2 mixtures by membrane technology is mostly found. In order to separate CO_2 from those mixtures, it depends on the pressure

difference across membrane; therefore, the supplied pressure is required for the feed gas. However, the use of membrane system has to importantly consider the energy requirement for gas compression.

CHAPTER III
LITERATURE REVIEWS

In this chapter, hydrogen production processes, especially the conventional steam reforming and the decomposition ones, are focused on and reviewed in Section 3.1. Their application for different fuel cells is also mentioned in this section. The related topics about methane decomposition process i.e. the catalysts used, the carbon generated, and the proposed mechanism are gathered in Sections 3.2-3.4. As considered biogas being a studied primary fuel for the decomposition system, the methods of biogas treatment by removing CO_2 with various techniques are proposed in Section 3.5.

3.1 Hydrogen Production Processes and Their Application for Fuel Cell

According to hydrogen production processes, there are various methods that have been disclosed in order to produce hydrogen such as steam reforming, partial oxidation, autothermal reforming, coal gasification, electrolysis, decomposition, etc. In Table 3.1, the energy efficiency of each hydrogen production technology is presented. It can be defined as the energy value of the hydrogen produced divided by the energy input required to produce the hydrogen. It could be recommended that the steam methane reforming process is an attractive choice as a result of providing the highest energy efficiency among several techniques for hydrogen production. However, the steam methane reforming and methane partial oxidation processes that give high value of energy efficiency currently produced large amount of carbon dioxide [6]. Therefore, the methane decomposition method as one of hydrogen production processes has been more interesting instead of the conventional one in terms of low carbon dioxide emission from the process.

Table 3.1 List of hydrogen production technologies [5].

Production technology	Energy efficiency (%)
Steam methane reforming	83
Partial oxidation of methane	70-80
Autothermal reforming	71-74
Coal gasification	63
Direct biomass gasification	40-50
Electrolysis (nuclear fission-powered)	45-55
Photocatalytic water splitting	10-14

For this research, the methane decomposition system is focused on. However, the conventional steam reforming process also needed to study and compare with in terms of reaction performances in order to investigate an appropriate process for hydrogen production. In addition, aim for different fuel cell types are also taken into account. Therefore, the introduction of the studied hydrogen production processes; i.e. steam reforming and decomposition systems is firstly mentioned in the following sections.

3.1.1 Steam Reforming

The steam reforming has been disclosed that this process provides high quantities of hydrogen produced per mole of reactant, leading to being widely used in industrial process. However, it required a lot of external heat due to the highly endothermic of the steam reforming reaction. Heat vaporization of water is a major factor related to high amount of required heat. Typically, natural gas can be simultaneously reacted via the steam reforming and WGS at 773 K by using Ni-based catalyst [44]. However, various fuels such as methane, ethane, methanol, ethanol, etc. can be processed by the steam reforming [22-26]. It was found that the coke deposition on the catalyst surface is generated under the steam reforming, resulting in the reduction the catalytic activity. The coke deposited is encapsulated the catalyst

surface and its pore. In order to overcome this major problem, the excess of steam has to be fed to the steam reforming reactor. The minimum ratio of steam to carbon atom of primary fuel is required for resolving the coke formation. It was revealed that the minimum ratio for the steam reforming of methane is around 1.4. In addition, air added to the reactant feed can also reduce the coke formation and energy consumption [45]. Moreover, Ni-based catalyst accompanied with additive such as ceria was possible to diminish the coke deposition [46]. In some cases, the study of adding the alkaline earth oxides such as MgO, CaO, and SrO into Ni-based catalyst was revealed that it can also inhibit the coke generation [47].

Regarding the use of steam reforming for fuel cell applications, it can be certainly used with SOFC since hydrogen and carbon monoxide produced from this process can be supplied as a feedstock for this kind of fuel cell. However, it is necessary to reduce the carbon monoxide concentration for PEMFC case via the secondary unit such as shift reactor and preferential oxidation reactor [2].

Currently, there is a significant disadvantage over the steam reforming process that is high quantities of CO_2 emission. Therefore, several researchers [5, 48] has been attempted to investigate another possible hydrogen production method in order to replace the steam reforming process. The decomposition is an alternative choice as reviewed in the next section.

3.1.2 Decomposition

The decomposition process has been known to be one of hydrogen production methods for decades. Compared to currently used steam reforming process in many industries, the decomposition obviously provides less quantities of hydrogen generated in case of the similar carbon atom in primary fuel. However, several researchers [5, 48] have been progressively interested in the decomposition system due to its capability of suppressing the greenhouse gas such as CO_2. In addition, the comparative study of various hydrogen production methods in term of total net cost

indicated that the decomposition process is economically selected [48]. Therefore, there are several attempts to develop this process for becoming another industrial hydrogen production system and subsequently diminishing the use of steam reforming system in industrial scale. Another topic that help gain more attraction is the co-generation of hydrogen product and the valuable carbon by-product. This form of carbon is different from coke that covers on the catalyst surface. The development of the co-generation system by the decomposition process in order to achieve higher hydrogen production with better carbon grade has been greatly investigated. However, the yields of product and by-products are dependent on the type of catalyst used in the decomposition reaction. Hence, in order to enhance the catalytic performances, the catalyst improvement has to be carried out as further mentioned in the next section. Nonetheless, the carbon sequestration from the decomposition process is a challenge topic because the carbon cannot easily separate from the catalyst surface. As reported in the previous researches [20, 21], the fluidized bed reactor has been employed in the decomposition process in order to promote the separation of the carbon produced while the reaction is processed. The presence of attrition phenomena from this reactor type is possible to remove the carbon on the external surface of catalysts. However, this method still cannot completely perform in some cases such as carbon nanotubes (CNT) deposited on the catalyst surface [11]. Therefore, this problem cannot clearly resolve yet, caused the uncertainty of the use of the decomposition process in industrial scale of hydrogen production. However, the decomposition process should preferably be carried out in the near future as a result of being a green technology.

As considered the decomposition process, the methane decomposition has been one of the interesting process for hydrogen production. However, methane-containing gas mixture such as biogas has been another option for being the primary fuel for the decomposition process. Moreover, the thermodynamic study of decomposition system fed by biogas was roughly investigated [35]. The hydrogen-rich gas product or synthesis gas with the valuable carbon by-product such as carbon nanofiber and carbon nanotube has been studied and being under investigations by several researchers [7, 32]. Nevertheless, there was no research for considering this process in order to equipped with fuel cell. However, the decomposition of

hydrocarbons, especially methane, has been accepted for PEMFC application due to the hydrogen production without CO_x emissions. In addition, it can be also employed with SOFC. Regarding the hydrogen production processed by biogas, it was found that the hydrogen production methods such as steam reforming, partial oxidation, autothermal reforming, dry reforming and dry oxidation reforming of biogas are not compatible with PEMFC [49]. However, it could be used with SOFC under some constraints. In this work, the decomposition process fed by biogas for fuel cell applications is concerned and further investigated in Section 5.2.2.

3.2 Catalysts Used in Methane Decomposition

The decomposition of methane typically generates the hydrogen product with by-products of solid carbon. Without the catalyst used, the methane decomposition reaction can be thermally carried out at around 1473-1573 K. However, the catalysts have been developed to employ in the decomposition reaction in order to improve the reaction performances. The operating temperature of the methane decomposition can be reduced by using the catalyst within the reactor. According to the study of catalyst development for decades, it has been found that the catalyst can be mainly divided into two types i.e. the metal-based catalyst and the carbon catalyst. Moreover, the metal-based catalyst can be operated in the methane decomposition at lower temperature, compared to the carbon catalyst.

Regarding the metal-based catalyst, the monometallic and bimetallic catalysts have been applied to the methane decomposition reaction. Transition metals such as Ni, Fe, Co, Pd, Pt, Cr, Ru, and Mo were tested in the decomposition reaction. The different forms of carbon generated can be appeared, relying on the operating temperature. At low operating temperature (773-973 K), the carbon filament can be achieved by using Ni-based catalyst. Fe-based catalyst preferably operated at higher temperature (923-1223 K) and the carbon filament can be also generated. In addition, graphitic turbostratic type of carbon can be obtained at high operating temperature (923-1323 K), catalyzed by Ni, Co, Fe, Pd, Pt, Cr, Ru, and Mo-based catalysts. The

support materials such as Al_2O_3, SiO_2, TiO_2, ZrO_2, and MgO were possible to use in the methane decomposition reaction. However, Ni-based catalyst has been mostly used to carry out in the decomposition reaction due to achieving high catalytic performances and providing long operational lifetime of the catalyst. The hydrogen purity of around 80% can be obtained by using the commercial Ni-based catalyst with 65 wt.% metal loading at temperature of 973 K. The Ni supported on Al_2O_3 has been investigated by comparing to that supported on other supports [50-52]. It was found that Ni/Al_2O_3 catalysts exhibit higher in catalytic activity and the stability of the methane decomposition, compared to Ni/SiO_2 catalysts. In case of using other monometallic catalysts such as Co-, Fe-, and Cu-based catalysts, lower carbon deposited was achieved, compared to Ni-based catalysts [8, 39, 53]. The carbon filament can be obtained by using the Ni-based catalyst at the moderate temperature (773-973 K). Several steps of carbon filament formation have been proposed [54] based on the deactivation of metal catalysts as listed in the following steps:

i) the methane decomposition reaction at the gas-metal interface
ii) the dissolution of carbon into the metal
iii) the diffusion of carbon through the metal particle
iv) the precipitation of carbon at the metal-support interface
v) the detachment of the metal particle from the support
vi) the carbon filament formation with the metal particle at its tip.

It was possibly indicated that the step of the diffusion of carbon through the metal particle is the rate-determining step. For the deactivation of the catalysts [55], the encapsulated carbon was formed on the catalyst surface. It can be presumably proposed that the catalyst deactivation occurred when the rate of carbon diffusion through the metal particle was slower than that of the carbon formation at the metal sites. After the carbon builds up at the catalyst surface, the catalyst was finally encapsulated, resulting in the deactivation of catalyst.

Besides the monometallic catalysts, the bimetallic catalysts were also investigated such as Ni-, Cu-, Fe-, and Pd-based bimetallic catalysts. These catalysts

are possible to obtain higher hydrogen production, compared to the use of the monometallic catalysts. For example, Ni-Cu/Al_2O_3 catalysts showed higher catalytic performance and longer periods of time, compared to Ni/Al_2O_3 catalysts [56]. The investigation of various Ni-containing catalysts such as Ni/Mn, Ni/Fe, Ni/Co, and Ni/Cu was carried out [10]. It was revealed that Ni/Mn shows high hydrogen production with carbon by-product in the form of carbon nanotube. Moreover, the multi-walled carbon nanotube can be achieved by using Mo-Fe/Al_2O_3 catalysts [30]. By using the Pd-based bimetallic catalysts, hydrogen purity higher than 94% and the carbon nanofiber were obtained at the operating temperature of 973-1123 K [29].

As considered the carbon catalysts, the activated carbon (AC) and carbon black (CB) are mostly used in the decomposition of methane. As reported from several researches [57-61], the carbon catalysts can provide the advantage over the metal-based catalysts such as

1) low cost
2) high temperature resistance
3) diminishing the CO_2 emission from the process
4) no need for the separation of carbon formation from the carbon catalysts
5) yielding the valuable carbon by-product.

From the research of Serrano *et al*. [62], it should be noted that the most active catalyst at short reaction times was AC, but a fast deactivation was occurred whereas CB provided high reaction rates at both short and long reaction times. The reduction in the catalyst deactivation can be obtained by increasing the surface area and pore volume [63]. In addition, the pore-size distribution is a key factor in indicating the long-term behavior of the catalyst.

However, the metal supported on the carbon catalyst such as Ni/AC has been studied by Bai *et al*. [64]. It was found that the Ni/AC shows higher catalytic activity, compared to the AC. In addition, the acceptable stability was achieved at 923 K.

3.3 Proposed Mechanism and Kinetic of Methane Decomposition

The kinetic model of the methane decomposition has been started to investigate since 1965 [65]. Until now, several proposed kinetic model of this reaction has been discovered [51, 58, 65-76]. It can be mainly divided into three categories: 1) the detailed mechanistic model, 2) the generated mathematic model, and 3) the global rate model. As considered the mechanism of methane decomposition in detail, the mechanism of this reaction was firstly expressed under the assumption of non-dissociative methane in the adsorption step [68-72]. This mechanism is presented step by step as listed below.

$CH_4 + I\ (\text{Vacant site}) \rightleftharpoons CH_4(ad)$ (3-1)

$CH_4(ad) \rightleftharpoons CH_3(ad) + H(ad)$ (3-2)

$CH_3(ad) \rightleftharpoons CH_2(ad) + H(ad)$ (3-3)

$CH_2(ad) \rightleftharpoons CH(ad) + H(ad)$ (3-4)

$CH\ (ad) \rightleftharpoons C(ad) + H(ad)$ (3-5)

$C(ad) \rightleftharpoons C(\text{dissolved})$ (3-6)

$2H(ad) \rightleftharpoons H_2 + 2I$ (3-7)

The differences in the developed models were proposed by different rate-determining step. The reaction (3-1), (3-2), or (3-3) was often used as the rate-limiting step. The Ni-based catalysts were typically used for developing the kinetic model, but the first model generated by Grabke [68] was tested by iron as the catalyst. These models were mostly developed in the temperature range of ca. 773-873 K. Grabke [68] and Bernando *et al*. [69] expressed the kinetic model in term of partial pressure of H_2 and CH_4 whereas Demicheli *et al*. [70], Snoeck *et al*. [71], and Kuvshinov *et al*. [72] incorporated the mechanism of carbon formation as shown in the following equations into their models.

Diffusion in Ni phase: C(dissolved) ⇌ C(nickel rear) (3-8)

Precipitation from Ni phase: C(nickel rear) ⇌ C(Carbon filamentous) (3-9)

Formation of encapsulating carbon: C(ad) ⇌ C(encapsulating) (3-10)

In addition, the carbon formation rate was performed, including the determination of maximum carbon deposited. Even though the kinetic model assuming non-dissociative adsorption of methane was often used, another model based on dissociative methane in adsorption step was also generated [73-76]. These mechanisms were illustrated as follows:

$CH_4 + I \text{ (Vacant site)} \rightleftharpoons CH_3(ad) + H(ad)$ (3-11)

$CH_3(ad) \rightleftharpoons CH_2(ad) + H(ad)$ (3-3)

$CH_2(ad) \rightleftharpoons CH(ad) + H(ad)$ (3-4)

$CH\ (ad) \rightleftharpoons C(ad) + H(ad)$ (3-5)

$C(ad) \rightleftharpoons C(dissolved)$ (3-6)

$2H(ad) \rightleftharpoons H_2 + 2I$ (3-7)

Alstrup and Tavares [73] model was fitted with the experimental data by applying the reaction (3-11) or (3-3) as the rate-determining step. Zavarukhin and Kuvshinov [74] used the reaction (3-11) and it was found that the specific carbon content on the catalyst at 823 K from the model and the experimental data exhibits the difference in value below 10%.

Considering the generated mathematic model, there is no need to define the reaction mechanisms for this model. However, it can predict the total carbon formation on the catalyst from the kinetic parameters in nucleation and filament growth steps. As reported in Villacampa *et al*. [51], the predicted data from the developed model was in a good agreement with the experimental data.

According to the simplest model, the global rate equation was presented. From the research of Fukada *et al*. [66], the first order of methane decomposition reaction was proposed for using Ni/SiO_2 as catalyst. The activation energy was 29.5 kJ mol^{-1}.

In case of using carbon catalysts, the reaction order was found to be 0.5 with the apparent activation energy of 160-201 kJ mol^{-1} and 205-236 kJ mol^{-1} for activated carbon or carbon black catalysts, respectively [58].

3.4 Carbon Generated from Decomposition Process

As mentioned previously (Section 3.2), relying on the operating conditions of the methane decomposition system, carbon can be produced in various structures: amorphous, turbostratic, and carbon fibers. The wide difference in the prices of different carbon modifications provided the importance of the carbon type produced in the methane decomposition process in terms of the reduction in cost of hydrogen production. For the useful carbon types, that are carbon nanofiber and carbon nanotube, several applications such as electronic applications, gas storage materials, composite materials, and catalyst supports can be conducted [13-17].

As a result of high catalytic activity, Ni catalyst has been the promising alternative for producing carbon nanofiber at moderate temperature (500-700^{o}C) from the methane decomposition process [64]. In case of Fe-based catalyst, high efficiency at higher temperature range could be gained. Moreover, the formation of carbon nanotube would be also achieved by adding the second metal such as Co and Ni. From the study of binary metallic catalysts, the generation of muti-walled carbon nanotubes could be obtained [30]. With the presence of carbon dioxide indicating as the biogas feed, the nanostructured carbon material could be exhibited, accompanied with gaseous product of hydrogen-rich gas or synthesis gas [7, 32].

3.5 Biogas Treatment Methods

The biogas treatment in term of CO_2 removal from gas streams has been of great interest, especially in large thermal power plants, due to its greenhouse effect [77]. Table 3.2 compares the different existing technologies. In this work, among

several CO_2 separation technologies, the CO_2 removal from gas streams of CO_2 capture type was also concerned in case of hydrogen production processed by biogas. Regarding various CO_2 separation techniques, it can be summarized in the following sections.

3.5.1 Absorption

It refers to the process by which one substance, such as a solid or liquid, takes up another substance, such as a liquid or gas, through minute pores or spaces between its molecules. The absorption capacity of the absorber depends on the equilibrium concentrations between gaseous phase and the liquid phase. For diluted concentrations in many gases and in a wide interval of concentrations, the equilibrium relation is given by Henry's law, which quantifies the gas absorption capacity in the fluid [78]. A gas absorbing unit should ensure complete contact between the gas and the solvent, in such a way that diffusion occurs at the inter-phase.

3.5.2 Adsorption

It refers to the process by which molecules of a substance, such as a gas or a liquid, collect on the surface of a solid. It differs from absorption, in which a fluid permeates or is dissolved by a liquid or solid [79]. It could be physical or chemical. In physical adsorption process, gas molecule adhere to the surface of the solid adsorbent as a result of the molecules attraction force (Van der Waals Forces). Chemical adsorption involves a chemical reaction. Usually, adsorbents are 12 μm to 120 μm high porosity solid grains, inert to the treated fluid. The most used adsorbents for CO_2 are activated charcoal, silica gel, zeolites and synthetic resins.

3.5.3 Condensation

It is the process of converting a gas into a liquid by reducing temperature and/or increasing pressure. Condensation occurs when partial pressure of the substance in the gas is lower than the vapor pressure of the pure substance at a given temperature.

3.5.4 Membranes

A membrane is a layer of material which serves as a selective barrier between two phases and remains impermeable to specific particles, molecules, or substances when exposed to the action of a driving force. The driving force is the pressure difference between both sides of the membrane. Gas permeability through a membrane is a function of the solubility and diffusivity of the gas into the material of the membrane. Membranes are expensive and their separation efficiencies are low [80].

Presently, the CO_2 emission generated by various processes, for example, the steam reforming affects the surroundings as this problem is called the global warming. Therefore, it is necessary to integrate the CO_2 separation system with the processes that release the greenhouse gas. There are several kinds of CO_2 sequestration units such as amine absorption, pressure swing adsorption, membrane, and carbonate looping [81]. Under the investigation of the adsorption method, it is not selected to use in the conventional process due to the limitation of its capacity and poor selectivity [82]. Therefore, other CO_2 separation methods are focused on.

Table 3.2 Alternatives to remove CO_2 from gas streams [83].

Method Option/Alternative	Advantages	Disadvantages
Absorption with water	High efficiency (>97% CH_4), Simultaneous removal of H_2S when H_2S< 300 cm^3/m^3, Capacity is adjustable by changing pressure or temperature, Low CH_4 losses (<2%), Tolerant to impurities	Expensive investment and operation, Clogging due to bacterial growth, Possible foaming, Low flexibility toward variation of input gas
Absorption with polyethylene glycol	High efficiency (>97% CH_4), Simultaneous removal of organic S components, H_2S, NH_3, HCN and H_2O, Energetic more favorable than water, Regenerative, Low CH_4 losses	Expensive investment and operation, Difficult operation, Incomplete regeneration when stripping/vacuum (boiling required), Reduced operation when dilution of glycol with water
Chemical absorption with amines	High efficiency (>99% CH_4), Cheap operation, Regenerative, More CO_2 dissolved per unit of volume (compared to water), Very low CH_4 losses (<0.1%)	Expensive investment, Heat required for regeneration, Corrosion, Decomposition and poisoning of the amines by O_2 or other chemicals, Precipitation of salts, possible foaming

Method	Option/Alternative	Advantages	Disadvantages
PSA/VSA	Carbon molecular sieves Zeolites Molecular sieves Alumina silicates	Highly efficient (95-98% CH_4), H_2S is removed, Low energy use: high pressure, Compact technique, also for small capacities, Tolerant to impurities	Expensive investment and operation, Extensive process control needed, CH_4 losses when malfunctioning of valves
Membrane technology	Gas/gas Gas/liquid	H_2S and H_2O are removed, Simple construction, Simple operation, High reliability, Small gas flows treated without proportional increase of costs • Gas/gas: removal efficiency: <92% CH_4 (1 step) or >96% CH_4, H_2O is removed • Gas/liquid: removal efficiency: >96% CH_4, cheap investment and operation, Pure CO_2 can be obtained	Low membrane selectivity: compromise between purity of CH_4 and amount of upgraded biogas, Multiple steps required (modular system) to reach high purity, CH_4 losses
Cryogenic separation		90-98% CH_4 can be reached, CO_2 and CH_4 in high purity, Low extra energy cost to reach liquid biomethane (LBM)	Extensive investment and operation, CO_2 can remain in the CH_4
Biological removal		Removal of H_2S and CO_2, Enrichment of CH_4, No unwanted end products	Addition of H_2, Experimental- not at large scale

According to the membrane method, polymer membrane is a promising type for separating CO_2. It was found that the best polyimide membranes attain a CO_2/N_2 selectivity of 30%. In term of energy consumption, the use of membrane consumes the energy around 0.04-0.07 kWh per CO_2 removal in case of using a coal-derived fuel. The CO shift reactor equipped with the membrane unit can possibly exhibit less energy losses due to the unnecessary syngas processing step [84].

As considered another CO_2 separation technique, the CO_2 removal processed by the carbonation of CaO to $CaCO_3$ is called the carbonate looping. This method is an attractive technique because the installation of this process in the syngas production can provide the increase in the reactant partial pressure and shift forward the WGS [85].

Chemical absorption technology is selected to be the capture unit in this work. The CO_2 separation efficiency can be gained in the range of 85-96% [42]. However, the optimum value of 90% is preferred to operate this technique [86, 87]. CO_2 is captured by using a chemical absorbent such as amine solution. Thermal energy is consumed to operate this capture in the absorber at temperature range of 320-340 K and to regenerate the chemical absorbent in the stripper around 400 K [88, 89].

Considering the amine absorption method, the possible chemical solvents such as monoetanolamine (MEA), diethanolamine (DEA), and methyl-diethanolamine (MDEA) are typically used to absorb CO_2. MEA is the most used absorbent in this system [90]. MEA is mostly used at the 30% concentration [91] and consumed at the rate of 1.5-3.1 kg ton^{-1} CO_2 removed [87, 91-95]. With the 30%wt of MEA solution, CO_2 is initially absorbed at the absorber unit [91] with the operating condition; temperature of 323 K and atmospheric pressure [96]. After that, CO_2 is absorbed until the MEA solution saturated. MEA solution is fed to regenerate at the stripper for reuse in the absorber. Temperature of this stripper unit is 393 K [96] and the thermal energy is required around 4 $GJ_{thermal}$ ton^{-1} CO_2 removed [87, 93-95, 97, 98].

The information provided for determining heat requirement of CO_2 capture employed in Section 5.2.2 for the systems as displayed in Figures 5.28 and 5.30 is listed below.

- The absorber temperature of 323 K
- CO_2 capture efficiency of 90%
- Heat consumption of CO_2 capture by means of MEA absorption of 4 GJ ton^{-1} CO_2

CHAPTER IV
SIMULATION

In this work, hydrogen production from decomposition and steam reforming processes is investigated by thermodynamic approach. Therefore, the topics related to the thermodynamic analysis are gathered in this chapter. Firstly, the equilibrium constants for all related reactions occurred in each system are presented in Section 4.1. Moreover, the thermodynamic study by means of Gibbs free energy minimization method is selected to employ in this work in order to consider the carbon formation in the process. Its technique with a proper equation of state is proposed in Section 4.2.

4.1 Equilibrium Constants for Related Reactions

In this research, the reaction performances from the decomposition and steam reforming processes such as the equilibrium conversion, the selectivity of hydrogen and by-products, hydrogen production, hydrogen purity, CO fraction, and carbon yield are firstly determined by using thermodynamic calculation. The direction of each reaction depends upon equilibrium constant (K_{eq}), which is a function of reaction temperature. The equilibrium constants of the related reactions as mentioned in Section 2.2 calculated by Aspen Plus program can be collected and further displayed in Figure 4.1.

4.2 Gibbs Free Energy Minimization Method

As mentioned previously (Section 2.2), the solid carbon can be certainly generated by the decomposition of hydrocarbon. The carbon activity (α_C) has been widely used as the thermodynamic indicator of carbon formation as addressed in a number of the previous researches [99-101]. Nonetheless, its value merely predicts

the carbon formation without providing the amount of carbon formed. For instance, the carbon activity of methane cracking can be expressed by the following equation:

$$\alpha_{C,CH_4} = \frac{K_1 p_{CH_4}}{p_{H_2}^2} \tag{4-1}$$

where K_1 is the equilibrium constant of methane decomposition and p_{CH_4} and p_{H_2} is partial pressure of CH_4 and H_2, respectively. The criterion of carbon formation is considered at the carbon activity value equal to 1. The carbon formation is observed when carbon activity is more than 1 whereas the equilibrium state is occurred when carbon activity is equal to 1 and the carbon unfavorably forms when carbon activity is less than 1. However, some researchers [102-105] determined the carbon formation by means of Gibbs free energy minimization, which is a function that indicates the tendency of the reaction at equilibrium state. The Gibbs free energy minimization method is commonly utilized to determine the equilibrium composition at desired temperature and pressure.

The composition of any reacting system is the equilibrium of the composition which can be calculated by Gibbs free energy equation [106]. Gibbs free energy reaction values would predict the chance for a reaction to occur by the minimization of total Gibbs free energy method. At the steady state, pressure and temperature of the system are constant, so the equations are given as follows:

$$dG = \sum_{i=1}^{N} \bar{\mu}_i dn_i \tag{4-2}$$

$$G = \sum_{i=1}^{N} \bar{\mu}_i n_i \tag{4-3}$$

a)

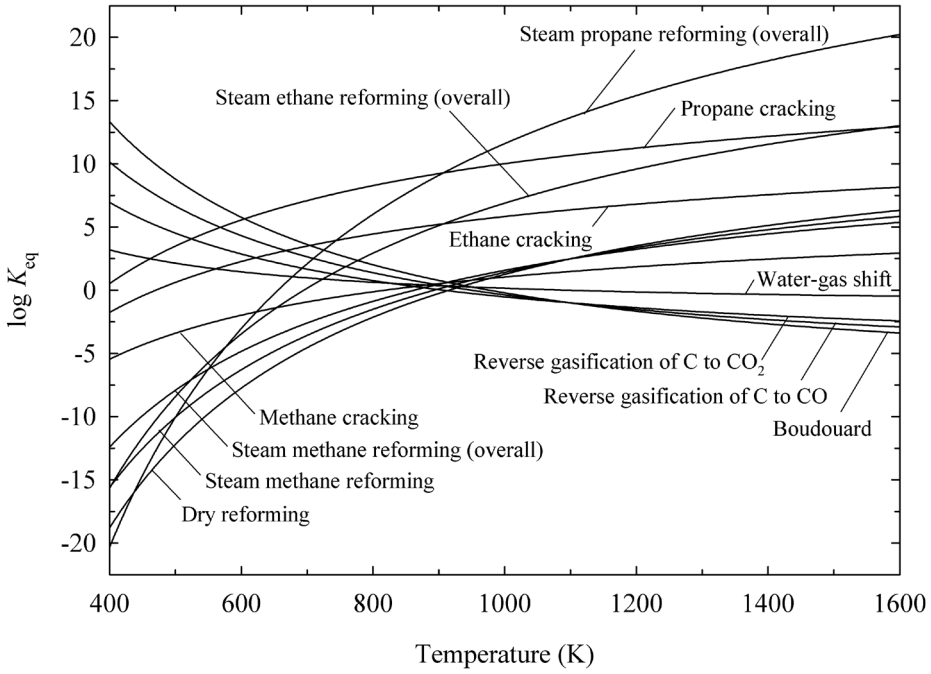

b)

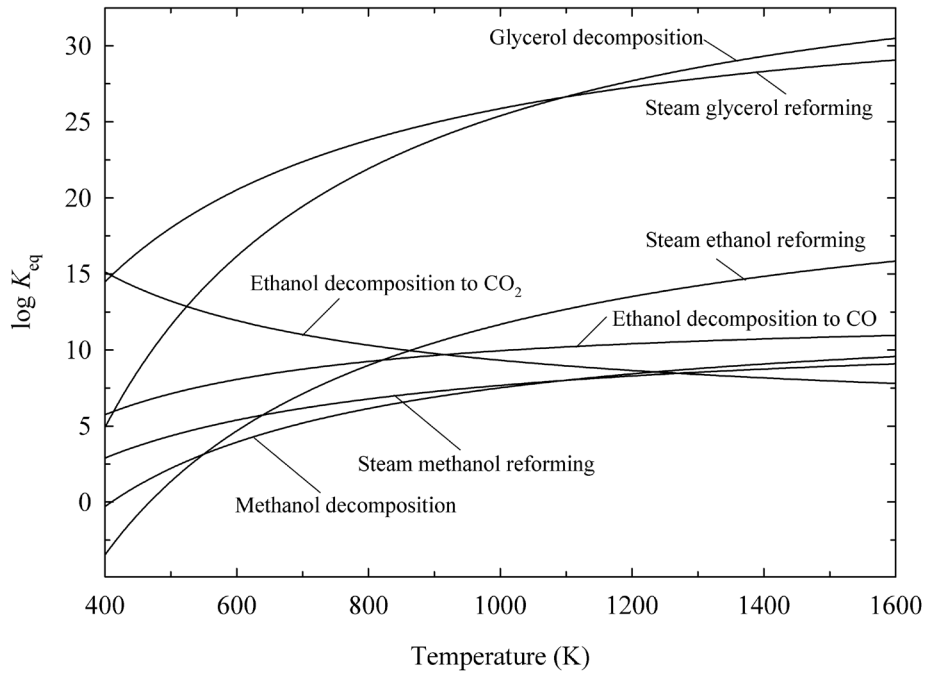

Figure 4.1 The equilibrium constants of reactions occurred in the decomposition and the steam reforming processes fed by (a) light hydrocarbons and (b) alcohols.

The total Gibbs function can be written as follows:

$$min(\mathrm{G^t}) = \sum n_i G_i^0 + RT \sum n_i ln \frac{\hat{f}_i}{f_i^0} \tag{4-4}$$

For reaction equilibrium in gas phase:

$$\hat{f}_i = \hat{\phi}_i y_i P \tag{4-5}$$

$$f_i^0 = P^0 \tag{4-6}$$

G_i^0 is set to zero for each chemical element in its standard state:

$$\Delta G^0 = \Delta G_{f_i}^0 \tag{4-7}$$

From these equations, N is the total number of components in the system; n_i is the variable that minimizes the value of Gibbs free energy. It can be solved two ways including 1) the stoichiometric thermodynamic approach which is determined by a set of stoichiometrically independent reactions, then typically chosen arbitrarily from a set of possible reactions, and 2) a non-stoichiometric thermodynamic approach value is set up by the direct minimization of the Gibbs free energy for a given set of species [106]. The advantages of non-stoichiometric thermodynamic approach included 1) a selection of the possible set of reactions in that system is not necessary 2) no divergence occurs during the consumption, and 3) an accurate estimation of the initial equilibrium composition is not necessary [107]. This research would be calculated by a non-stoichiometric thermodynamic approach. Lagrange's undetermined multiplier method was expressed as:

$$\Delta G_{f_i}^0 + RTln \frac{\hat{\phi}_i y_i P}{P^0} + \sum_k \lambda_k a_{ik} = 0, \tag{4-8}$$

$$\sum_{i=1}^{N} n_i \left(\Delta G_{f_i}^{0} + RTln \frac{\hat{\phi}_i y_i P}{P^0} + \sum_k \lambda_k a_{ik} \right) = 0, \quad (4\text{-}9)$$

From the constraints of elemental balances:

$$\sum_{i=1}^{N} n_i \, a_{ik} = A_k. \quad (4\text{-}10)$$

where a_{ik} is the number of atoms of element k in component i, A_k is the total number of atoms of element k in the reaction mixture, and N is the total number of elements.

When solid carbon (graphite) is considered in the system, Gibbs energy of carbon is usually considered [108]:

$$\overline{G}_{C(g)} = \overline{G}_{C(s)} = G_{C(s)} \cong G_{f_{C(s)}}^{0} = 0 \quad (4\text{-}11)$$

However, for a temperature-steady process:

$$dG_{C(s)} = V_C dP \quad (4\text{-}12)$$

V_C is the mole volume of solid carbon, and it can be regarded as a constant because it is less affected by temperature and pressure then, equation (4-12) can be expressed as equation (4-13):

$$G_{C(s)}(T,P) - G_{C(s)}(T,P^0) = V_C(P - P^0) \quad (4\text{-}13)$$

where $G_{C(s)}(T,P^0)$ is assumed to be zero and $V_C = 4.58 \times 10^{-6}$ m^3 mol^{-1}. Equation (4-13) is further expressed as equation (4-14).

$$G_{C(s)}(T,P) = 4.58 \times 10^{-6}(P - P^0) \quad (4\text{-}14)$$

The minimization function of Gibbs energy as following equation (4-15) is obtained by substituting equation (4-4) by equation (4-8) for gaseous species and by equation (4-14) for solid species.

$$\sum_{i=1}^{N\text{-}1} n_i \left(\Delta G_{f_i}^{0} + RTln \frac{\hat{\phi}_i y_i P}{P^0} + \sum_k \lambda_k a_{ik} \right) + n_C G_{C(s)}(T,P) = 0 \qquad (4\text{-}15)$$

The fugacity coefficient $\hat{\phi}_i$ of each component in the gas mixture can be calculated according to the Peng-Robinson equation of state; that is

$$P = \frac{RT}{V - b} - \frac{a\,(T)}{V(V+b) + b\,(V - b)} \qquad (4\text{-}16)$$

$$a\,(T) = a\,(T_c)\,\alpha\,(T_r, \omega) \qquad (4\text{-}17)$$

$$a\,(T_c) = 0.45724 \frac{R^2 T_c^2}{P_c} \qquad (4\text{-}18)$$

$$\alpha\,(T_r,\omega) = [1 + \kappa\,(1 - T_r^{0.5})]^2 \qquad (4\text{-}19)$$

$$T_r = \frac{T}{T_c} \qquad (4\text{-}20)$$

$$\kappa = 0.37464 + 1.54226\omega - 0.26992\omega^2 \qquad (4\text{-}21)$$

$$b = 0.07780 \frac{RT_c}{P_c} \qquad (4\text{-}22)$$

In polynomial form:

$$A = \frac{aP}{R^2 T^2} \qquad (4\text{-}23)$$

$$B = \frac{bP}{RT} \tag{4-24}$$

$$Z = \frac{PV}{RT} \tag{4-25}$$

Accordingly, the fugacity coefficient $\hat{\phi}_i$ can be calculated from the following equation:

$$\ln \hat{\phi}_i = \frac{b_i}{b_{\mathrm{m}}}(Z - 1) - \ln (Z - B) - \frac{A}{2\sqrt{2}B} \times \left(\frac{2\sum_j y_j a_{ji}}{a} - \frac{b_i}{b_{\mathrm{m}}} \right) \ln \left(\frac{Z + \left(1+\sqrt{2}\right)B}{Z + \left(1-\sqrt{2}\right)B} \right) \tag{4-26}$$

The mixture parameters used above in equation (4-26) are defined by the mixture rules

$$a_{\mathrm{m}} = \sum_i \sum_j y_i y_j a_{ij} \tag{4-27}$$

$$b_{\mathrm{m}} = \sum_{\mathrm{i}} y_i b_i \tag{4-28}$$

$$a_{\mathrm{ij}} = \left(a_i a_j\right)^{0.5} \left(1 - \delta_{ij}\right) \tag{4-29}$$

The processes of simulation were operated by Aspen Plus software. It is a software program designed to build a process model and then simulate the model without tedious calculations for conceptual design, optimization, and performance monitoring. It can be also used for a wide variety of chemical engineering tasks. This program was used for all calculations consisting of material balances, energy balances, net of energy equals zero, and minimization of total Gibbs free energy for studying the effects of variables at each condition of the system. The RGibbs model was chosen in this analysis in order to minimize Gibbs free energy.

In this work, the calculation of the equilibrium values at different reaction temperatures is determined by Gibbs free energy minimization. The vapor-solid phases with Peng-Robinson equation of state were used in this simulation. This equation of state has been known to use in the refinery and natural gas processing industries. The Peng-Robinson equation of state could provide the results similar to the Soave-Redlich-Kwong equation of state [109]. As considered the possible solid carbon generated by hydrogen production, the solid carbon is assumed to be graphite in every reaction that generated the carbon. No reaction is necessary to state in the Gibbs free energy minimization module but the possible products converted from the related primary fuel and process have to be input in the calculation, which can be found elsewhere [22, 104, 110-112].

For both hydrocarbon cracking processes and the steam reforming of hydrocarbons yields H_2, carbon, and low hydrocarbons but additional CO and CO_2 can be obtained from the steam reforming processes as by-products. On the other hand, the use of methanol in both processes can reasonably gain dimethyl ether (CH_3OCH_3), formaldehyde (HCHO), CH_4, H_2, CO, CO_2, H_2O and carbon. In case of using ethanol as a fuel source, acetaldehyde (CH_3CHO), acetone (CH_3COCH_3), diethyl ether ($C_2H_5OC_2H_5$), C_2H_6, C_2H_4, CH_4, H_2, CO, CO_2, H_2O and carbon would be produced. Further, the decomposition and steam reforming of glycerol can presumably produce acetaldehyde, acrolein (C_3H_4O), acetone, methanol, ethanol, acetic acid (CH_3COOH), C_3H_6, C_2H_6, C_2H_4, CH_4, H_2, CO, CO_2, H_2O and carbon. Each reactant used in the decomposition and steam reforming was fed to their systems at 298 K. Regarding the steam reforming system, the appropriate mole of feeding water was calculated according to its stoichiometric coefficient of overall steam reforming reaction, which consequently gives the maximum mole of hydrogen produced. In addition, the reaction temperatures were studied in the range of 400-1600 K at pressure of 1 bar. According to the simulation in this work, RGibbs reactor was employed in decomposition and steam reforming units. It was also applied in order to consider the carbon formation at the SOFC inlet with the SOFC temperature in the range of 900-1300 K for investigating the range of possible uses.

CHAPTER V
RESULTS AND DISCUSSION

In this chapter, the simulation results of hydrogen production systems are presented and further discussed in details. This can be mainly divided into two sections including comparison of reaction performances between steam reforming and decomposition processes with different primary fuels (Section 5.1) and study of decomposition system fed by biogas (Section 5.2). According to the first section, the characteristics of the steam reforming and decomposition systems are firstly presented as a function of the operating temperature for different primary fuels such as light hydrocarbons and alcohols. In addition, the systems under thermally self-sustained condition, which are the systems with no external heat source, are carried out to be fair comparison of reaction performances between both systems. Lastly, the appropriate primary fuel of hydrogen production for low and high temperature fuel cells is selected. Methane decomposition system has been one of the interesting alternatives for hydrogen production. However, the methane-containing gas mixture such as biogas is another promising choice to employ in the decomposition system as investigated in the second section. Moreover, the influence of CO_2/CH_4 ratio on the reaction performances is further taken into account. Finally, the suitable operating condition of the decomposition system which is compatible with different types of fuel cells is determined.

5.1 Comparison of Reaction Performances between Steam Reforming and Decomposition Processes with Different Primary Fuels

In this section, the thermodynamic analyses of the steam reforming and decomposition systems were determined by means of Gibbs free energy minimization method as mentioned in Section 4.2. These systems were fed by different primary fuels such as light hydrocarbons (methane, ethane and propane) and alcohols (methanol, ethanol and glycerol). From this point forward, the decomposition (D) and steam reforming (SR) systems of primary fuel *i* were denoted as D-*i* and SR-*i*, respectively.

Each reactant used in the decomposition and steam reforming was fed to their systems at 298 K. A basis of 1 mole feed of each primary fuel was assumed for all systems. For the steam reforming system, the appropriate mole of feeding water was calculated according to its stoichiometric coefficient of overall steam reforming reaction, which consequently gives the maximum mole of hydrogen produced. The reaction temperatures were studied in the range of 400-1600 K at pressure of 1 bar. The related reactions for both systems fed by different primary fuels are listed in Section 2.2. In addition, the possible products for each process that have to be input in the simulator and the necessary assumptions were gathered in Section 4.2.

In a comparative study of the reaction performances on the steam reforming and decomposition processes, the simulation results in terms of the equilibrium conversion, selectivity of hydrogen and by-products, hydrogen yield, carbon yield, and hydrogen purity are calculated by equations summarized in Table 5.1.

Table 5.1 Expressions of the equilibrium conversion $(X_{i,\mathrm{e}})$, hydrogen and by-product selectivities $(S_{\mathrm{H_2},i}$ and $S_{j,i})$, carbon yield $(Y_{\mathrm{C},i})$, and hydrogen purity from different primary fuels i ($\mathrm{C}_a\mathrm{H}_b\mathrm{O}_c$).

Variable	Expression (× 100)	
	Decomposition	Steam reforming
$X_{i,\mathrm{e}}(\%)$	$\frac{n_{i,\mathrm{in}}-n_{i,\mathrm{out}}}{n_{i,\mathrm{in}}}$	
$S_{\mathrm{H_2},i}(\%)$	$\frac{n_{\mathrm{H_2,out}}}{\frac{b_i}{2}\left(n_{i,\mathrm{in}}-n_{i,\mathrm{out}}\right)}$	$\frac{n_{\mathrm{H_2,out}}}{\frac{b_i}{2}\left(n_{i,\mathrm{in}}-n_{i,\mathrm{out}}\right)+\left(n_{\mathrm{H_2O,in}}-n_{\mathrm{H_2O,out}}\right)}$
$S_{j,i}(\%)$	$\frac{n_{j,\mathrm{out}}}{\frac{a_i}{a_j}\left(n_{i,\mathrm{in}}-n_{i,\mathrm{out}}\right)}$	
$Y_{\mathrm{H_2},i}(\%)$	$\frac{n_{\mathrm{H_2,out}}}{\frac{b_i}{2}\times n_{i,\mathrm{in}}}$	$\frac{n_{\mathrm{H_2,out}}}{\frac{b_i}{2}\times n_{i,\mathrm{in}}+n_{\mathrm{H_2O,in}}}$
$Y_{\mathrm{C},i}(\%)$	$\frac{n_{\mathrm{C,formed}}}{a_i\times n_{i,\mathrm{in}}}$	
$\mathrm{H_2}$ Purity (%)	$\frac{n_{\mathrm{H_2,out}}}{\sum_i n_{i,\mathrm{out}}}$	

b_i is number of H atom in primary fuel i

$n_{i,\mathrm{in}}$ and $n_{i,\mathrm{out}}$ are mole of primary fuel i at inlet and outlet of the system

j is by-product species

5.1.1 Effect of Operating Temperature on Reaction Performances

In this part, reaction performances are proposed in terms of the equilibrium conversion of each primary fuel, the selectivity of the product, hydrogen, and of by-products, CH_4, CO, and CO_2, and carbon yield as a function of temperature for different primary fuels, processing by the decomposition and the steam reforming for comparison purposes. Starting with the equilibrium conversion for each primary fuel (Figure 5.1), it was found that the equilibrium conversion of methane from either D-CH_4 or SR-CH_4 is increased with increasing reaction temperature. Since the methane cracking and the methane steam reforming are endothermic reactions, the increase in temperature resulted in enhancing the value of the equilibrium constant, leading to higher methane consumption and product generation. Therefore, the equilibrium methane conversion was subsequently lifted up until the value close to 100% at ca. 1500 K for D-CH_4. It should be noted that the equilibrium conversion of methane shows the similar simulation results and is in good agreement with the results reported by Ogihara *et al.* [29]. Moreover, the equilibrium compositions from SR-CH_4 of this work were also validated with those of Seo *et al.* [113]. It is worthy to note that although lower equilibrium constant of SR-CH_4 is observed at low temperature comparing to D-CH_4 [Figure 4.1(a)], higher equilibrium conversion is achieved. This was because of WGS, which could shift forward the main reaction of methane steam reforming and further enhance the equilibrium conversion. At high temperature, higher in the equilibrium constant resulted in providing higher equilibrium conversion from SR-CH_4. Therefore, not only the equilibrium constant, but also the occurrence of side reaction, WGS, could play an important role in obtaining high conversion when compared to D-CH_4. On the other hand, other light hydrocarbons and alcohols were entirely consumed over temperature range of the study and gave 100% conversion. Such complete conversion was observed for light hydrocarbons and alcohols in both cracking and steam reforming systems.

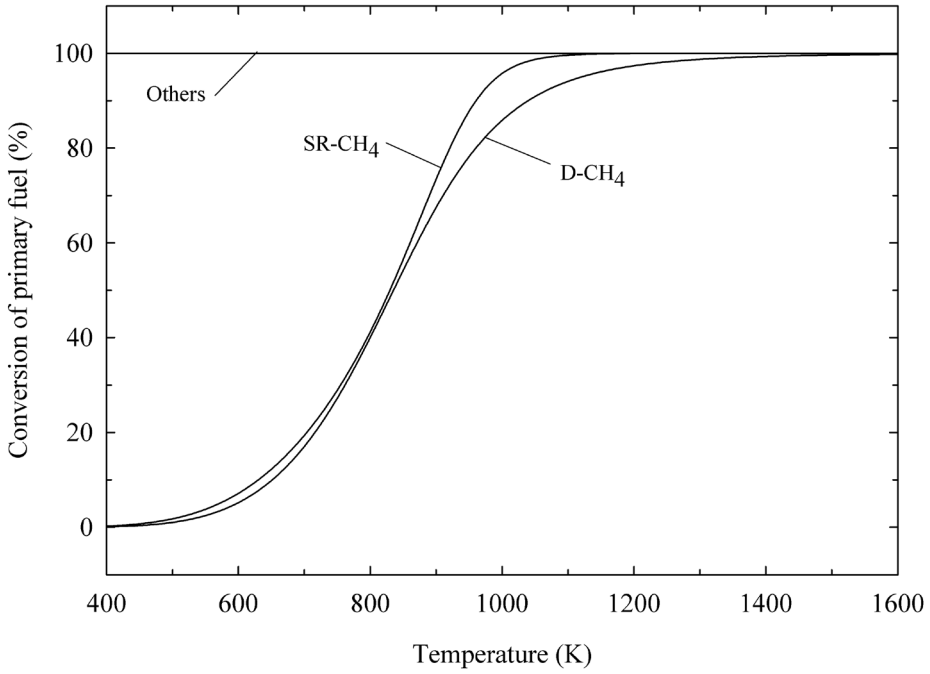

Figure 5.1 The equilibrium conversion of each primary fuel obtained from the decomposition and the steam reforming processes.

In Figure 5.2(a) is shown percent selectivity of hydrogen at different temperatures. When the primary fuel was methane, it was observed as expected that D-CH_4 and SR-CH_4 give 100% selectivity of hydrogen regardless of temperature. This result was because no other products containing H atom are formed for both systems. For other primary fuels, including light hydrocarbons and alcohols, at low temperature, low hydrogen selectivity was observed as methane was generated as a by-product. The hydrogen selectivity increased when temperature was raised due to the by-product, methane, reacted via methane cracking or methane steam reforming.

a)

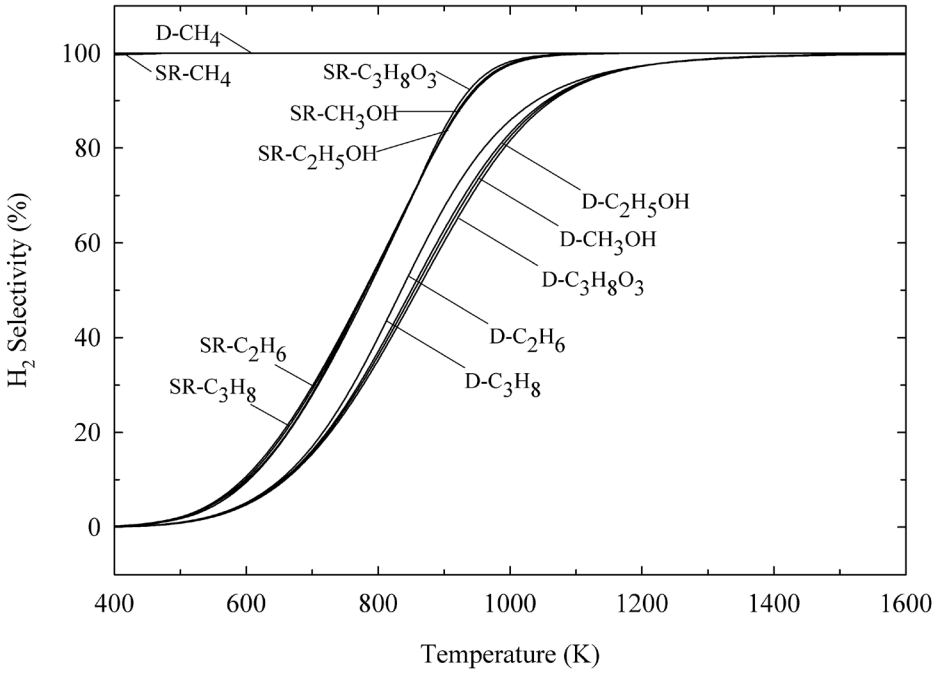
D-CH4
SR-CH4
SR-C3H8O3
SR-CH3OH
SR-C2H5OH
D-C2H5OH
D-CH3OH
D-C3H8O3
D-C2H6
D-C3H8
SR-C2H6
SR-C3H8
H2 Selectivity (%)
Temperature (K)
0
20
40
60
80
100
400
600
800
1000
1200
1400
1600

b)

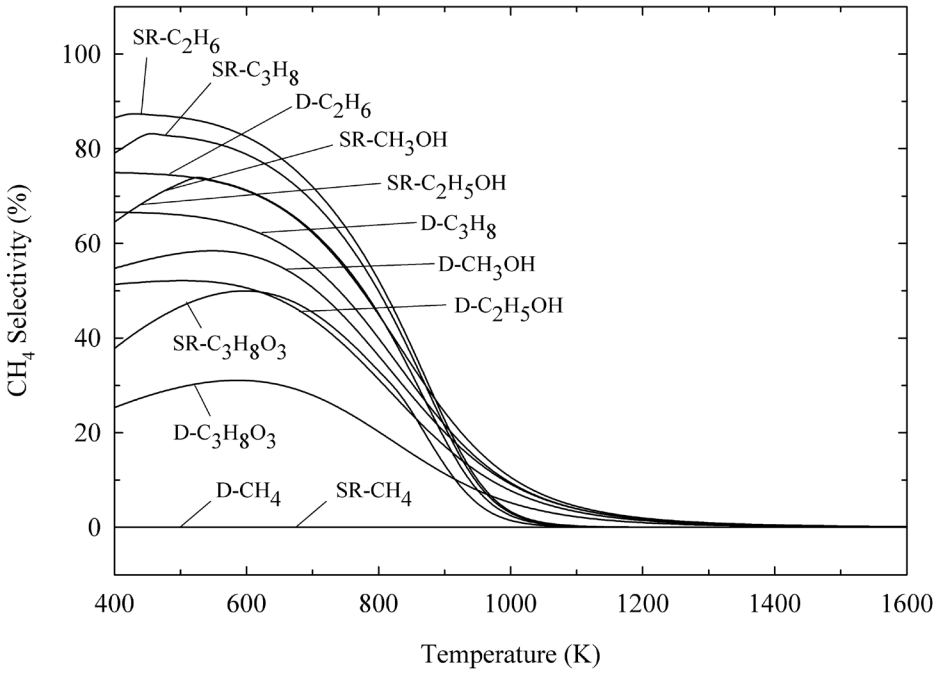
SR-C2H6
SR-C3H8
D-C2H6
SR-CH3OH
SR-C2H5OH
D-C3H8
D-CH3OH
D-C2H5OH
SR-C3H8O3
D-C3H8O3
D-CH4
SR-CH4
CH4 Selectivity (%)
Temperature (K)
0
20
40
60
80
100
400
600
800
1000
1200
1400
1600

c)

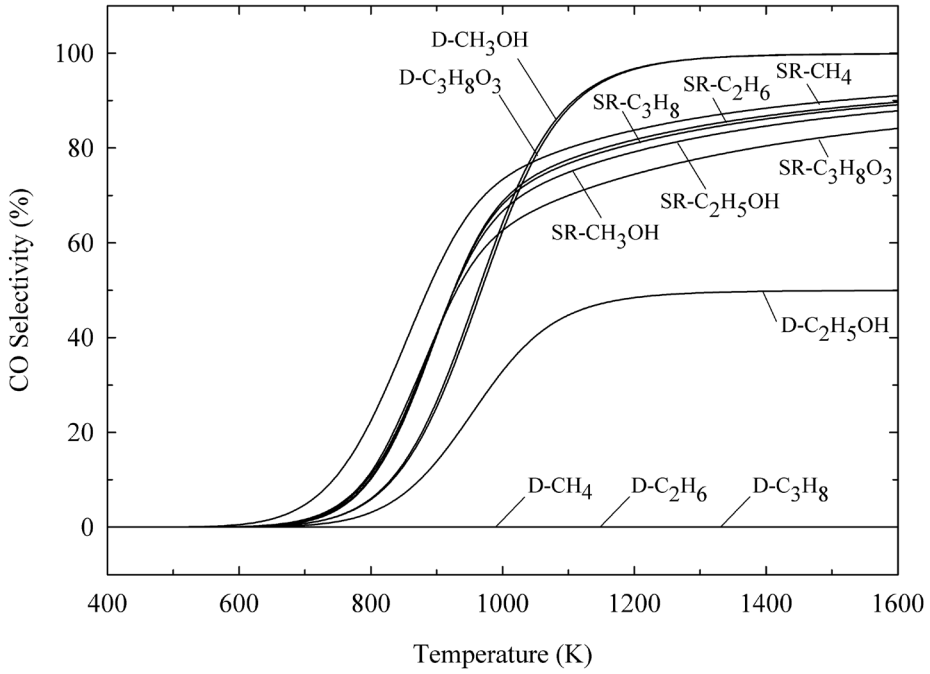

d)

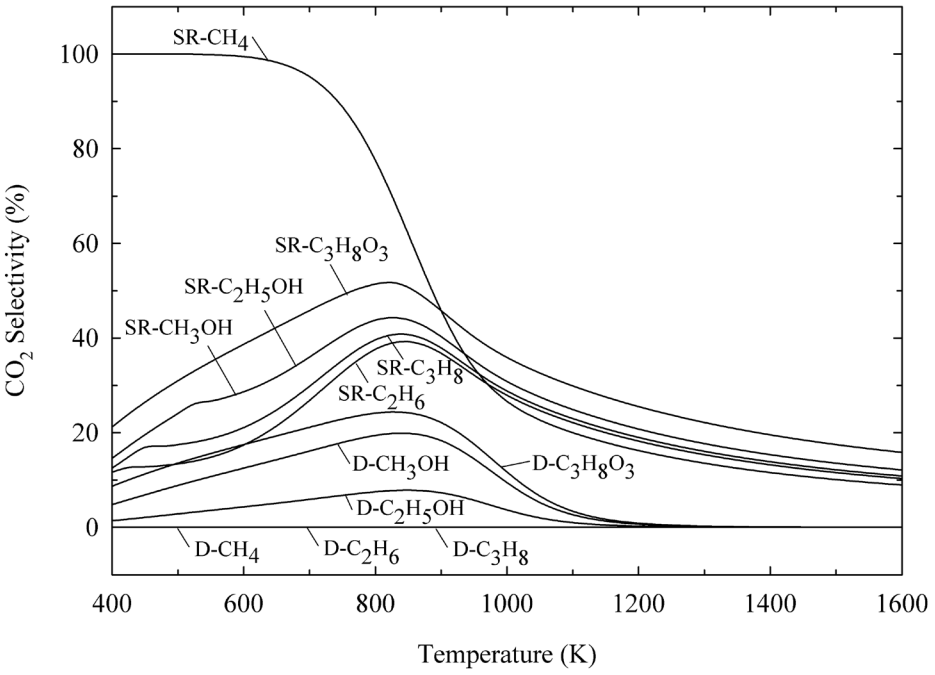

Figure 5.2 The selectivities of product (a) H_2 and by-products of (b) CH_4, (c) CO and (d) CO_2 obtained from the decomposition and the steam reforming processes.

It is noted that the hydrogen selectivity from the steam reforming of other hydrocarbon feeds is higher than those obtained from the decomposition process. It was reasonably suggested that the steam reforming accompanied with WGS can produce more hydrogen, whereas the decomposition generally obtains high solid carbon and consequently reduces the hydrogen production via the reverse methane cracking [reverse of reaction (2-1)]. It is also noted that no significant difference in hydrogen selectivity of steam reforming is observed whereas those of the decomposition of light hydrocarbons are higher than alcohols. As seen in reactions (2-2) and (2-3), light hydrocarbon cracking typically generates hydrogen and solid carbon. The hydrogen produced could be further consumed in reverse methane cracking leading to less hydrogen remained. However, CO, CH_4, CO_2 and carbon, by-products, can be occurred in the decomposition of alcohol as shown in reactions (2-4)-(2-7). These by-products can be reacted with hydrogen by various side reactions such as reverse methane cracking, methanation [reverse of reaction (2-8)], and reverse gasification. As a result, hydrogen remained from decomposition of alcohol was less than those remained from decomposition of light hydrocarbon, leading to less hydrogen selectivity. In addition, D-$C_3H_8O_3$ gave the lowest hydrogen selectivity among all systems studied. This phenomenon can be explained as glycerol could be thermally cracked into high ratio of CO/H_2 [reaction (2-7)] comparing to ethanol and methanol. This high CO/H_2 ratio can enhance either methanation by reverse of reaction (2-8) or reverse gasification of C to CO [reaction (2-16)], leading to high water content.

For the by-products selectivity, based on C atom balance, the possible by-products such as CH_4, CO, CO_2, and solid carbon were taken into account. The methane selectivity [Figure 5.2(b)] was high at low temperature and gradually decreased until approaching to zero at temperature approximately 1500 K. By considering the equilibrium constant, methane was easily formed at low temperature by reverse methane cracking or methanation and was decomposed or reformed with steam at higher temperature.

In Figure 5.2(c) is presented the selectivity of CO as a function of temperature. It was observed that CO selectivity increases when temperature is elevated. At low temperature, CO could be entirely consumed via the related reactions, including WGS, Boudouard reaction and reverse gasification. At high temperature, the reverse of those reactions evidently occurred, resulting in higher concentration of CO and CO selectivity. In addition, as a result of WGS and Boudouard reaction, CO_2 generation gradually increased at low temperature until around 800-900 K and then declined at higher temperature by the reverse of those reactions as displayed in Figure 5.2(d) in term of CO_2 selectivity.

Regarding the solid product in term of carbon yield (Figure 5.3), at low temperature, the solid carbon could be obviously formed with help of the related CO reactions. In case of no CO produced in the system, carbon formation could obtain from light hydrocarbon cracking and it still tended to increase at higher temperature. According to the decomposition reactions, the sequence of carbon yield value from D-light hydrocarbon was in the order of D-C_3H_8 > D-C_2H_6 > D-CH_4. However, D-alcohol exhibited higher carbon yield at low temperature compared to D-light hydrocarbon as higher CO was formed and high ratio of CO/H_2 was observed, resulting in the production of carbon according to the Boudouard reaction. The highest CO intermediate generation was achieved from D-$C_3H_8O_3$, resulting in obtaining the highest carbon formation. At a certain value of C and H atoms in primary fuel, carbon obtained from D-alcohols was higher than those obtained from D-light hydrocarbon depending on the routes of carbon formation. As considered the equilibrium constant, Boudouard reaction occurred in D-alcohols was preferred to form carbon rather than D-light hydrocarbon. Although CO was also occurred from the steam reforming process, it showed lower carbon yield than the decomposition one. Due to high amount of water acting as a diluent in the steam reforming system, it could reduce the concentration of CO intermediate, leading to suppressing the carbon formation. In addition, it was found that SR-alcohols could obtain higher carbon formation compared to SR-light hydrocarbons. It was reasonably pointed out that the O atom in alcohol can play an important role in forming a number of CO that further

obtains high carbon deposition. Like D-$C_3H_8O_3$, glycerol still provided the highest carbon yield among the steam reforming systems.

Considering the processes at high temperature, 100% of carbon yield could be achieved in case of light hydrocarbon fuel because the decomposition reaction of light hydrocarbon was completed. For the systems with the presence of CO_2 and H_2O, no carbon was observed at high temperature because it could react via the reverse of reactions (2-15)-(2-17). However, it was found that high carbon is produced from D-C_2H_5OH at high temperature. This was presumably due to methane produced as a major by-product and it was further decomposed to carbon at high temperature.

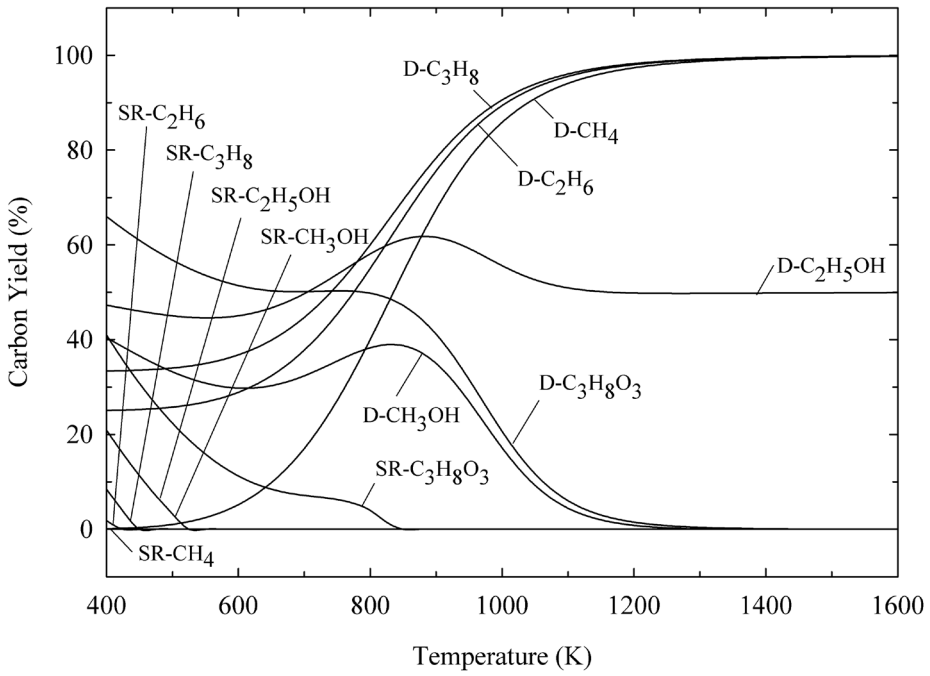

Figure 5.3 The percentage of carbon yield obtained from the decomposition and the steam reforming processes.

Based on C atom balance, the selectivities of by-products (CH_4, CO and CO_2) and carbon yield were related to one another. At low temperature, gaseous methane and solid carbon were generated from D-C_2H_6 and D-C_3H_8. The CH_4 selectivity from D-C_3H_8 was less than from D-C_2H_6 whereas the former gave higher carbon formation.

Among D-alcohols, glycerol was decomposed to gain highest carbon and CO_2 selectivity. This was due to high CO/H_2 ratio enhances Boudouard reactions rather than methanation. For SR-CH_4, no carbon was occurred over the range of temperature studied and CO selectivity was around zero at low temperature due to shifting CO by WGS to produce CO_2 gaining high CO_2 selectivity (around 100%). Considering SR-C_2H_6, SR-C_3H_8 and SR-alcohols, it showed the similar trend as D-alcohols that these systems mainly produced CH_4, CO, CO_2 and carbon as by-products. Excluding SR-CH_4, SR-alcohols could gain higher CO_2 selectivity than those of SR-light hydrocarbon. The alcohol with higher O atom in steam reforming system resulted in a lower amount of CO but higher CO_2 formation. The CO_2 selectivities of D-alcohols were less than SR-alcohols systems because larger amount of CO_2 produced by WGS from steam reforming process compared to Boudouard reaction from decomposition process. In these systems, CO was an important intermediate to convert into carbon, CO_2, and CH_4 selectivity. Moreover, SR-CH_3OH exhibited the same profiles of by-products selectivities as those profiles from SR-C_2H_5OH. It was revealed that the ratios of CO/H_2 from both processes are equal, causing no difference in carbon, CO_2, and CH_4 production.

At high temperature, complete reaction of light hydrocarbon decomposition was occurred and no methane was remained. Considering D-alcohols, CO selectivity relied on reaction approach of each alcohol as summarized in reactions (2-4), (2-7) and (5-1).

Ethanol decomposition:

$$C_2H_5OH \rightleftharpoons C + CO + 3H_2 \qquad \Delta H^0 = 124.8 \text{ kJ mol}^{-1} \qquad (5\text{-}1)$$

It was noticed that CO selectivities from D-CH_3OH and D-$C_3H_8O_3$ almost reaches 100% whereas the value from D-C_2H_5OH approaches ca. 50%. This behavior was due to ethanol could decompose into by-products, carbon and CO equally in D-C_2H_5OH whereas only CO was formed in D-CH_3OH and D-$C_3H_8O_3$. For CH_4 and CO_2, the selectivity values were around zero because both by-products could be entirely consumed to other products. Methane was typically decomposed into carbon

and hydrogen, while CO_2 was generally consumed to form CO by RWGS [reverse water gas shift, reverse of reaction (2-18)] and Boudouard reaction at high temperature. In case of steam reforming, no carbon and CH_4 selectivity were observed for all primary fuels. The CO_2 selectivity was dependent on ratio of CO/H_2. Regarding CO_2 selectivity, SR-CH_4 and SR-$C_3H_8O_3$ showed the lowest and the highest values, respectively, and the opposite tendency was found in CO selectivity.

5.1.2 Energy Self-Sustained Systems

Owing to the endothermic reaction of the steam reforming and decomposition systems, it requires the external heat source to operate these systems. However, the systems under thermally self-sustained condition should be carried out to be fair comparison of reaction performances between the decomposition and the steam reforming. To operate these systems under energy self-sustained condition as shown the system configurations in Figure 5.4, it could be achieved from the aid of the combustion of a portion of primary fuel [Figure 5.4(a)] or product stream [Figure 5.4(b)]. As considered these operations, a portion of primary fuel or product stream was introduced to a burner to generate heat (Q_c) for supplying to the reactor until the heat requirement of reactor (Q_r) is reached, resulting in zero net heat of the system ($Q_{net} = Q_r + Q_c = 0$). The complete combustion in the burner and the exhausted gases from the burner at exit temperature of 373 K were assumed. For the heat generation at the burner, it could be determined from the difference in enthalpy or heat of formation between its outlet and inlet as presented in the equation below.

$$Q_c = \sum_i n_{i,out} H_{i,out} - \sum_i n_{i,in} H_{i,in} \quad (5\text{-}2)$$

In addition, the determination of feed fraction to reactor (f_d) and gas product fraction (g_d) under energy self-sustained operation was proposed in APPENDIX B.

a)

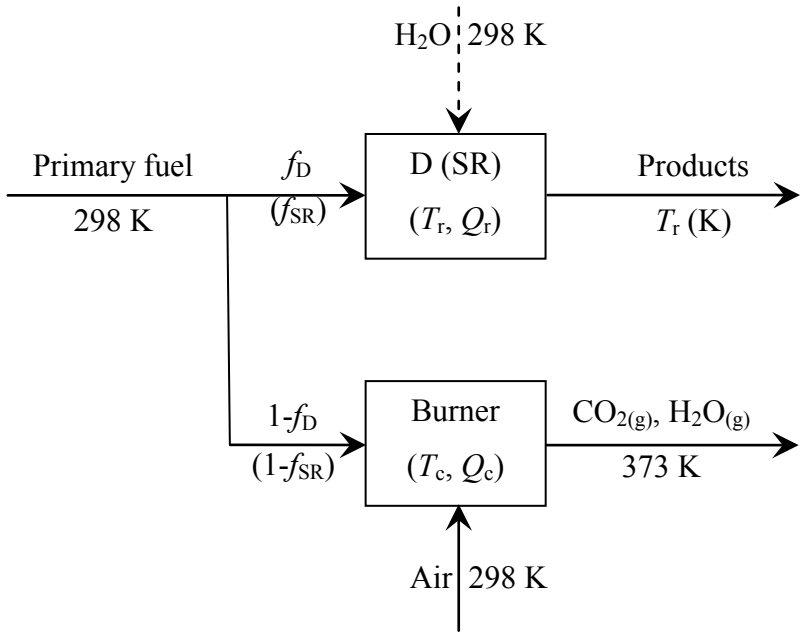

b)

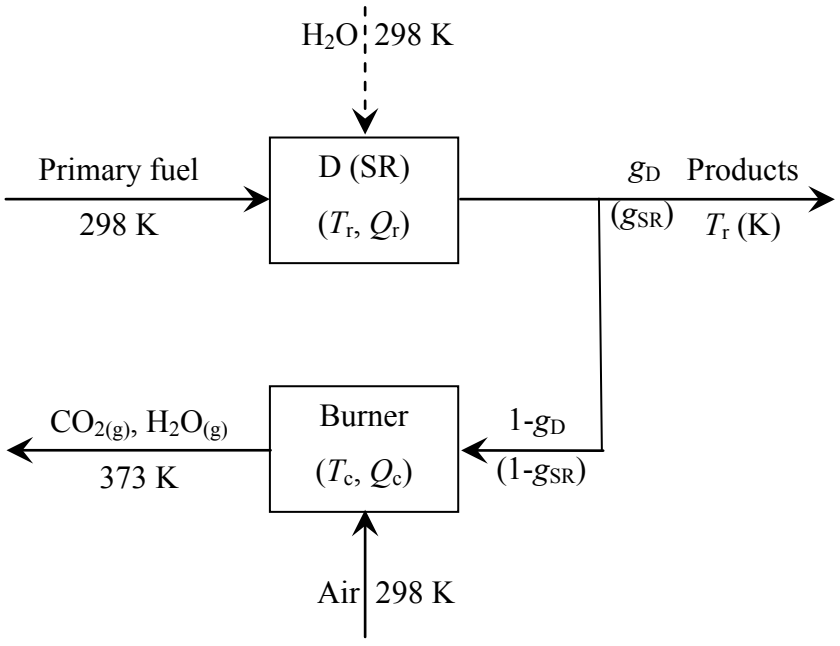

Figure 5.4 The system configurations under energy self-sustained operation of the decomposition and the steam reforming in case of (a) splitting primary fuel and (b) splitting gas product stream.

In order to study the decomposition and steam reforming under thermally self-sustained condition, it was firstly necessary to concentrate on the heat requirement of each system as illustrated in Figure 5.5. Typically, the main reactions of decomposition and steam reforming were endothermic reaction. It was apparently revealed that the steam reforming systems are higher endothermic reaction. Since the requirement of water for steam reforming system, heat of vaporization should be taken into account. Higher water supplied to the system caused higher in heat of system as obviously seen in SR-C_3H_8. Therefore, heat requirement of the steam reforming system mainly relied on the amount of water fed into the system. Regarding the decomposition system, heat requirement of D-$C_3H_8O_3$ was the highest at high temperature among all decomposition processes due to largely high enthalpy of glycerol compared to those of other primary fuels. However, it was found that the system can operate under exothermic reaction at low temperature because the possible exothermic side reactions such as reverse methane cracking, methanation, Boudouard reaction, and reverse gasification can take place even the endothermic of main reaction is involved.

Under the energy self-sustained condition, the systems of hydrogen production could be performed as illustrated the operation modes in Figures 5.4 (a) and (b). In order to control the net heat of each system, the change in feed fraction to the burner (1-f_D or 1-f_{SR}) or gas product fraction to the burner (1-g_D or 1-g_{SR}) was observed that depends upon the reaction temperature. Owing to the heat of reaction as shown in Figure 5.5, the values of feed and product fraction as shown in Figures 5.6 and 5.7, respectively, tended to decrease when the system was conducted at higher operating temperature. The f_D values of every primary fuel was greater than the f_{SR} because of greatly higher in heat requirement for steam reforming. Due to no heat required for exothermic system at low temperature, it was not necessary to separate the primary fuel to the burner; hence, f_D of each primary fuel was equal to 1. In addition, the tendency of gas product fraction profiles was also found to be similar to that of feed fraction to reactor ones. It could be presumed that the thermally self-sustained operations affect not only feed fraction of each primary fuel to the reactor or product fraction, but also the reaction performances.

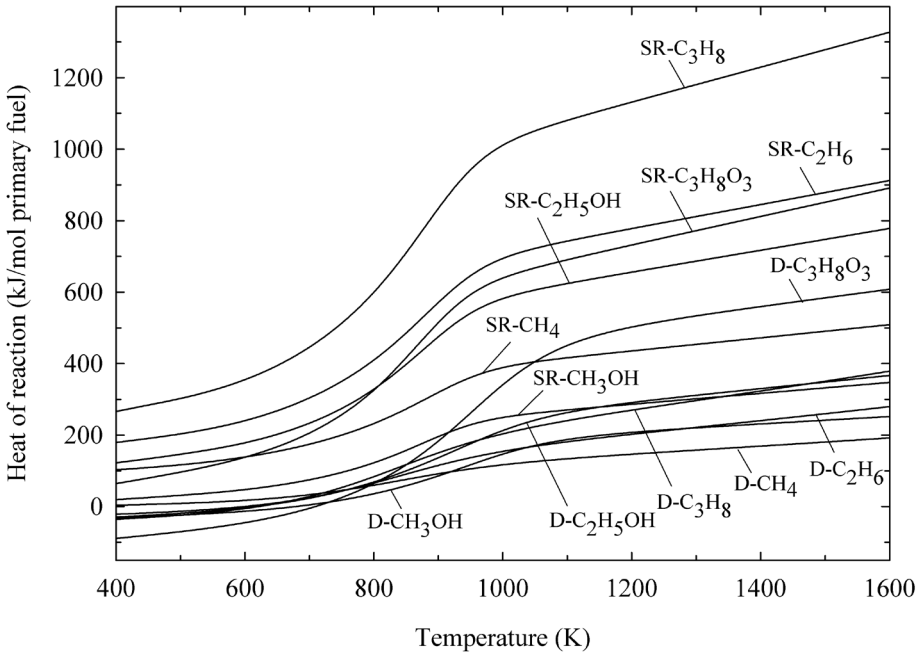

Figure 5.5 The heat requirement of the decomposition and the steam reforming processes.

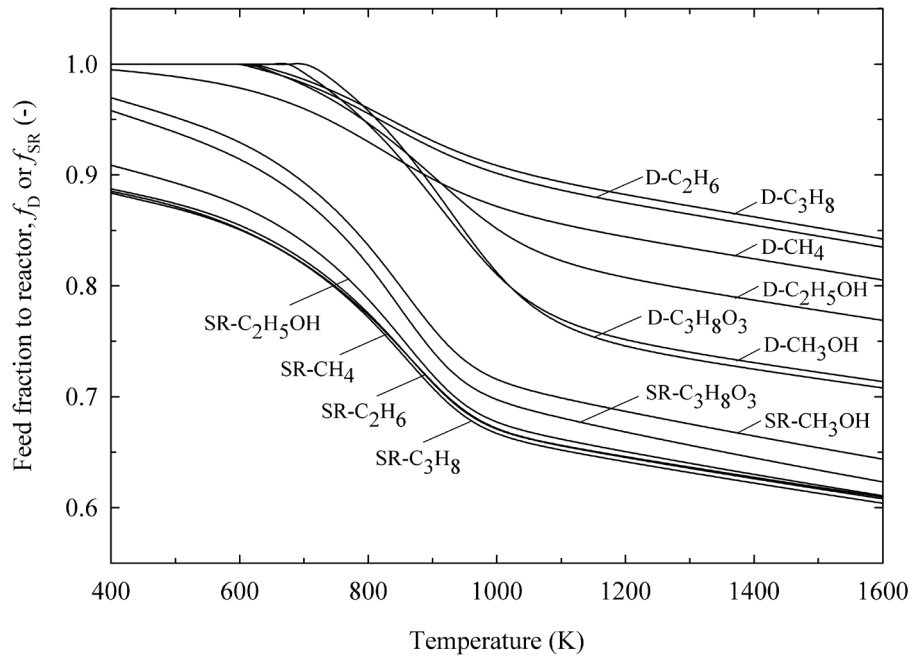

Figure 5.6 The feed fraction to reactor obtained from the decomposition and the steam reforming processes under energy self-sustained condition.

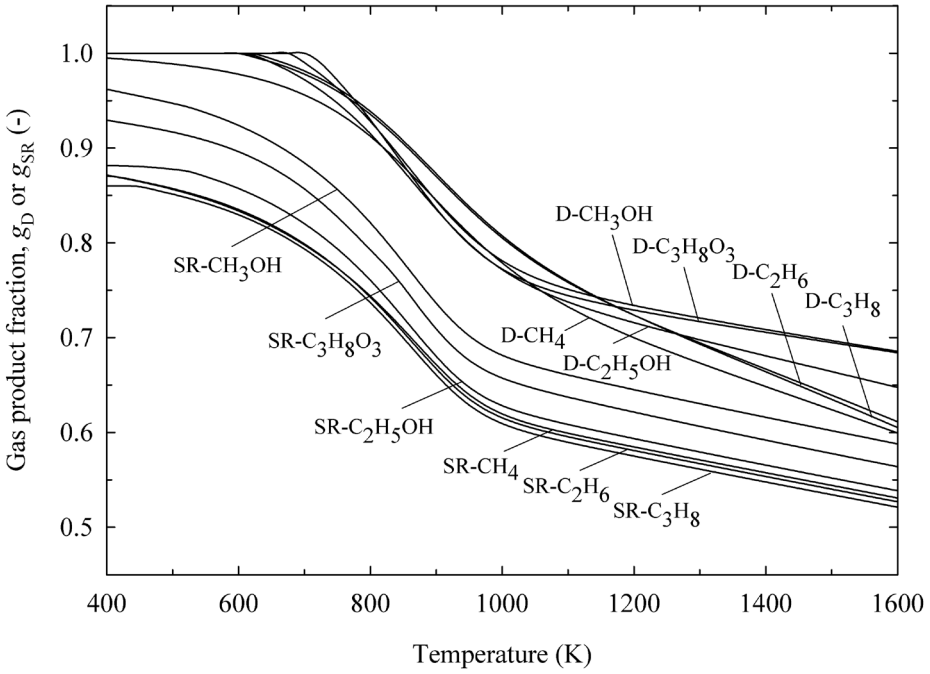

Figure 5.7 The gas product fraction obtained from the decomposition and the steam reforming processes under energy self-sustained condition.

The major reaction performances obtained from the systems under the thermally self-sustained operations such as hydrogen production, purity of hydrogen, mole fraction of CO in product stream and carbon yield were also investigated in this work. The simulation results are illustrated in Figures 5.8-5.12. It was revealed that the differences in hydrogen production (Figure 5.8), hydrogen yield (Figure 5.9) and carbon yield (Figure 5.12) can be reasonably appeared between splitting feed and gas product but the hydrogen purity and CO fraction in both cases are similar (Figures 5.10 and 5.11). As seen in Figure 5.8, it is clearly indicated that high hydrogen produced can be obtained from splitting feed for each primary fuel. The SR-C_3H_8 gave the highest hydrogen production at temperature ca. 1050 K. Below this temperature, WGS played an important role in increasing the hydrogen generation. However, RWGS could be easily taken place at high temperature, hence more hydrogen was consumed by this reaction. Therefore, the hydrogen produced was decreased beyond the maximum point. Similar profiles of hydrogen production were

found in the steam reforming fed by other primary fuels. The decrement in hydrogen production profiles corresponded to lower in stoichiometric coefficient of hydrogen in their overall steam reforming of primary fuels. Nonetheless, SR-C_2H_6 and SR-$C_3H_8O_3$ should be achieved the similar maximum mole of hydrogen of 7, the hydrogen produced of the former showed higher profile than the latter. It was probably suggested that higher concentration of CO_2 in the latter causes higher hydrogen reduction by consuming via RWGS. As considered the decomposition systems, the tendency of hydrogen production related to their reaction approaches [reactions (2-1)-(2-4), (2-7), and (5-1)] at high temperature. At similar C and H atoms in primary fuel such as CH_4 and CH_3OH etc., it should be gained the mole of hydrogen produced identically at high temperature but D-light hydrocarbon produced hydrogen higher than D-alcohol over the temperature range studied. Hydrogen was obtained from thermal cracking and could further consumed by reverse methane cracking in D-light hydrocarbon but lower amount of hydrogen remained in D-alcohol due to higher hydrogen consumption by the reaction of CO by-product such as methanation, reverse gasification and reverse methane cracking. Therefore, CO was a major factor affected lesser hydrogen production for D-alcohol. However, the feed fraction to reactor also influenced hydrogen production. It was apparently revealed that D-light hydrocarbon exhibit significantly higher f_D value compared to D-alcohol. In case of splitting gas product, it was found that the hydrogen produced was less than the case of splitting feed for all D- and SR-reactant feed. In addition, the difference in hydrogen production was more pronounced from the system fed by primary fuel with containing higher C atom. The decrement in hydrogen produced was observed and it further decreased at high temperature because of the reduction in gas product fraction (Figure 5.7). However, concerning primary fuels with the same C and H atoms, the hydrogen gained did not follow the tendency of splitting feed case, especially at high temperature. The hydrogen produced from D-alcohol was higher than that from D-light hydrocarbon due to higher $g_{D.}$ In case of the steam reforming, the profiles of splitting feed were similar to that of splitting gas product, of which SR-light hydrocarbons gave higher H_2 yield than that of SR-alcohols for similar C and H atoms.

a)

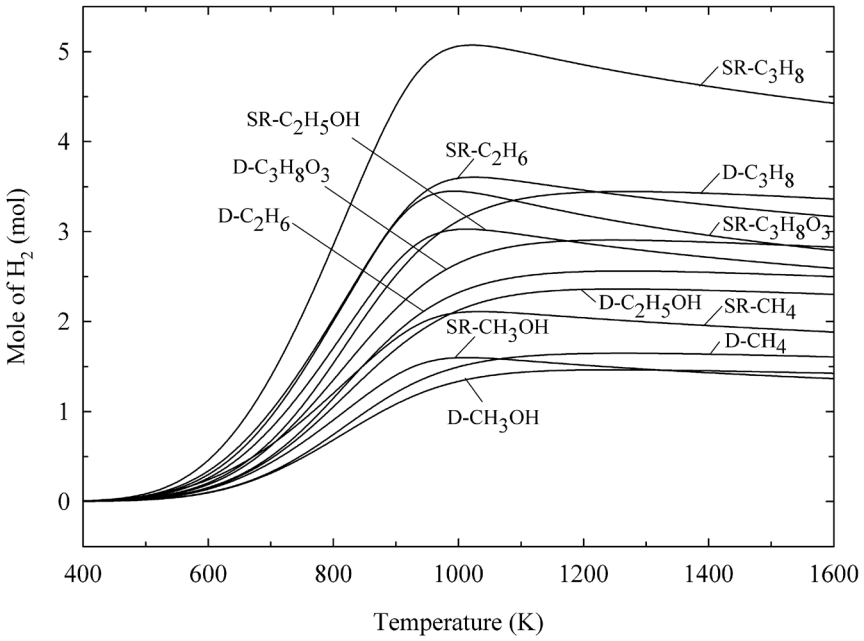

b)

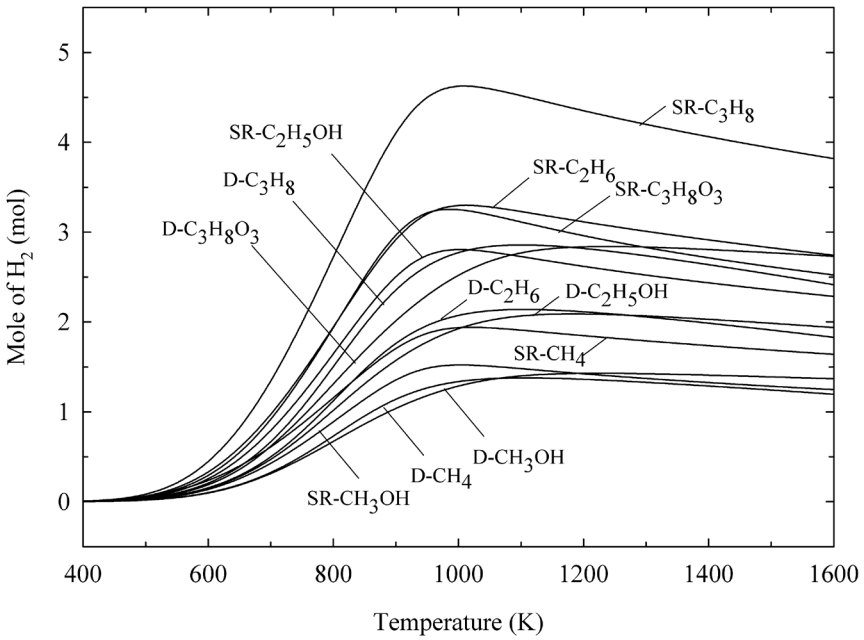

Figure 5.8 The amount of H_2 produced obtained from the decomposition and the steam reforming processes under energy self-sustained condition in case of (a) splitting primary fuel and (b) splitting gas product stream.

According to hydrogen yield in case of splitting primary fuel as shown in Figure 5.9(a), it was found that the decomposition can obtain hydrogen yield higher than the steam reforming as obviously seen at high temperature. The sequence of hydrogen yield values corresponded to the feed fraction to reactor values. In addition, the decrease in hydrogen yield was likely affected by the increase in ratio of amount of hydrogen consumed by side reactions to amount of H atom in feed. The side reactions in D-alcohols mostly related to CO by-product reactions that were more significant than those in D-light hydrocarbons, resulting in less hydrogen yield. Regarding the steam reforming systems at high temperature, RWGS played an important role in lowering the hydrogen yield. Moreover, SR-light hydrocarbon exhibited higher hydrogen yield than SR-alcohol in consequence of lower value of hydrogen consumption per H atom in feed via RWGS. The hydrogen yield profiles in Figure 5.9(b) were lower compared to the splitting feed case. As apparently seen at high temperature, the decomposition systems gave hydrogen yield more than the steam reforming ones. Like the result of hydrogen production, among the decomposition processes, D-alcohol exhibited higher hydrogen yield, compared to D-light hydrocarbon. However, the hydrogen yield was certainly dependent on the gas product fraction. Concerning the steam reforming systems, the hydrogen yield presumably relied on the hydrogen consumed by RWGS per H atom in feed. The highest hydrogen yield from SR-CH_3OH among the steam reforming processes could be achieved by having the highest gas product fraction. In addition, the hydrogen yields from D-CH_3OH and D-$C_3H_8O_3$ in case of splitting gas product stream were not different from those in case of splitting feed.

a)

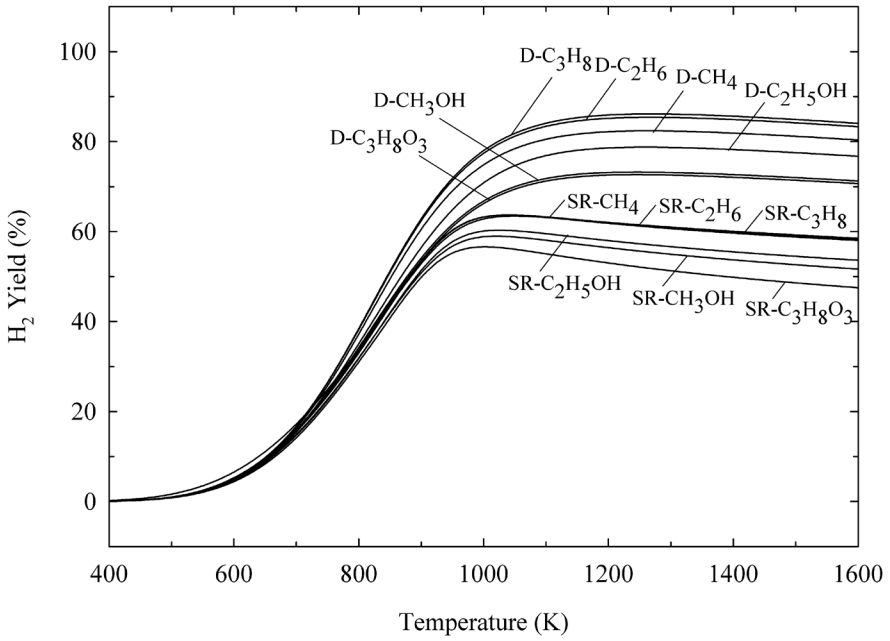

b)

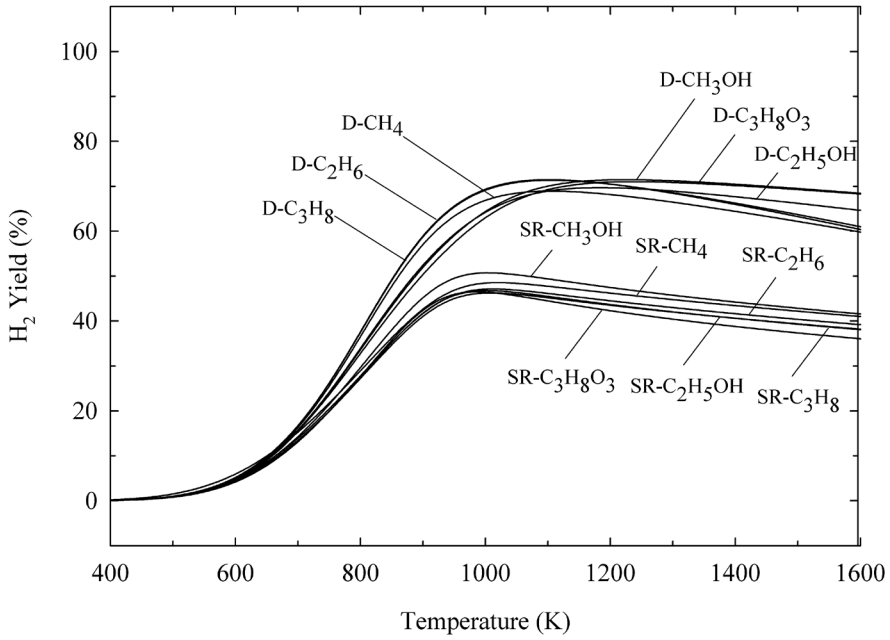

Figure 5.9 The percentage of H_2 yield obtained from the decomposition and the steam reforming processes under energy self-sustained condition in case of (a) splitting primary fuel and (b) splitting gas product stream.

For purity of hydrogen, the results are displayed in Figure 5.10. Owing to the absence of any gaseous by-products in the decomposition of light hydrocarbon, the purified hydrogen (100%) could be achieved at high temperature. Since requirement of water in steam reforming, the steam reforming of each primary fuel could obtain less hydrogen purity than the decomposition one. Various by-products were formed in D-alcohol compared to D-light hydrocarbon, leading to lower hydrogen purity. Among D-alcohols, the highest purity of hydrogen could be gained from D-C_2H_5OH. Furthermore, the hydrogen purity from decomposition of each primary fuel related to concentration of hydrogen in product stream based on the complete reaction of each system at high temperature. It was disclosed that the hydrogen purity from D-$C_3H_8O_3$ was less than SR-light hydrocarbon. Generally, amount of by-products of CO and CO_2 greatly occurred from D-$C_3H_8O_3$ and SR-light hydrocarbon. However, glycerol might be decomposed into higher concentration of by-products due to containing high O atom in this primary fuel.

In Figure 5.11 is demonstrated the mole fraction of CO as a function of temperature. The decomposition of alcohol showed high level of CO concentration and the highest CO fraction was obtained from D-$C_3H_8O_3$. It was indicated that the fraction of CO from all systems followed the ratio of CO/H_2 in each reaction approach. In case of D-alcohols, CO fraction increased with increasing temperature until the value is constant at temperature around 1200 K, whereas the CO fraction keep increasing as a function of temperature over the range of study in the steam reforming process (both alcohols and light hydrocarbons). This was probably due to the occurrence of RWGS in the steam reforming systems at high temperature. In the steam reforming, SR-alcohol gave higher CO concentration than SR-light hydrocarbon. This result was probably due to lower hydrogen content obtained in case of SR-alcohol as depicted in Figure 5.10. At high temperature, CO and H_2O fractions were similar accompanied with less portion of CO_2. Therefore, the fractions of H_2 and CO reasonably related to each other. Among the steam reforming processes, it was found that SR-$C_3H_8O_3$ exhibits the highest CO fraction since the highest CO produced and the lowest H_2 content.

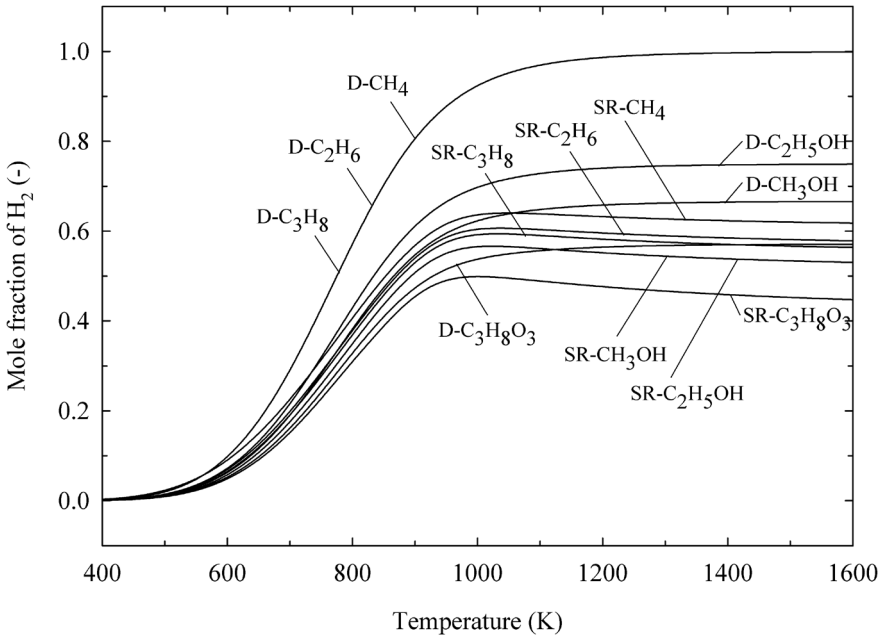

Figure 5.10 The H_2 fraction obtained from the decomposition and the steam reforming processes under energy self-sustained condition.

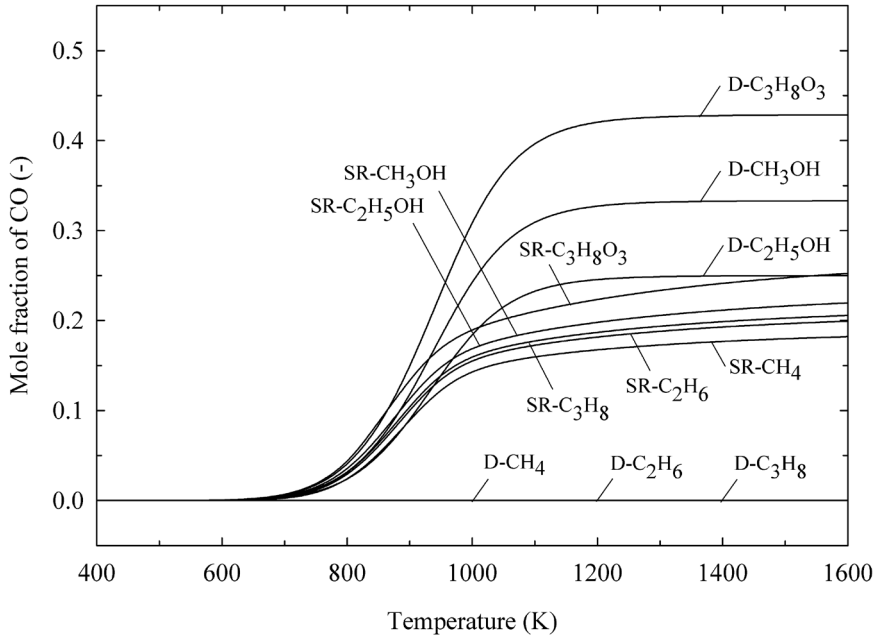

Figure 5.11 The CO fraction obtained from the decomposition and the steam reforming processes under energy self-sustained condition.

Lastly, the carbon yields of all systems are illustrated in Figure 5.12. The profiles in case of splitting gas product stream were displayed in Figure 5.3 and already discussed in previous section (where f_D or f_{SR} equal to 1). Compared between splitting feed and splitting gas product stream, the carbon yields in case of splitting feed were found to be lower than those of splitting gas product as particularly seen in the decomposition processes at high temperature. For instance, the maximum carbon yield values of D-light hydrocarbon reduced from 100% to around 80%. The decrease in the carbon yield obtained from each system resulted from the change in feed fraction value. Moreover, the value of carbon yield tended to gradually decrease at high temperature as a result of the reduction in f_D values. In the case of the steam reforming processes, splitting feed gave slightly lower carbon yield than that of splitting gas product.

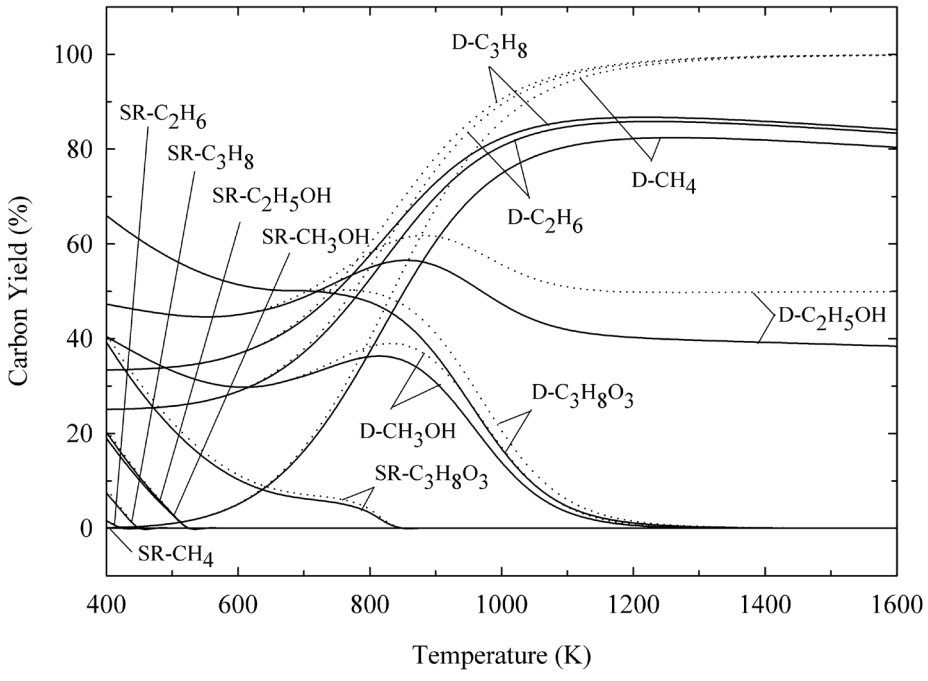

Figure 5.12 The percentage of carbon yield obtained from the decomposition and the steam reforming processes under energy self-sustained condition (solid line – case of splitting primary fuel, dotted line – case of splitting gas product stream).

However, the steam reforming as widely used in many industries was typically processed by using an excess of steam to prevent carbon formation on the catalyst. The requirement of steam in order to avoid the presence of coke should be higher than the minimum ratio of steam to carbon atom of primary fuel (*S/C*). The results from this work were revealed that those minimum ratios are 1.6, 2.1, 2.5, 2.0, 2.5, and 2.6 for the steam reforming of methane, ethane, propane, methanol, ethanol, and glycerol, respectively. It was clearly seen that the value of *S/C* for SR-CH_4 (*S/C* = 2) is in the range of no carbon formation whereas those values for the steam reforming of other primary fuels are lower than the boundary of minimum ratio, resulting in forming the carbon especially at low temperature. In the case of SR-C_2H_6 and SR-C_3H_8 at low temperature, these primary fuels preferred to be converted to lighter hydrocarbon, H_2, and carbon rather than were reacted via the steam reforming reaction as a result of higher value of the equilibrium constant. However, methane was then produced by the reverse of methane cracking. The methane steam reforming accompanied with WGS was occurred to produce CO and CO_2 as by-products. In addition, CO was an intermediate by-product to generate carbon via Boudouard reaction and reverse gasification of C to CO. For SR-alcohols, alcohols could be converted to H_2 and CO via both cracking and steam reforming reactions. Higher CO intermediate presented at low temperature, compared to SR- light hydrocarbon systems, could be further reacted by WGS, methanation, Boudouard reaction, and reverse gasification of C to CO and was eventually formed the carbon. With the excess of steam in the range of no carbon formation, the combination of the steam reforming reaction and WGS was mainly performed in the steam reforming of all primary fuels and the related reactions of carbon formation could be suppressed.

Regarding the steam reforming systems with the excess of steam that was lower and higher than the minimum ratio of steam to carbon atom of primary fuel, higher steam fed to the reactor generally caused higher heat requirement of the system. In order to provide more heat, higher amount of fuel had to be supplied to the burner; hence, the feed fraction to reactor and gas product fraction were decreased when *S/C* increased. Although the increase in hydrogen production in term of mole of hydrogen produced for the systems with spitting feed or gas product was observed at

higher value of *S/C*, mole fractions of H_2 and CO were found to be lower due to higher content of water. In addition, the reduction in carbon yield was found at higher S/C and the disappearance of carbon could be noticed when *S/C* was higher than the minimum value as mentioned above.

5.1.3 Selection of Suitable Primary Fuel of Hydrogen Production for Fuel Cell

The appropriate system for different fuel cell grades is dependent on the limitation of each fuel cell type. For low temperature fuel cell (PEMFC), CO concentration was restricted to be lower than 10 ppm. However, CO was useful in case of high temperature fuel cell (SOFC) because it could be used as another fuel besides hydrogen. In general, hydrogen purity and hydrogen production were firstly considered in this determination. Nevertheless, the carbon capture in term of carbon yield was also taken into account. Under the environmental concern, the solid carbon by-product, acting as energy storage, could reasonably reduce the CO_2 emission.

Regarding PEMFC based on the CO limitation, the system had to be operated at low temperature to minimize the CO concentration, as shown in Figure 5.11 but the hydrogen production and hydrogen purity were very low. However, the absence of CO was appeared in D-light hydrocarbon processes. Therefore, D-light hydrocarbon systems at high temperature were the promising choices. It was revealed that the systems in case of splitting feed exhibit higher in hydrogen production but lower in carbon yield compared to the systems in case of splitting gas product. Based on maximum hydrogen production, the suitable process among D-light hydrocarbon processes was D-C_3H_8 with splitting feed that should be operated at ca. 1275 K. This process could gain the hydrogen purity up to 99% with impurity of methane and the carbon yield around 87%. Considering the carbon capture and CO_2 emission, D-light hydrocarbon in case of splitting gas product was preferred to produce the feedstock for PEMFC even obtaining lower hydrogen production, compared to that in case of splitting feed. The CO_2 emission from the burner was generated from oxidation of

carbon-containing reactant such as light hydrocarbons and alcohols from primary fuels, and by-products i.e. CH_4 and CO from the reactor. However, for D-light hydrocarbon at high temperature, lower CO_2 emission from the burner was found in case of splitting gas product. It was revealed that methane by-product in case of splitting gas product is fed to the burner lower than light hydrocarbon (on carbon atom basis) in case of splitting primary fuel. In addition, the decomposition of light hydrocarbon systems with splitting gas product should be carried out at ca. 1100 K to obtain the maximum value of hydrogen production. At this temperature, 97% of hydrogen purity with methane as impurity and 97% of carbon yield could be obtained. Among D-light hydrocarbons, ethane and propane could achieve higher hydrogen production, compared to methane. However, ethane and propane has been widely used for producing higher product value, but methane is available and often used as heating source. Hence, methane was possibly suggested to be employed in the decomposition process for supplying to PEMFC. Nonetheless, the product stream from D-alcohol and the steam reforming systems could also be fed to PEMFC after reducing the CO concentration by water gas shift and preferential oxidation reactors.

For high temperature fuel cell such as SOFC, no limitation of CO fraction was involved. In this case, H_2 and CO can be used as fuel source, whereas CH_4, CO_2, and H_2O were diluent. Therefore, D-light hydrocarbon with high hydrogen purity and D-alcohol with major products of H_2 and CO were preferred to match SOFC. Like the PEMFC case, since the criteria of carbon capture and CO_2 emission were concerned, the decomposition processes in case of splitting gas product were reasonably selected. For D-light hydrocarbons, it should be operated at ca. 1100 K as mentioned above. In the case of D-alcohol, the operating temperature of this system should be around 1175 K to achieve the highest hydrogen production, D-C_2H_5OH could obtain the highest values of the ratio of H_2/CO, hydrogen purity, and carbon yield. The hydrogen purity of 74% and CO 24% content were obtained from this system with 2% impurity of CH_4, CO_2 and H_2O. Moreover, in case of splitting gas product, D-alcohol gave higher CO_2 emission from the burner than D-light hydrocarbon as a result of higher CO generation. However, D-CH_3OH and D-$C_3H_8O_3$ with lower ratio of H_2/CO were also possible to carry out at operating temperature of ca. 1225 K. Under the criteria of the

highest hydrogen production, D-C_3H_8 in case of splitting primary fuel was preferable among the decomposition systems. Compared to the decomposition systems, the product stream from the steam reforming systems could be also applied to SOFC but lower power density of fuel cell would be achieved, relying on the criteria. Nevertheless, hydrogen production from the steam reforming process could be improved by additionally conventional processes such as shift reactor and preferential oxidation reactor.

Practically, the steam reforming gives higher hydrogen production than the decomposition, but the former is more complicate. The vaporizer should be equipped with the steam reforming reactor to heat up the water supply to the system. Moreover, it is necessary to operate with larger volume of reactor due to additional water. For example, SR-C_3H_8 gives the highest mole of hydrogen produced but it requires larger amount of water 6 times of propane. In addition, higher cost should be appeared due to more complexity of the process. For the decomposition process, no vaporizer is required and the reactor is smaller compared to the steam reforming even obtaining lower hydrogen production. Furthermore, the steam reforming requires other reactors to reduce the CO concentration and to enhance the hydrogen production for applying to fuel cell whereas it is not necessary for the decomposition system at high temperature. Moreover, no carbon capture is observed from the steam reforming at high temperature but it is apparently obtained via the decomposition. In conclusion, the decomposition process was preferable to be compatible with various kinds of fuel cells such as PEMFC and SOFC.

5.2 Study of Decomposition System Fed by Biogas

According to the previous section, it was disclosed that the decomposition system is the promising choice under the environmental criteria, although less hydrogen production is obtained comparing to the steam reforming systems. When considering the issues on carbon capture and CO_2 emission, methane decomposition was found to be an attractive process, therefore, it was very useful to further investigate this system in details.

Generally, methane can be gained from various sources such as natural gas and fermentation process. However, the interesting methane source is currently obtained from biogas generated by the fermentation process. Hence, biogas as the methane-containing gas mixture that mainly composes of methane and high concentration of carbon dioxide has been another alternative in order to employ in the decomposition process since it is available and being renewable energy source. In addition, biogas as a primary fuel can be apparently utilized because both methane and carbon dioxide representing as greenhouse gases can be diminished. From the previous report [29], methane content in biogas varies in the range of 40-65%, relying on the source of biogas and the fermentation process.

Pointing out the use of methane-containing gas mixture as a primary fuel, it was revealed that the advantage of the system fed by this kind of feedstock is the enhancement of equilibrium methane conversion as illustrated in Figure 5.13. In this system, methane mixed with nitrogen was fed to the decomposition unit with the study of various mole fraction of methane (y_{CH_4}). It can be confident that only methane cracking is occurred without any side reactions. It was evidently indicated from this figure that the dilution of methane with nitrogen can help improving the equilibrium conversion. From this result, even nitrogen did not react within the methane decomposition system, it could possibly affect the equilibrium content because the nitrogen concentration was included in the calculation of the equilibrium constant. This resulted in the lowered concentration of the reaction product and

eventually the increased equilibrium conversion. Therefore, using biogas as a primary fuel in the decomposition system should also provide higher equilibrium conversion accompanied with the occurrence of many side reactions. The possible reactions related to this system are previously mentioned in Section 2.2.

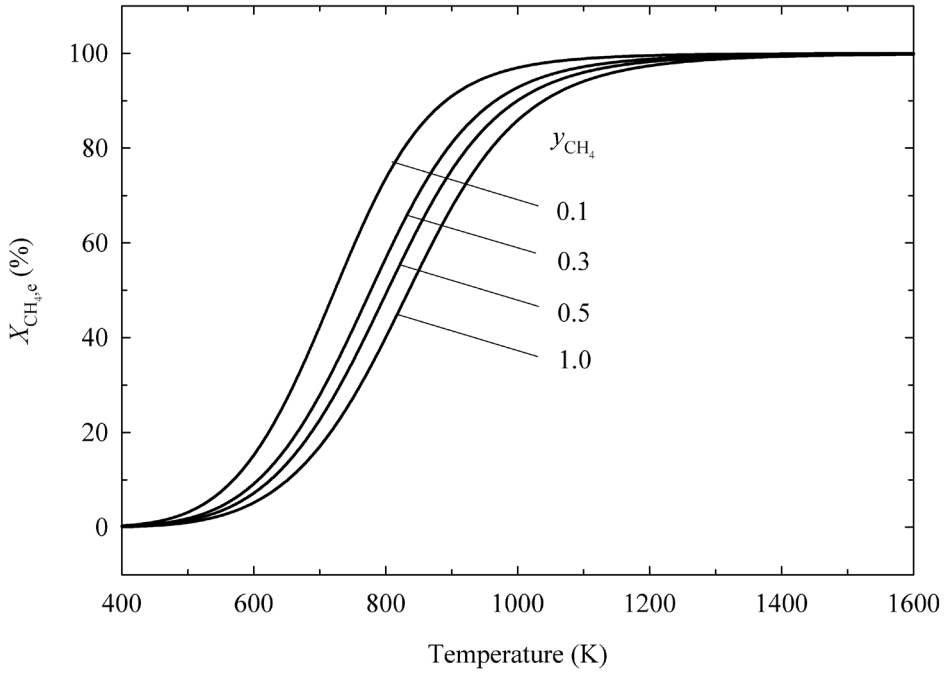

Figure 5.13 The equilibrium conversion of methane obtained from the decomposition process fed by CH_4/N_2 mixture with various mole fraction of methane (y_{CH_4}).

In this research, the investigation of biogas or CH_4/CO_2 mixture being a primary fuel for the decomposition process was carried out. The biogas was firstly assumed to be the mixture at CO_2/CH_4 ratio of 40:60. The reaction products determined by thermodynamic approach are presented in Figure 5.14. Starting with methane and carbon dioxide at 0.6 and 0.4 kmol/s, methane and carbon dioxide are consumed by ca. 57% and 85%, respectively, at the temperature of 400 K. At low temperature, methane and carbon dioxide were consumed by dry reforming reaction to produce carbon monoxide and hydrogen. These products could be further reacted by the side reactions such as Boudoard reaction and reverse gasification of carbon to carbon monoxide or carbon dioxide to form water and the solid carbon as obviously

seen from the highest product generation at low temperature. Although methane was mostly reacted by methane decomposition and dry reforming, it could be generated by carbon monoxide and carbon dioxide methanation. Therefore, methane slightly increased at low temperature due to favorable methanation. The increase in carbon dioxide content was observed at low temperature as well. It inclined to higher content at higher temperature because carbon dioxide was mainly produced from Boudouard reaction. The water gas shift reaction also gave the generation of carbon dioxide but it provided less quantity compared to Boudouard reaction. For the gaseous products of carbon monoxide and hydrogen, the similar trend of product distribution was demonstrated. Carbon monoxide primarily achieved from dry reforming, but it was possibly consumed by Boudouard reaction, reverse gasification of carbon to carbon monoxide, water gas shift reaction and carbon monoxide methanation at low temperature. At high temperature, it was mostly introduced by dry reforming and higher content could be also gained from carbon and steam gasification of carbon to carbon monoxide, reverse of water gas shift reaction and steam methane reforming. For the hydrogen production, it was mainly introduced by dry reforming and methane decomposition, leading to higher concentration at higher temperature. Considering the solid carbon formation, Boudouard reaction, reverse gasification of carbon to carbon monoxide or carbon dioxide, and methane decomposition were taken into account for forming carbon at low temperature and then the reduction in carbon content was displayed at higher temperature. At high temperature, even carbon formation was higher due to the endothermic methane decomposition, the carbon could be progressively converted by the reverse of Boudouard reaction and gasification of carbon to carbon monoxide or carbon dioxide, resulting in lower in the carbon content. The product distribution at high temperature consisted of carbon monoxide, hydrogen and carbon while methane, carbon dioxide and water were entirely consumed. It could be noticed that the product contents at high temperature can be indicated the associated reactions, which are dry reforming and methane decomposition.

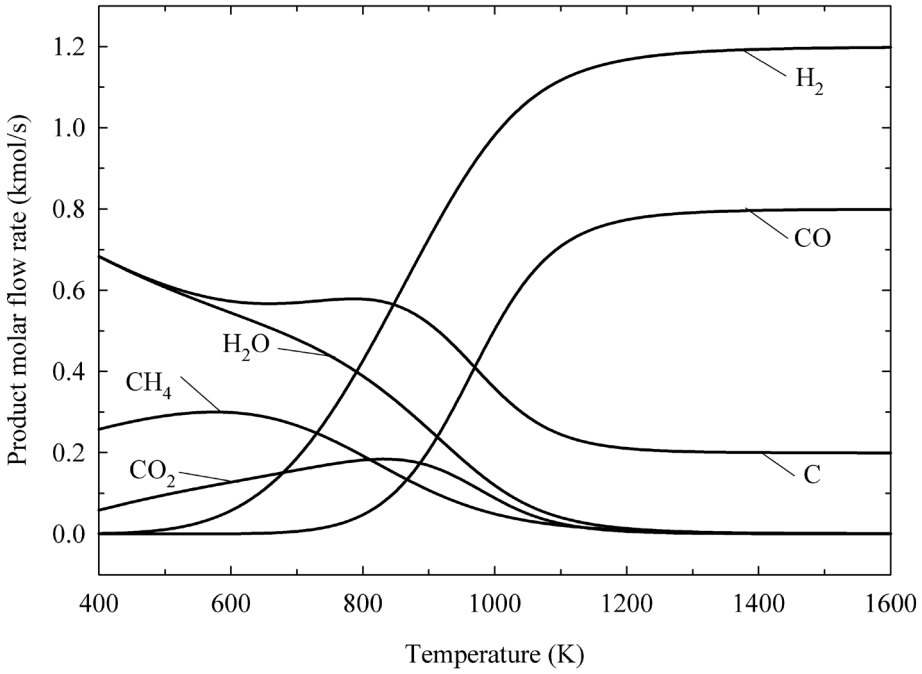

Figure 5.14 Product distribution profiles obtained from the decomposition process fed by CH_4/CO_2 mixture with CO_2/CH_4 ratio of 40:60 (0.67) at 1 bar (total feed molar flow rate of 1 kmol/s).

Regarding the study of the decomposition fed by biogas in this section, it was examined in terms of the reaction performances such as the equilibrium conversion of methane ($X_{CH_4,e}$), hydrogen purity, hydrogen yield and carbon yield. These terms can be determined as defined in the following equations.

$$X_{CH_4,e}(\%) = \left[\frac{\text{mole of } CH_4 \text{ at inlet - mole of } CH_4 \text{ at outlet}}{\text{mole of } CH_4 \text{ at inlet}}\right] \times 100 \quad (5\text{-}3)$$

$$H_2 \text{ Yield } (\%) = \left[\frac{\text{mole of } H_2 \text{ at outlet}}{2 \times \text{mole of } CH_4 \text{ at inlet}}\right] \times 100 \quad (5\text{-}4)$$

$$H_2 \text{ Purity } (\%) = \left[\frac{\text{mole of } H_2 \text{ at outlet}}{\text{mole of all gases at outlet}}\right] \times 100 \quad (5\text{-}5)$$

$$\text{C Yield (\%)} = \left[\frac{\text{mole of C formed}}{\text{mole of C at inlet}}\right] \times 100 \quad (5\text{-}6)$$

5.2.1 Effect of CO_2/CH_4 ratio on Reaction Performances

As mentioned above, the characteristics of the decomposition system fed by CH_4/CO_2 mixture with the certain CO_2/CH_4 ratio were investigated. In addition, the influence of several CO_2/CH_4 ratios in the range of 0.00001-1 on the reaction performances are thoroughly discussed in this section. For the studied CO_2/CH_4 ratios, their values consist of 0.001:99.999 (0.00001), 1:99 (0.01), 5:95 (0.05), 10:90 (0.11), 20:80 (0.25), 30:70 (0.43), 40:60 (0.67), and 50:50 (1.00).

Firstly, the gaseous product and by-products such as H_2, CH_4, CO, CO_2, and H_2O are presented in term of mole percent as shown in Figure 5.15. It was found that the gaseous product profiles as a function of the operating temperature at different CO_2/CH_4 ratios show the difference in quantity of each product, but the tendency for these profiles is similar to those presented in Figure 5.14. Firstly, considering the hydrogen production [Figure 5.15(a)], it was obviously seen its reduction at high temperature when CO_2/CH_4 ratio increased. This was because the addition of carbon dioxide into the decomposition system resulted in higher by-product of carbon monoxide occurred via dry reforming as indicated in Figure 5.15(b). Moreover, it was revealed that the production in percent of hydrogen accompanied with carbon monoxide is around 100% at high temperature for all studied CO_2/CH_4 ratios. It could be reasonably explained that the overall reactions for this system at high temperature are dry reforming accompanied with methane cracking.

For other gaseous products (CH_4, CO_2, and H_2O), it was apparently found that the changes of these production particularly occur at low temperature range while those values are zero at high operating temperature. Pointing out the methane profiles [Figure 5.15(c)], those profiles represented as the methane decomposition one, that is methane content decreased with increasing operating temperature, for very low

CO_2/CH_4 ratio cases (0.00001 and 0.01). Like methane profile in Figure 5.14, there was a peak at low temperature for higher CO_2/CH_4 ratio cases as a result of methanation.

a)

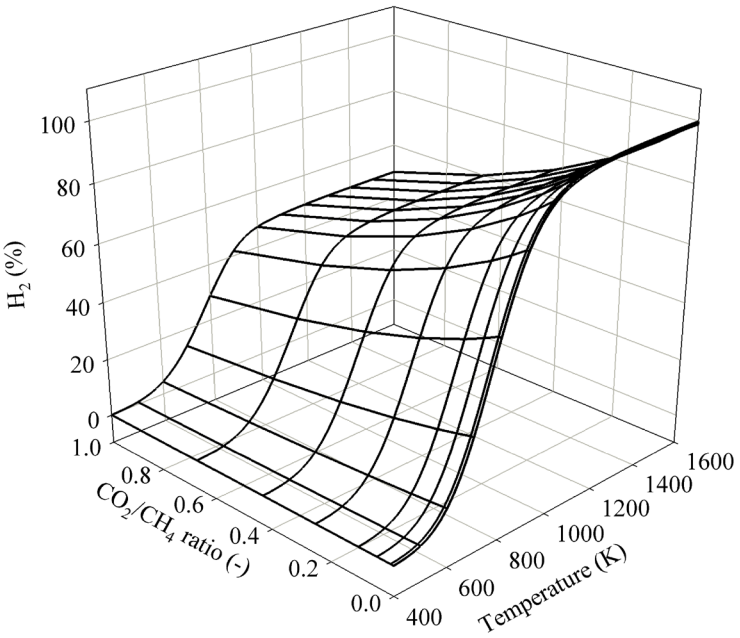

b)

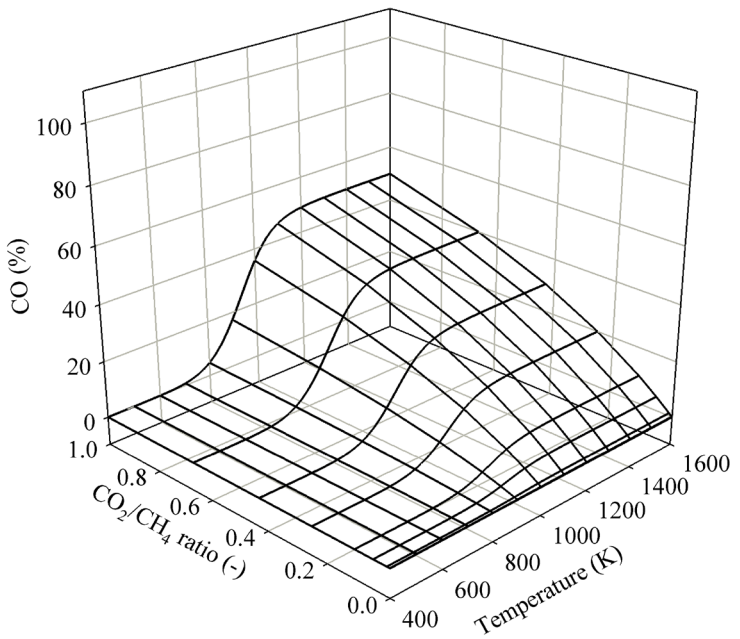

c)

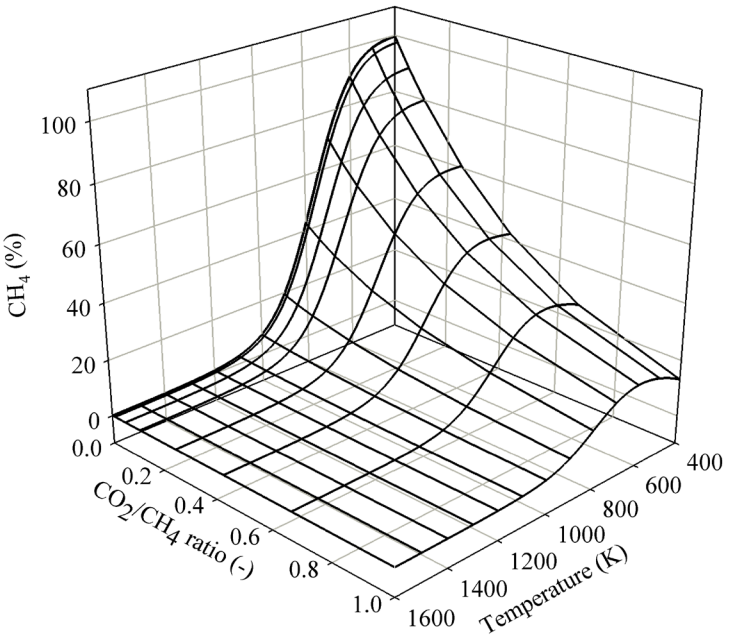
100
80
60
40
20
0
CH4 (%)
0.0
0.2
0.4
0.6
0.8
1.0
CO2/CH4 ratio (-)
400
600
800
1000
1200
1400
1600
Temperature (K)

d)

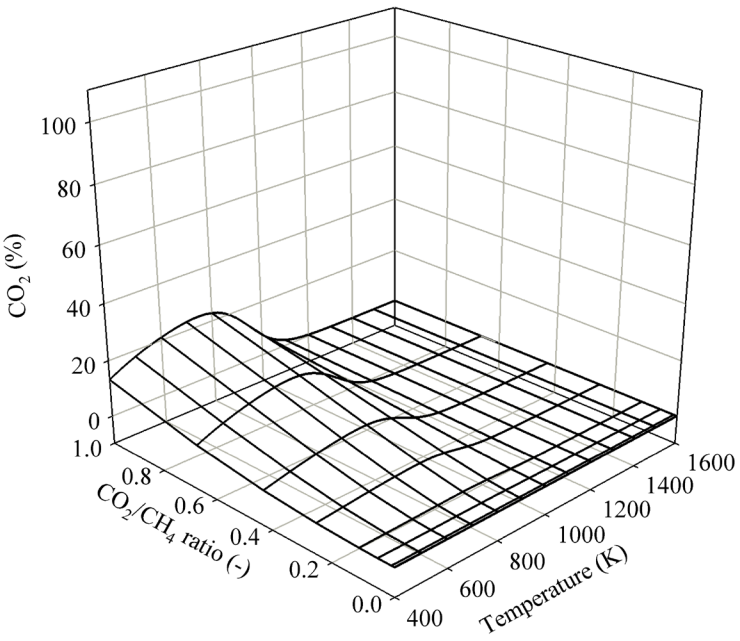
100
80
60
40
20
0
CO2 (%)
1.0
0.8
0.6
0.4
0.2
0.0
CO2/CH4 ratio (-)
1600
1400
1200
1000
800
600
400
Temperature (K)

e)

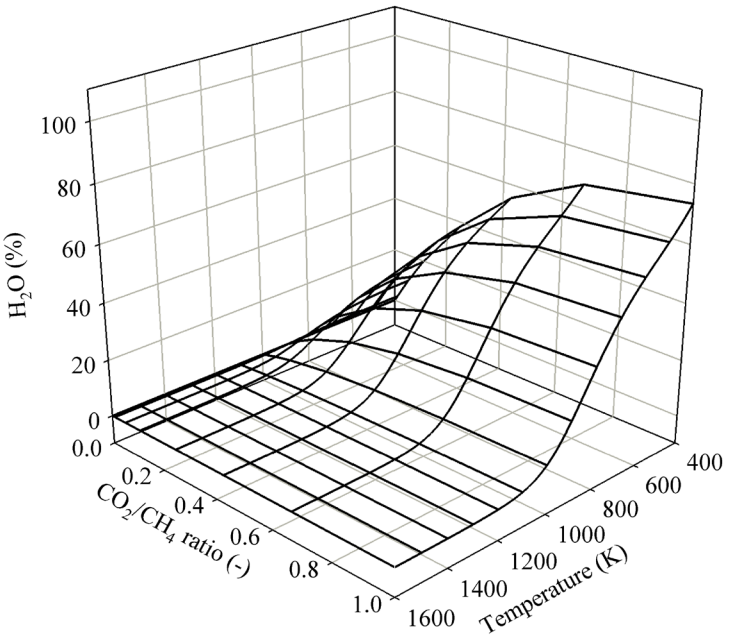

Figure 5.15 The percentage of gaseous products of (a) H_2, (b) CO, (c) CH_4, (d) CO_2, and (e) H_2O obtained from the decomposition process fed by CH_4/CO_2 mixture with various CO_2/CH_4 ratios at 1 bar (total feed molar flow rate of 1 kmol/s).

Regarding carbon dioxide and water profiles as illustrated in Figures 5.15 (d) and (e), respectively, the increase in CO_2/CH_4 ratio caused higher in the production values. Additionally, water content produced at low temperature was surely more than carbon dioxide content in the product stream. It could be described that less carbon dioxide, acting as a reactant, is appeared due to its consumption via dry reforming while higher water content is generated as a by-product from several reactions such as methanation from carbon monoxide and carbon dioxide, and reverse gasification of carbon to carbon monoxide and carbon dioxide even it is partly consumed by water gas shift.

Furthermore, the main by-products such as hydrogen and carbon monoxide generated from the decomposition process fed by CH_4/CO_2 mixture are presented in term of CO/H_2 product ratio as illustrated in Figure 5.16. According to the moles of

hydrogen and carbon monoxide in percent from Figures 5.15 (a) and (b), respectively, Figure 5.16 then shows that the CO/H_2 product ratio increases with increasing CH_4/CO_2 feed ratio. It was apparently revealed that the product ratio of CO/H_2 exhibits the similar value of CO_2/CH_4 feed ratio at high temperature (> 1300 K). Therefore, at this temperature range, the carbon dioxide content in the feed stream could be known since the desired carbon monoxide concentration was set. From these results, the synthesis gas, that is gases consisting of hydrogen and carbon monoxide at CO/H_2 ratio of 1, could be achieved from the decomposition process fed by CH_4/CO_2 mixture at CO_2/CH_4 ratio of 1. This product is another alternative source that can be employed in various well-known industries such as Fischer-Tropsch synthesis of liquid fuels and methanol production [31, 114].

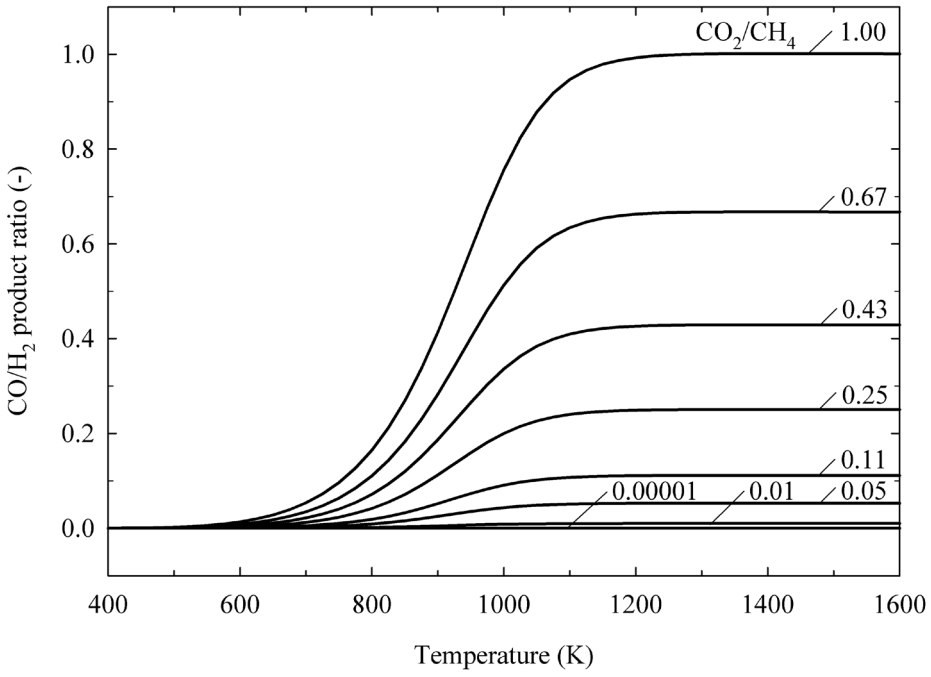

Figure 5.16 The CO/H_2 product ratio obtained from the decomposition process fed by CH_4/CO_2 mixture with various CO_2/CH_4 ratios.

In order to study the reaction performance, the equilibrium conversion of methane is firstly exhibited in Figure 5.17. It was clearly seen that 74% methane conversion can be reached with feeding 50% of carbon dioxide at the temperature of

400 K. It was probably due to high carbon dioxide content affecting the dry reforming to shift forward gaining better equilibrium conversion. At CO_2/CH_4 ratios higher than 0.43, the methane conversion was reduced until temperature of 600 K and it was then increased. The decrease in the methane conversion at low temperature resulted from carbon monoxide or carbon dioxide methanation, which produced more methane concentration. At higher temperatures, the enhancement of the equilibrium conversion of methane was obviously presented, depending on the mainly endothermic reaction and it finally approached to 100% at ca. 1500 K.

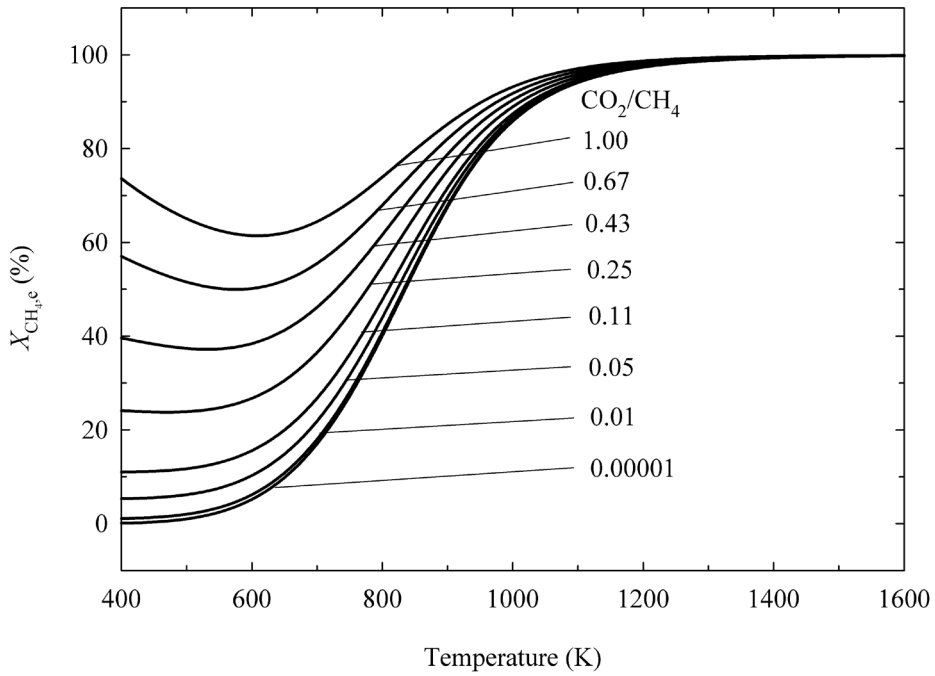

Figure 5.17 The equilibrium methane conversion obtained from the decomposition process fed by CH_4/CO_2 mixture with various CO_2/CH_4 ratios.

According to the hydrogen yield as shown in Figure 5.18, it was found that even higher methane conversion is achieved with higher carbon dioxide presented at low temperature (400-600 K), the hydrogen yield as well as the hydrogen purity (Figure 5.19) are barely different. The apparently difference in hydrogen yield was observed in the temperature range of 700-1100 K. In this range, hydrogen could be generated from the source of methane and water as seen the product distribution in

Figure 5.14. Less CO_2/CH_4 ratio exhibited higher hydrogen yield. It could be indicated that methane was more pronounced than water in order to convert to hydrogen product. Moreover, the slight difference was introduced with the maximum value of the difference in hydrogen yield of ca. 7% at 900 K. Without water produced at high temperature, methane was totally reformed to hydrogen, affecting no difference in hydrogen yield. As mentioned earlier, only hydrogen and carbon monoxide as the gaseous product were appeared at high temperature with the CO/H_2 product ratio presented in Figure 5.16. Therefore, higher in hydrogen yield at lower CO_2/CH_4 ratio resulted in higher in hydrogen purity as seen in Figure 5.19. In addition, the maximum value of hydrogen purity in the case of CO_2/CH_4 ratio of 1.00 was limited at ca. 50%.

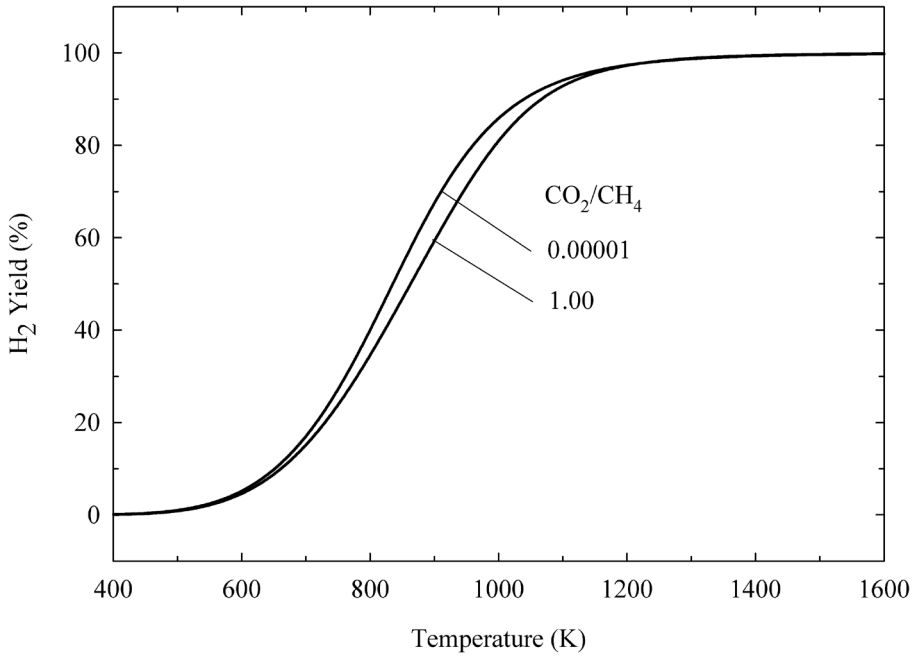

Figure 5.18 The percentage of H_2 yield obtained from the decomposition process fed by CH_4/CO_2 mixture with various CO_2/CH_4 ratios.

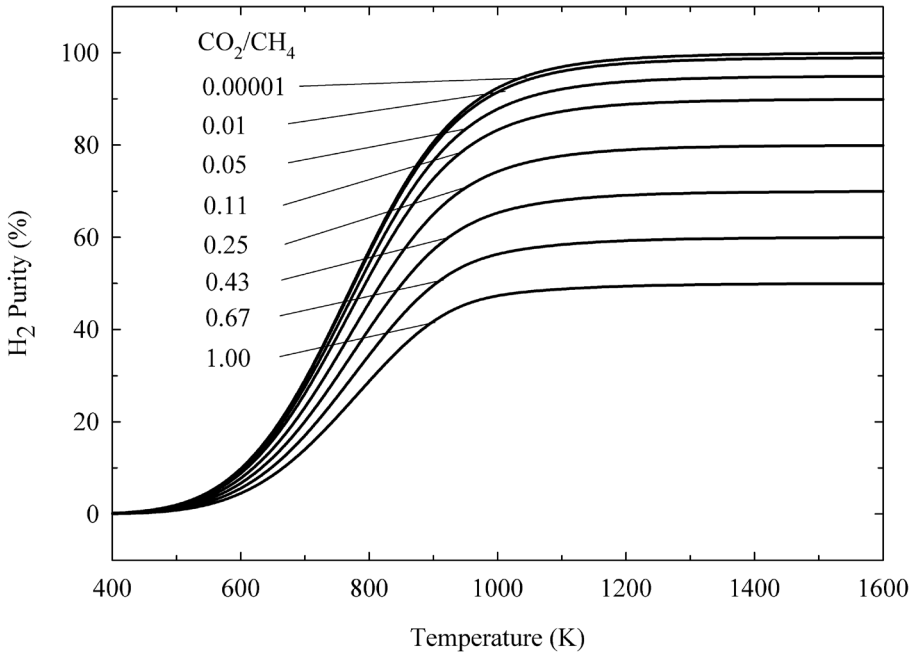

Figure 5.19 The percentage of H_2 purity obtained from the decomposition process fed by CH_4/CO_2 mixture with various CO_2/CH_4 ratios.

At very low CO_2/CH_4 ratio (0.00001), the carbon yield profile (Figure 5.20) could be represented as that from the decomposition process fed by 100% of methane. When adding the amount of carbon dioxide, carbon yield increased over the temperature range of 400-800 K since the presence of carbon dioxide in methane could generate various products i.e., carbon monoxide, hydrogen, water, and carbon, causing higher accumulation of carbon formation. At high CO_2/CH_4 ratio (> 0.25), lower in carbon yielded at low temperature could be explained as mentioned in Figure 5.14. At temperatures higher than 900 K, the opposite trend was observed, that is higher carbon dioxide concentration affected lower in carbon yield. It was due to dry reforming mainly occurred at high carbon dioxide content. Considering the carbon formation, it was mostly generated by methane cracking. In addition, steam or carbon dioxide gasification of carbon could largely occur at high temperature, resulting in less carbon remained in the system. From the overall reactions at high temperature, the dry reforming accompanied with methane cracking was proposed. Higher

CO_2/CH_4 ratios influenced higher methane conversion from the dry reforming, leading to less carbon formation from cracking of the remaining methane.

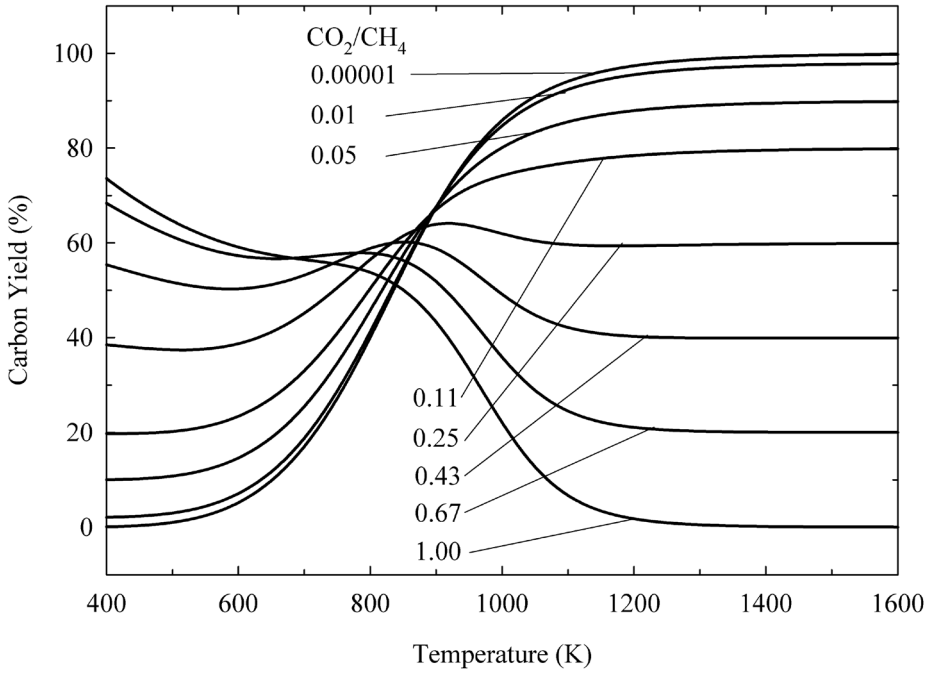

Figure 5.20 The percentage of carbon yield obtained from the decomposition process fed by CH_4/CO_2 mixture with various CO_2/CH_4 ratios.

As considered the reaction performance as shown in Figures 5.17-5.20, higher in CO_2/CH_4 ratio at high temperature could give the similar value of the equilibrium conversion of methane and hydrogen yield approaching 100%, but hydrogen purity and carbon yield was found to be lower.

5.2.2 Compatibility of Decomposition System with Fuel Cells

This section focuses on determining ranges of operating condition of decomposition system which offers gaseous products suitable for different fuel cells including PEMFC and SOFC. For the case of PEMFC, carbon monoxide concentration of 10 ppm was allowed [3, 4]. This criteria was set to investigate the reaction performances as illustrated by the results shown in Figures 5.21 and 5.22. These figures indicate the reaction performances such as the equilibrium conversion of methane, hydrogen yield, carbon yield, and hydrogen purity in percent obtained from the decomposition process fed by biogas with various CO_2/CH_4 ratios under the restriction of carbon monoxide content in the product stream. It was clearly seen that the required CO_2/CH_4 ratio decreases with increasing the operating temperature (Figure 5.21). This could be explained from the relation as mentioned in the previous section that carbon monoxide fraction increases with increasing temperature at a certain CO_2/CH_4 ratio, while the decrease in CO_2/CH_4 ratio results in the reduction in carbon monoxide content at a certain temperature. Therefore, when the CO_2/CH_4 ratio reduced, it was necessary to raise the operating temperature in order to keep the constant value of carbon monoxide fraction. The range of possible uses providing carbon monoxide concentration less than 10 ppm was presented in the region below the boundary profile as shown in Figure 5.21.

As considered the reaction performances, there were no results presented at the temperature below 500 K since carbon monoxide content from the process was less than 10 ppm for all studied CO_2/CH_4 ratios. From Figure 5.22, the methane conversion and carbon yield at low temperature were high and then swiftly reduced when the operating temperature was increased. This trend corresponded to the results from Figures 5.17 and 5.20 at high CO_2/CH_4 ratio. In addition, the increase in temperature and the reduction in CO_2/CH_4 ratio affected higher in reaction performances until the value approached to 100% as shown in Figures 5.17-5.20. Moreover, it was found that the equilibrium conversion of methane, hydrogen yield, and carbon yield are similar at temperature higher than 650 K. This behavior was like the case of the decomposition process fed by pure methane. Thus, low carbon dioxide

content in the feed stream at those temperatures with CO_2/CH_4 ratio in the order of 0.001 could not influence the reaction performances. At high temperature, the value of CO_2/CH_4 ratio of 10^{-5} was achieved. Like the results in Figure 5.16, it was further revealed that the carbon dioxide content in the feed stream has to be around 10 ppm in order to obtain the carbon monoxide concentration of 10 ppm in the product stream. In conclusion, high reaction performances could be gained from very low CO_2/CH_4 ratio case. Hence, it was necessary to separate carbon dioxide before feeding to the decomposition unit when the desired feedstock was biogas with high CO_2/CH_4 ratio such as 40:60 (0.67).

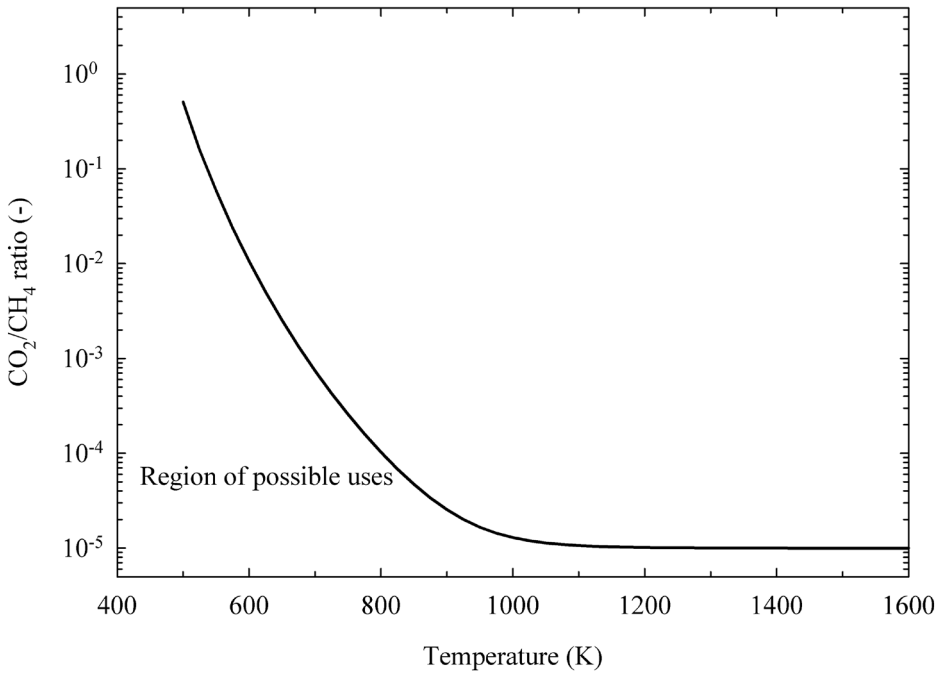

Figure 5.21 The boundary profile of the required CO_2/CH_4 ratio obtained from the decomposition process fed by CH_4/CO_2 mixture under the limitation of CO concentration of 10 ppm.

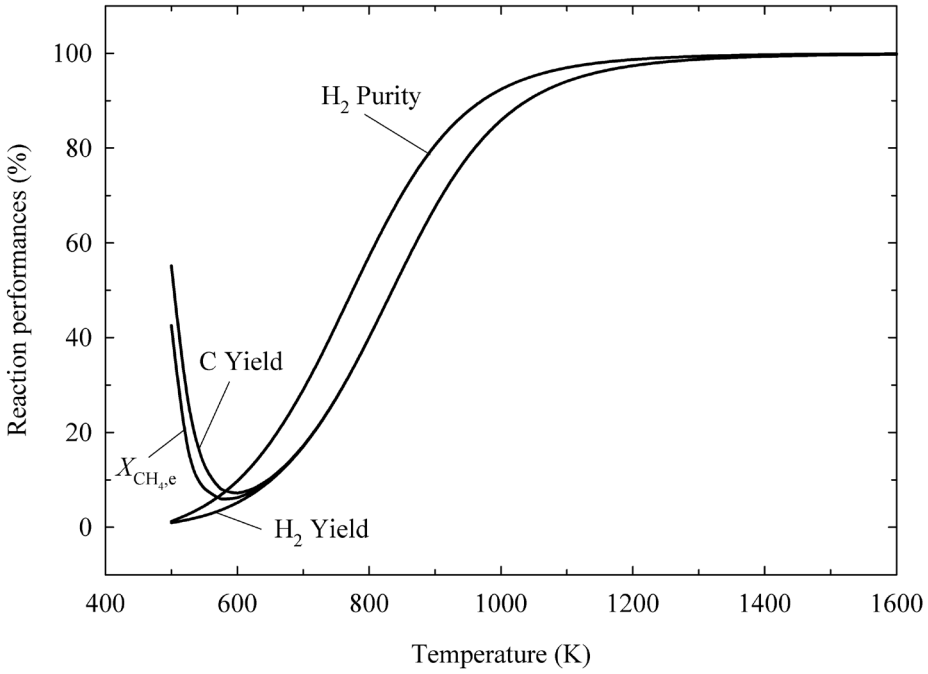

Figure 5.22 The boundary profiles of the reaction performances related to the required CO_2/CH_4 ratio obtained from the decomposition process fed by CH_4/CO_2 mixture under the limitation of CO concentration of 10 ppm.

In Figure 5.23, the decomposition reactor equipped with SOFC was studied. For this kind of fuel cell, the condition of no carbon formation at the SOFC inlet was necessary to take into account. According to this requirement, the equilibrium state at the inlet of SOFC was assumed. Moreover, the equilibrium compositions of product gases and solid carbon could be estimated by means of Gibbs free energy minimization method with the studied operating temperature of SOFC (T_{SOFC}) in the range of 900-1300 K. From Figures 5.23(a)-(e), the carbon formation at the SOFC inlet was expressed as the function of decomposition temperature and CO_2/CH_4 ratio with the operating temperature of SOFC of 900, 1000, 1100, 1200, and 1300 K, respectively.

a)

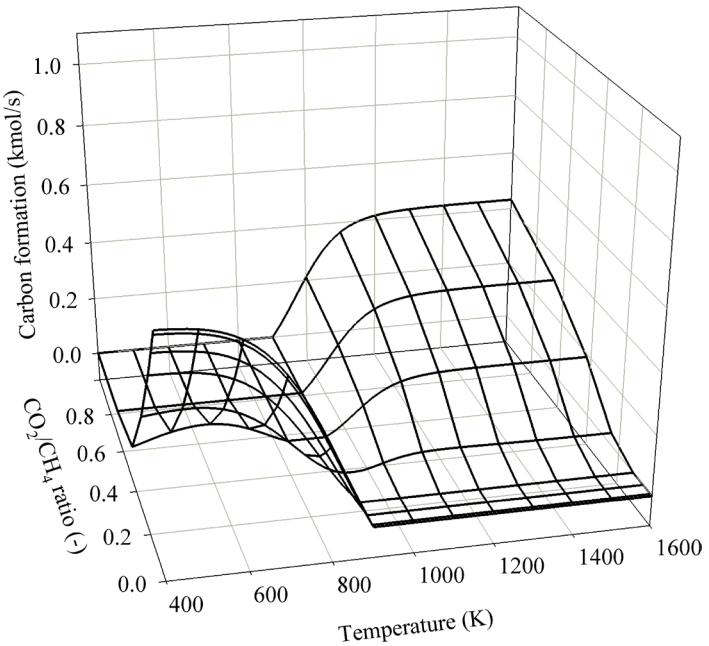
Carbon formation (kmol/s)
1.0
0.8
0.6
0.4
0.2
0.0
CO2/CH4 ratio (-)
0.0
0.2
0.4
0.6
0.8
400
600
800
1000
1200
1400
1600
Temperature (K)

b)

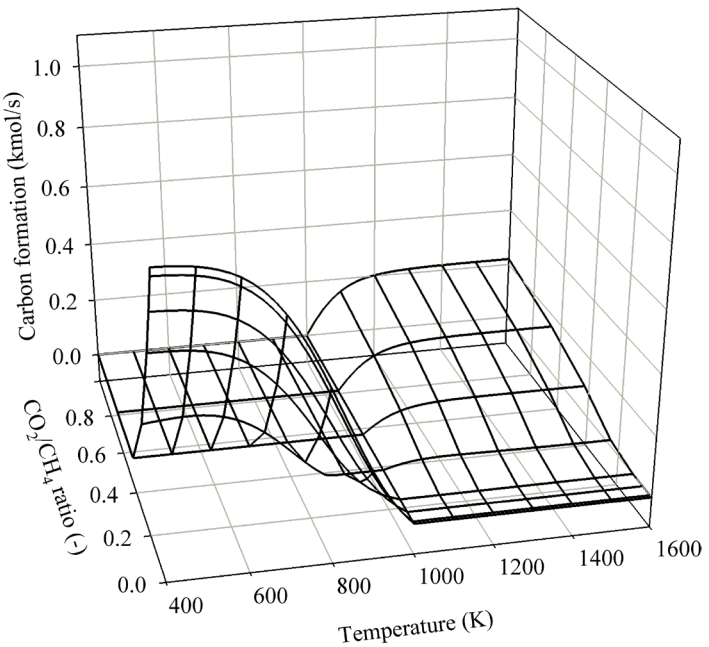
Carbon formation (kmol/s)
1.0
0.8
0.6
0.4
0.2
0.0
CO2/CH4 ratio (-)
0.0
0.2
0.4
0.6
0.8
400
600
800
1000
1200
1400
1600
Temperature (K)

c)

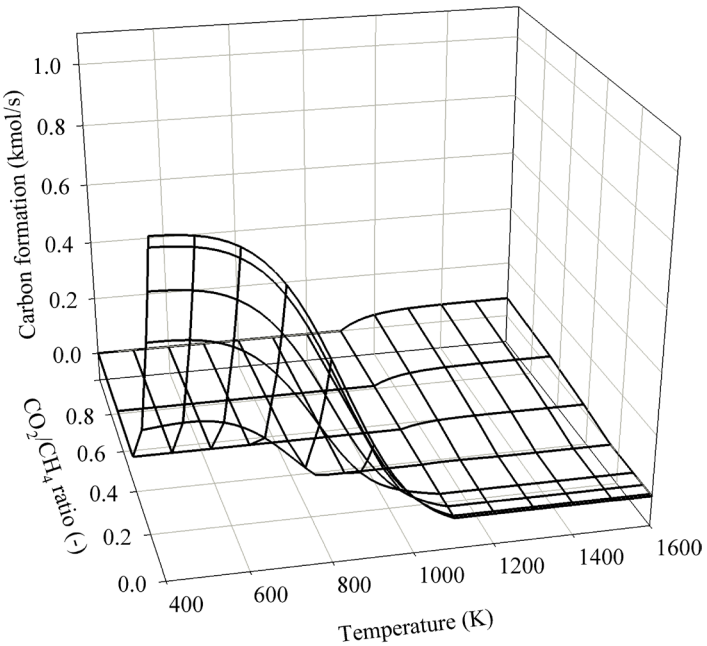
Carbon formation (kmol/s)
1.0
0.8
0.6
0.4
0.2
0.0
CO2/CH4 ratio (-)
0.0
0.2
0.4
0.6
0.8
400
600
800
1000
1200
1400
1600
Temperature (K)

d)

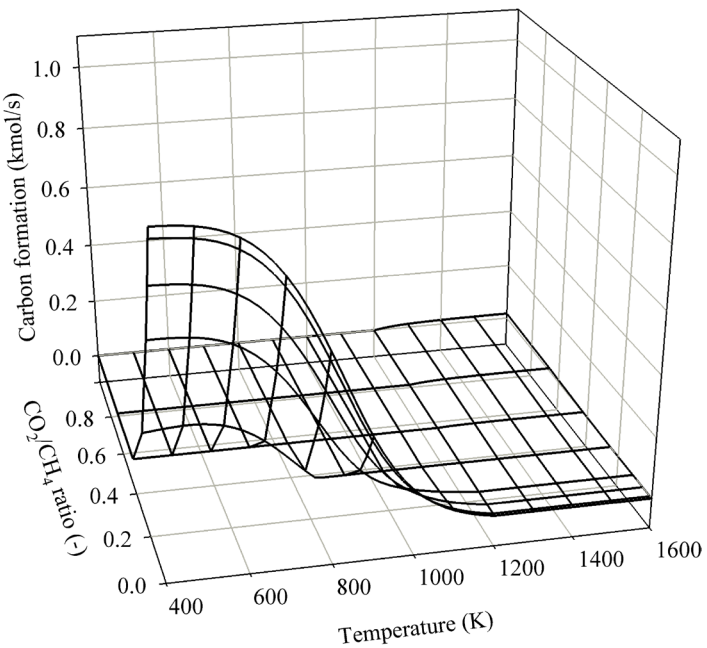
Carbon formation (kmol/s)
1.0
0.8
0.6
0.4
0.2
0.0
CO2/CH4 ratio (-)
0.0
0.2
0.4
0.6
0.8
400
600
800
1000
1200
1400
1600
Temperature (K)

e)

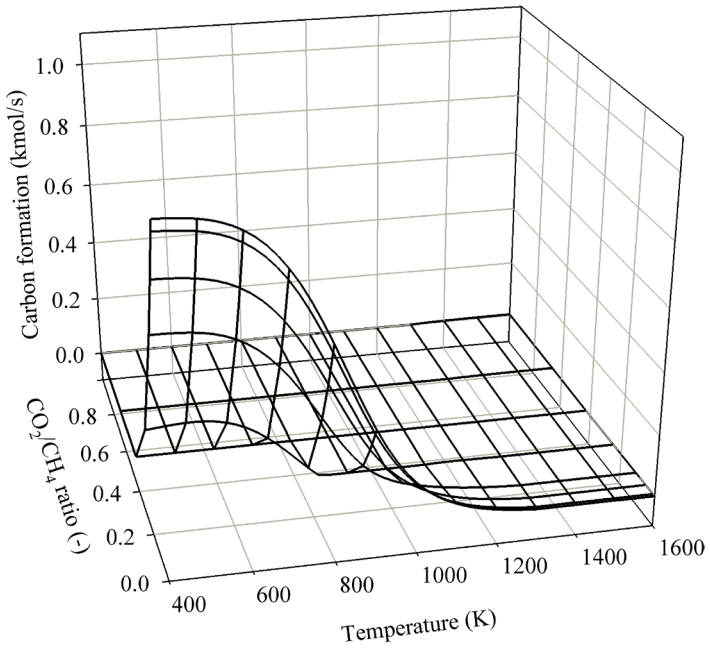

Figure 5.23 Carbon formation generated at the SOFC temperature of (a) 900 K, (b) 1000 K, (c) 1100 K, (d) 1200 K, and (e) 1300 K obtained from the decomposition process fed by CH_4/CO_2 mixture with various CO_2/CH_4 ratios.

As seen in this figure, it could be noticed that, at high CO_2/CH_4 ratio, no carbon formation is observed when the operating temperature of SOFC is higher than the decomposition temperature ($T_r<T_{SOFC}$), whereas carbon is generated in case of the decomposition temperature higher than the operating temperature of SOFC ($T_r>T_{SOFC}$) and higher carbon formation is presented as a result of lower operating temperature of SOFC. Regarding the first case ($T_r<T_{SOFC}$), high water content was generated at low reaction temperature as shown in Figure 5.15(e). It could help prevent the carbon formation at the SOFC inlet for high SOFC temperature case. At high decomposition temperature, the products composing of high concentrations of carbon monoxide and hydrogen fed to SOFC with lower temperature compared to the decomposition one ($T_r>T_{SOFC}$) might result in the occurrence of carbon via Boudouard reaction and reverse gasification of carbon to carbon monoxide [reactions (2-15) and (2-16)]. Furthermore, higher in the difference between the operating temperature of

decomposition unit and SOFC exhibited higher carbon content appeared at the SOFC inlet.

At low value of CO_2/CH_4 ratio, the opposite trend from high CO_2/CH_4 ratio case was apparently disclosed. The carbon formation was occurred in case of $T_r<T_{SOFC}$ because high amount of the unconverted methane at low decomposition temperature fed to SOFC with higher operating temperature reasonably caused the generation of carbon from methane cracking. More carbon was gained when SOFC was operated at higher temperature, compared to the decomposition temperature as displayed in Figures 5.23(a)-(e). This was obviously due to the endothermic reaction of methane cracking. In case of $T_r>T_{SOFC}$, there was no carbon formation since hydrogen with low amounts of by-products (CH_4, CO, and CO_2) as the product from the decomposition unit was fed to SOFC.

According to the results from Figure 5.23, it could be concluded the preferable operating condition of the decomposition process without carbon formation at the SOFC inlet as summarized in Table 5.2. From this table, the operating temperature of SOFC was considered in the range of 900-1300 K. However, SOFC is typically carried out at very high operating temperature of 1200-1300 K. With lower operating temperature (900-1100 K), it is suitable for intermediate-temperature SOFC (IT-SOFC) which is a useful application and being the promising topic for current investigations and developments by several researchers [115, 116]. It was revealed that broader operating windows for IT-SOFC are achieved compared to SOFC ones. Regarding the desired operations, the decomposition unit was necessary to operate at lower temperature compared to the SOFC temperature at high CO_2/CH_4 ratio, whereas the opposite trend was occurred at low CO_2/CH_4 ratio. However, the different operating conditions was appeared in case of CO_2/CH_4 ratio of 0.25 since the carbon could be generated from reaction of methane for $T_r<T_{SOFC}$ case and from reactions of carbon monoxide for $T_r>T_{SOFC}$ case. At this ratio, it was the transition state between the effect of methane or carbon monoxide on the carbon formation considering at the SOFC inlet.

Table 5.2 The operating temperature of decomposition unit under the condition of no carbon formation at the SOFC inlet.

T_{SOFC} (K)	Decomposition temperature (K)							
	CO_2/CH_4 ratio (-)							
	0.00001	0.01	0.05	0.11	0.25	0.43	0.67	1.00
900	900-1600				900-925	800-900	400-900	
1000	1000-1600				875-1000	400-1000		
1100	1100-1600				850-1100 1325-1600	400-1100		
1200	1200-1600				850-1150 1200-1600	400-1200		
1300	1300-1600				850-1100 1300-1600	400-1300		

The study of reaction performances for the range of operation are shown in Figures 5.24-5.27. The operating temperature of SOFC was studied in the range of 900-1300 K. From these figures, each line of a certain value of CO_2/CH_4 ratio represents the reaction performances for all range of T_{SOFC}. Therefore, the decomposition and CO_2/CH_4 ratio for each T_{SOFC} can be firstly obtained from Table 5.2 and eventually indicated the value of reaction performance (Figures 5.24-5.27). For the equilibrium conversion of methane and carbon yield (Figures 5.24 and 5.25), it could be referred to those values from Figures 5.17 and 5.20, respectively. The maximum value of methane conversion for high CO_2/CH_4 ratio was limited by T_{SOFC} (maximum at 1300 K). However, its value could be gained at the decomposition temperature of 1600 K for low CO_2/CH_4 ratio. In addition, the carbon yield could be maximized when CO_2/CH_4 ratio was low at high operating temperature of decomposition unit.

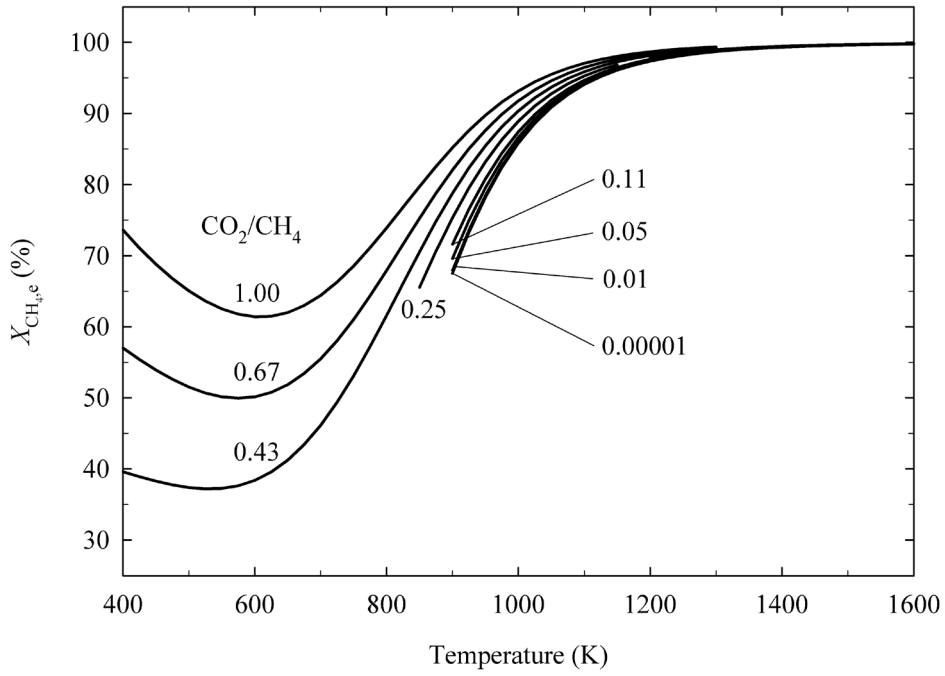

Figure 5.24 The equilibrium methane conversion obtained from the decomposition process fed by CH_4/CO_2 mixture with various CO_2/CH_4 ratios accompanied with SOFC (T_{SOFC} = 900-1300 K).

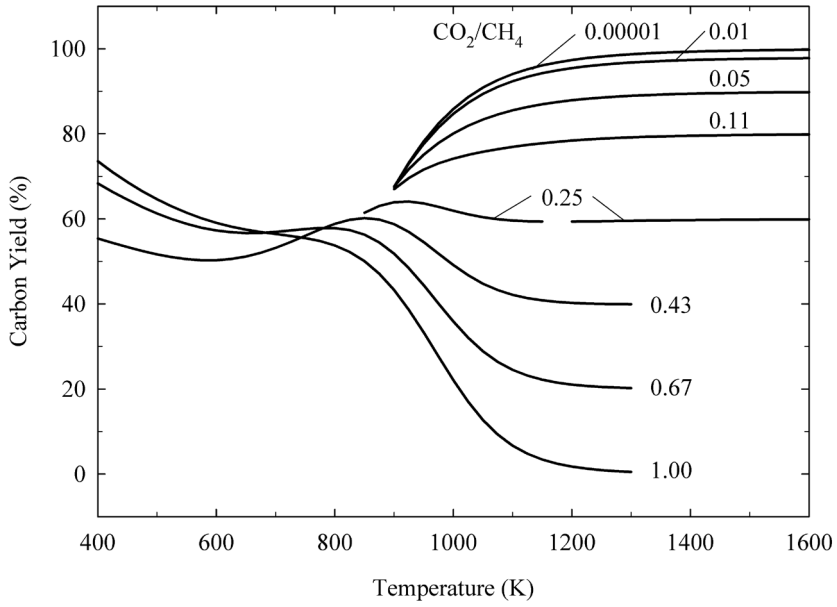

Figure 5.25 The percentage of carbon yield obtained from the decomposition process fed by CH_4/CO_2 mixture with various CO_2/CH_4 ratios accompanied with SOFC (T_{SOFC} = 900-1300 K).

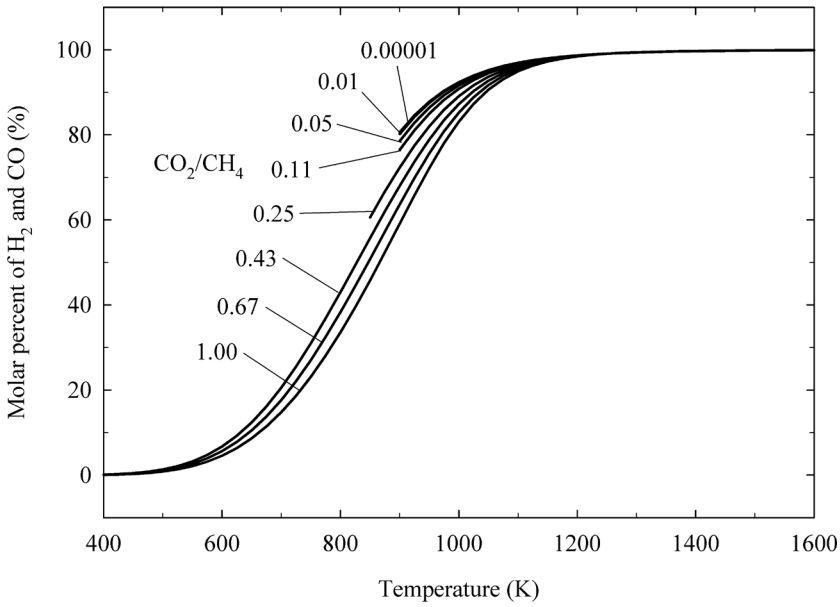

Figure 5.26 The percentage of H_2 and CO obtained from the decomposition process fed by CH_4/CO_2 mixture with various CO_2/CH_4 ratios accompanied with SOFC (T_{SOFC} = 900-1300 K).

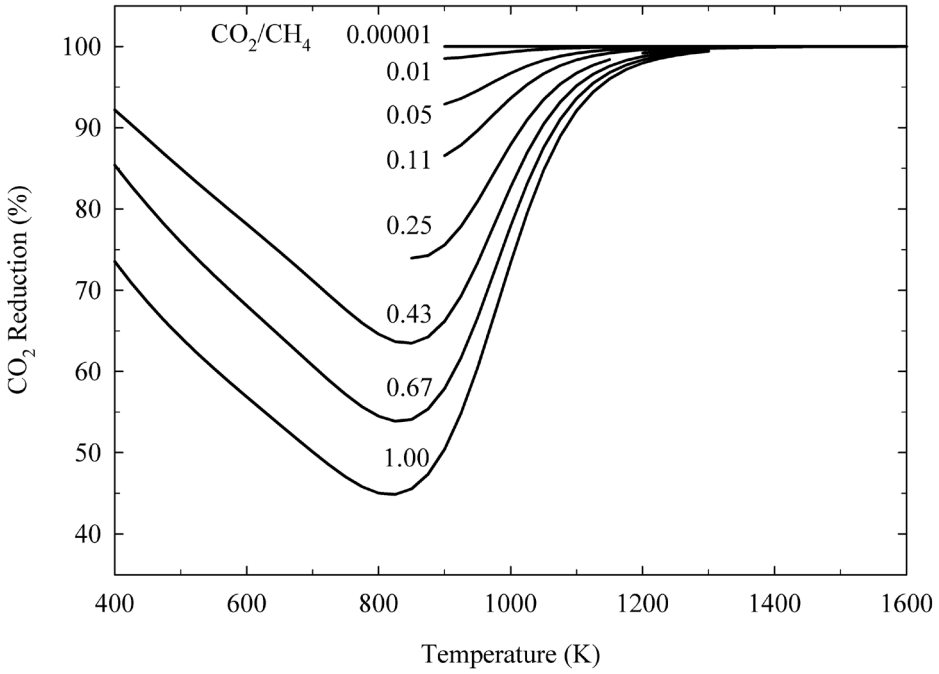

Figure 5.27 The CO_2 reduction obtained from the decomposition process fed by CH_4/CO_2 mixture with various CO_2/CH_4 ratios accompanied with SOFC (T_{SOFC} = 900-1300 K).

Since hydrogen and carbon monoxide could be used as a fuel source for SOFC, the concentration of both gases was another variable to take into account as shown in Figure 5.26. It was found that higher amount of fuel source in percent is achieved at lower CO_2/CH_4 ratio. This was probably due to higher in the generation of by-products in case of higher CO_2/CH_4 ratio. Considering the CO_2 reduction (Figure 5.27), it could be determined from the amount of CO_2 reduced, compared to the amount of CO_2 at the inlet of decomposition process. It was found that the CO_2 reduction increases with decreasing the CO_2/CH_4 ratio. The tendency of these profiles was related to the results from Figure 5.15(d).

Generally, biogas composes of methane and carbon dioxide with high CO_2/CH_4 ratio such as 40:60 (0.67). Therefore, according to the results from Figures 5.24-5.27, it was necessary to reduce the amount of carbon dioxide until the value of

CO_2/CH_4 ratio was less than 0.25 when high value of reaction performances was desired. In other words, it required at least ca. 63% of CO_2 capture from biogas with CO_2/CH_4 ratio of 40:60 for the decomposition process.

As considered biogas with CO_2/CH_4 ratio of 40:60 as a primary fuel in this work, the CO_2 separation unit before feeding to the decomposition reactor was needed as shown the system configuration in Figure 5.28. Among several options of CO_2 capture unit, MEA absorption is an attractive choice as described in Section 3.5. The percentage of CO_2 removal was typically set at 90% [86, 87]. Thus, CO_2/CH_4 product ratio obtained from the CO_2 capture unit was about 0.067. For this ratio indicating in the range of 0.05-0.11 (Table 5.2), the operating temperature of decomposition reactor had to be higher than the SOFC temperature.

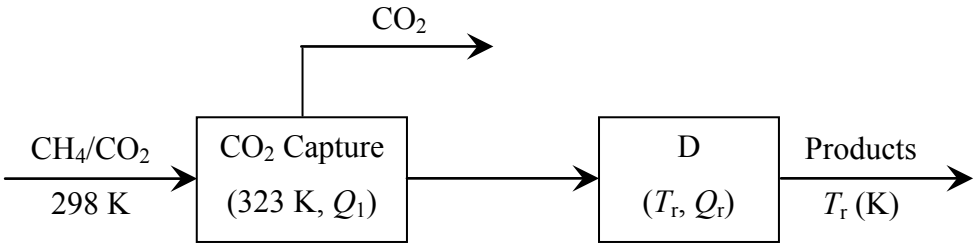

Figure 5.28 System configuration of the decomposition process with CO_2 capture.

However, the product from the CO_2 capture providing CO_2/CH_4 ratio of 0.067 fed to the decomposition unit could not be suitable for PEMFC because the carbon monoxide concentration of 10 ppm could not be achieved. In addition, it could be also confirmed from the results in Figure 5.22. Hence, from this point, it was focused on investigation of the system configuration for SOFC application.

Several reaction performances for this case are gathered in Figure 5.29. The operating temperature of decomposition reactor was displayed in the range of 900-1600 K, which corresponded to the operation without carbon formation at the SOFC inlet for the SOFC temperature range of 900-1300 K. It was clearly seen that most reaction performances reach the maximum value of 100% at high operating

temperature, except for the carbon yield that was maximized at ca. 88%. According to these results, it could be not found the optimum value. Therefore, it was further studied the decomposition process under energy self-sustained condition (Q_{net} = 0) as illustrated in Figure 5.30. Regarding these system configurations, total heat of the system can be determined as follows:

$$Q_{net} = Q_1 + Q_2 + Q_r + Q_c \quad (4\text{-}2)$$

Moreover, the comparison of the reaction performances between the systems with splitting feed and splitting product was concerned. Splitting feed or product stream to the burner was designed in order to provide heat for the system. In this case, the decomposition and CO_2 capture units certainly required heat to operate this process as a result of mainly endothermic reactions occurred in both units.

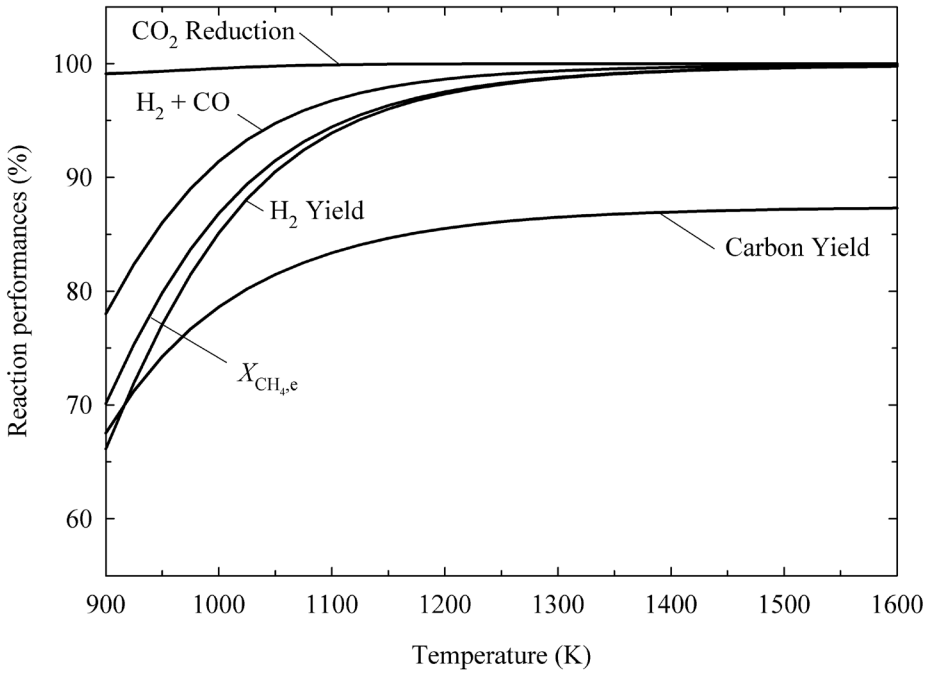

Figure 5.29 The reaction performances obtained from the decomposition process with CO_2 capture fed by CH_4/CO_2 mixture accompanied with SOFC (CH_4/CO_2 ratio of 40:60 and T_{SOFC} = 900-1300 K).

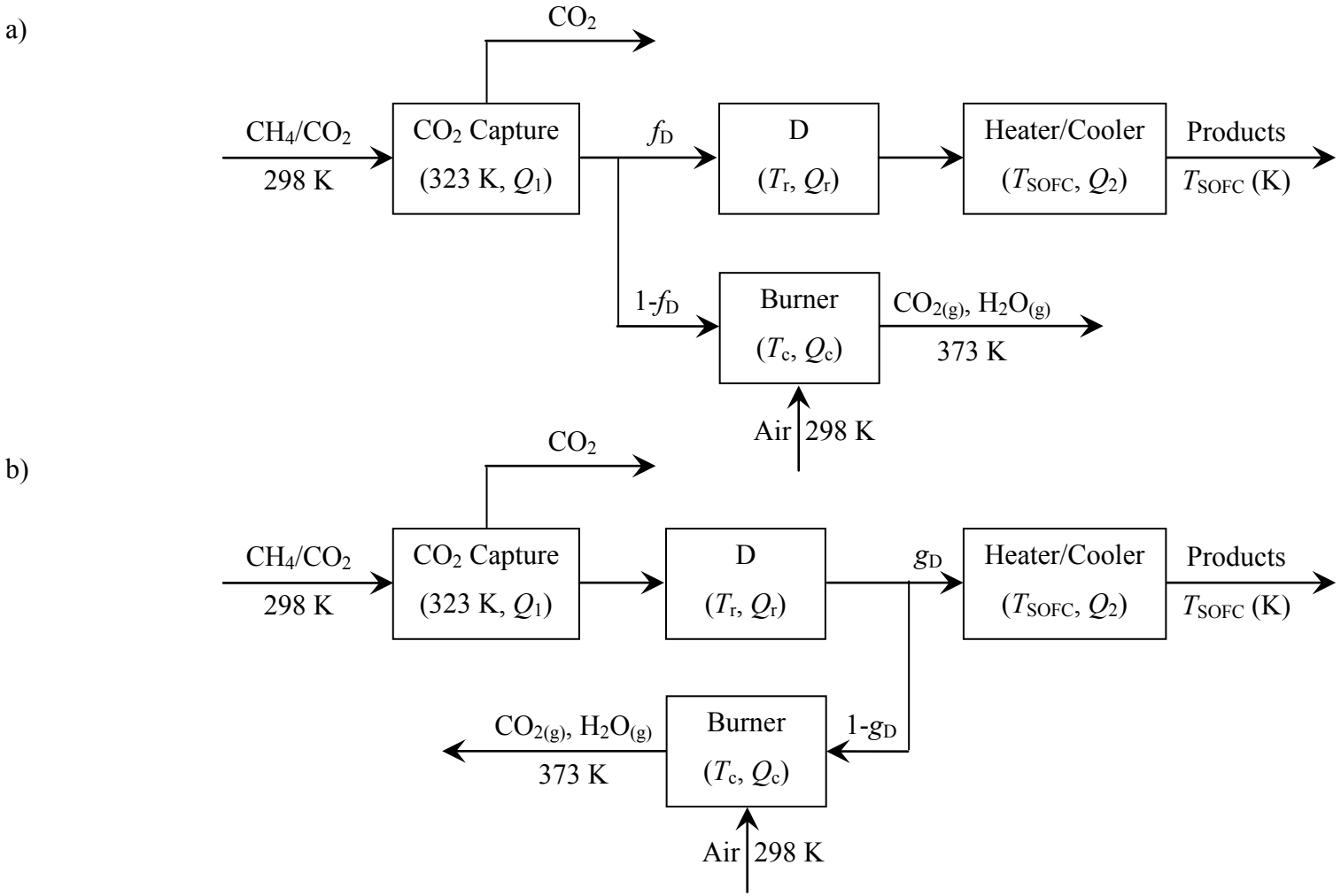

Figure 5.30 The system configurations under energy self-sustained operation obtained from the decomposition process with CO_2 capture fed by CH_4/CO_2 mixture accompanied with SOFC in case of (a) splitting primary fuel and (b) splitting gas product stream.

The heat requirement of CO_2 removal (Q_1) was referred to the calculation as expressed in Section 3.5. Pointing out the decomposition process under thermally self-sustained condition, it was obviously presented that f_d and g_d decrease with increasing the operating temperature (Figure 5.31) due to the endothermic system. In addition, f_d exhibited higher than g_d because heat combustion of methane-containing primary fuel was higher than that of hydrogen-containing product.

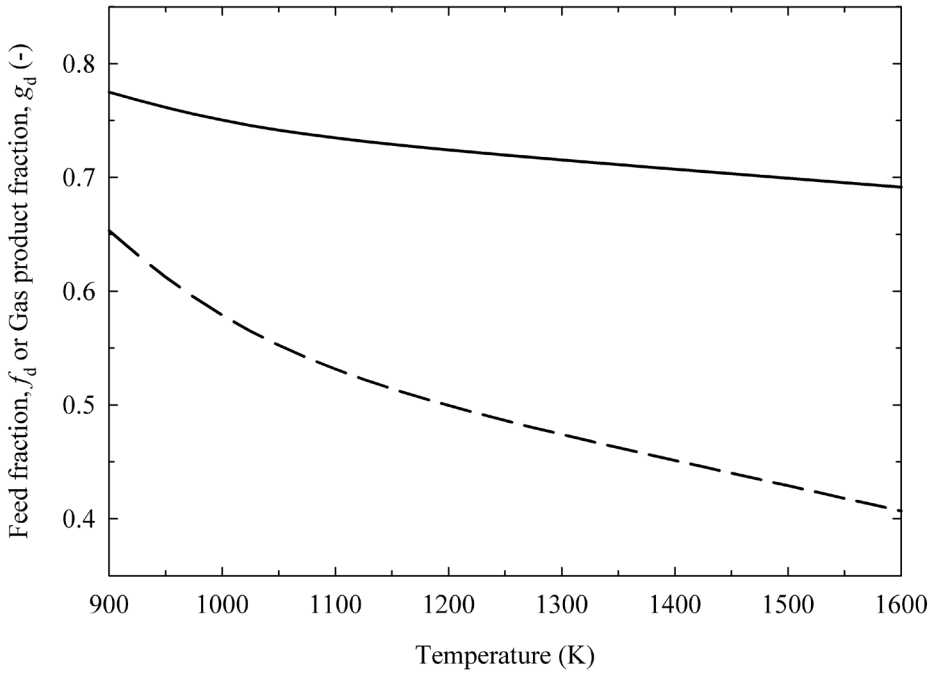

Figure 5.31 The feed fraction or gas product fraction under energy self-sustained operation obtained from the decomposition process with CO_2 capture fed by CH_4/CO_2 mixture with CH_4/CO_2 ratio of 40:60 accompanied with SOFC for T_{SOFC} = 900-1300 K (solid line – case of splitting primary fuel, dashed line – case of splitting gas product stream).

As shown in Figure 5.32, it represents the reaction performances of the system with splitting feed or splitting product gas stream. For overall range of T_{SOFC} (900-1300 K), insignificant difference in reaction performances was observed. This was because heat generation at the SOFC inlet (Q_3) was a small portion of the overall heat of the system, resulting in no effect to the reaction performances. From this figure, it

was found that hydrogen and carbon monoxide concentration is similar for both cases while CO_2 reduction is insignificantly different. These reaction performances still approached to 100% at high operating temperature. Considering another reaction performance, higher hydrogen yield in case of splitting primary fuel was gained, compared to that in case of splitting gas product stream. The maximum hydrogen yield of 70.7% was obtained at temperature of 1275 K. For the carbon yield profiles, the system with splitting gas product gave higher value than that with splitting feed, providing the maximum value of 87.3% at 1600 K. Referred to the hydrogen yield and carbon yield profiles in Figure 5.29, the appearance of a peak was observed in Figure 5.32 and their values tended to decrease at higher temperatures since the feed fraction to reactor and gas product fraction reduced along with the increased operating temperature.

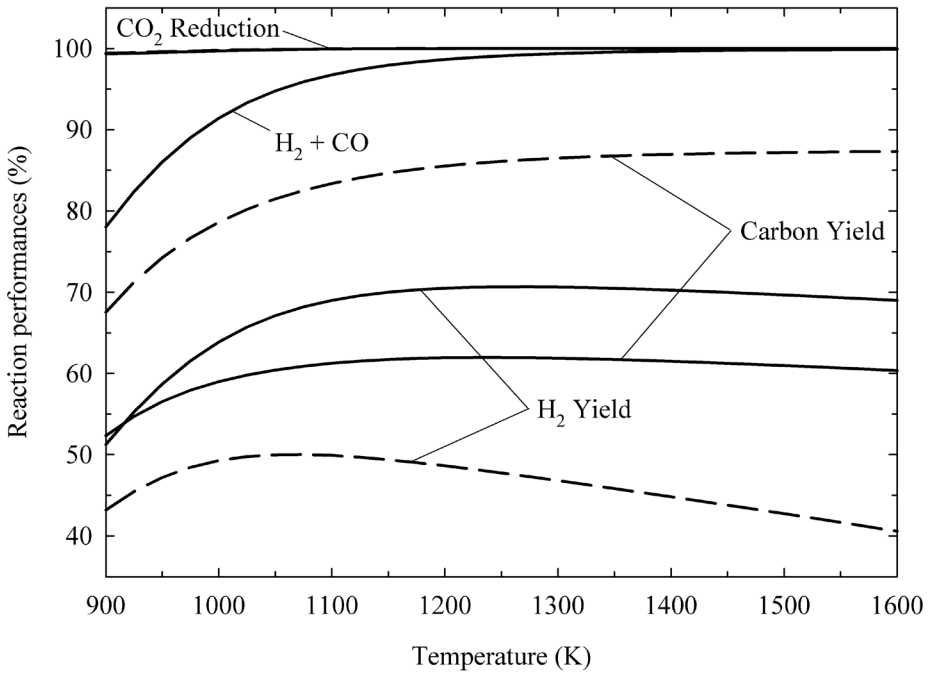

Figure 5.32 The reaction performances under energy self-sustained operation obtained from the decomposition process with CO_2 capture fed by CH_4/CO_2 mixture with CH_4/CO_2 ratio of 40:60 accompanied with SOFC for T_{SOFC} = 900-1300 K (solid line – case of splitting primary fuel, dashed line – case of splitting gas product stream).

Regarding the reaction performance in term of the amount of fuel for SOFC (H_2 and CO) as shown in Figure 5.33, the optimum operation was carried out at 1275 K for the system with splitting primary fuel. Higher difference between the system with splitting feed and product at higher temperature since the tendency of the reduction in feed fraction and gas product fraction was observed (Figure 5.31).

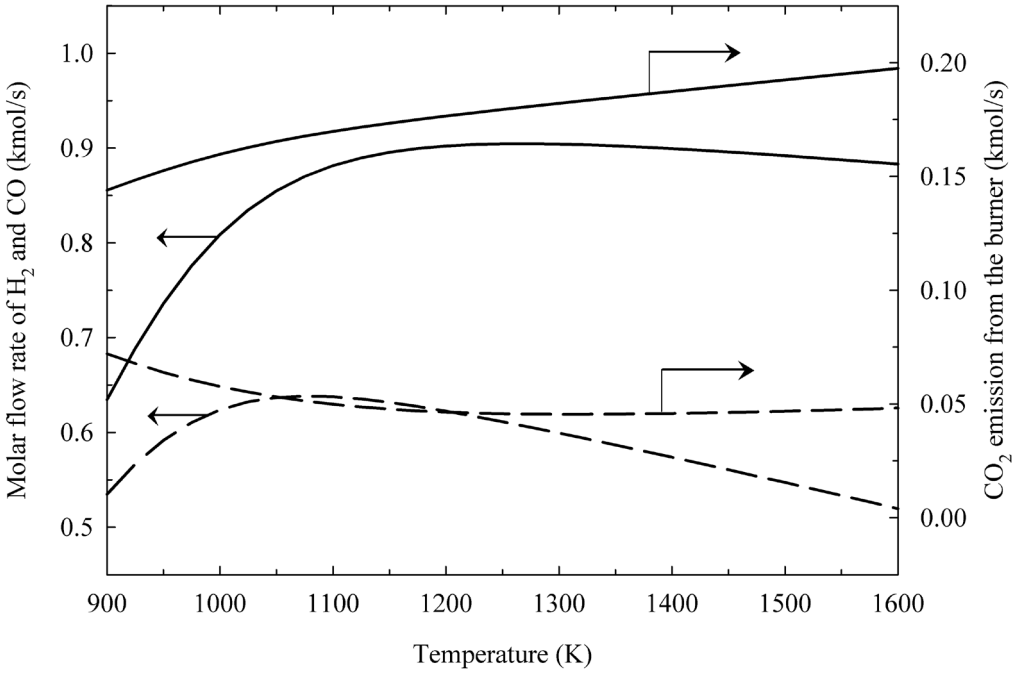

Figure 5.33 The H_2 and CO production and CO_2 emission from the burner under energy self-sustained operation obtained from the decomposition process with CO_2 capture fed by CH_4/CO_2 mixture with CH_4/CO_2 ratio of 40:60 accompanied with SOFC for T_{SOFC} = 900-1300 K (solid line – case of splitting primary fuel, dashed line – case of splitting gas product stream).

Under the criteria of hydrogen and carbon monoxide production and hydrogen yield, the maximum value could be achieved from the system with splitting feed at the operating temperature of 1275 K (Figure 5.33), exhibiting hydrogen yield of 70.7% and carbon yield of 61.9%. At this operation, it was suitable for processing with SOFC at the SOFC temperature range of 900-1200 K.

In order to take into account the environmental concern in term of CO_2 emission, the system in case of splitting feed gave higher CO_2 emission from the burner, compared to splitting gas product stream case (Figure 5.33). For this reaction performance, the amount of CO_2 exhaust from the process was not necessary to include in CO_2 emission term due to very low quantity of CO_2 presented in the product stream compared to the CO_2 emission from the burner. The system with splitting product gas stream provided the lowest CO_2 emission from the burner at the temperature of 1300 K. At the minimum CO_2 emission, the hydrogen yield of 46.8% and carbon yield of 86.5% was obtained. In addition, the SOFC could be operated for all studied temperature range (900-1300 K). Thus, this operation could give high carbon capture in term of carbon yield with low level of CO_2 emission, but the hydrogen and carbon monoxide production was low.

In this work, CO_2 capture was considered to reduce the carbon dioxide content before processing to the decomposition reactor. It could obviously affect the reaction performances. However, in case of separating carbon dioxide after the decomposition unit (data not shown), it was found that insignificant effect is observed in terms of the reaction performances and the range of operations, but it is useful in a part of the reduction in CO_2 emission. Therefore, the post-combustion capture for removing carbon dioxide after the SOFC application was not examined.

Therefore, for the aim of high production of fuel for SOFC, the system with splitting primary fuel at the decomposition temperature of 1275 K and the SOFC temperature of 900-1200 K was selected, while the appropriate system in term of environmental concern as totally carbon capture was the system with splitting gas product at the decomposition temperature of 1300 K and the SOFC temperature of 900-1300 K. Nevertheless, it was disclosed that even at low operating temperature of SOFC for IT-SOFC, the process provides no difference in reaction performances compared to high SOFC temperature. Moreover, IT-SOFC has been more interesting application than SOFC based on the economic factor. Hence, the decomposition process had an ability to operate with IT-SOFC.

Several hydrogen production methods from biogas for fuel cell application have been proposed and researched as reported previously [49]. The steam reforming, partial oxidation reforming, autothermal reforming, dry reforming, and dry oxidation reforming can be processed by biogas. It was reported that biogas reforming is not suitable for PEMFC as presented the similar result in this work. However, the range of possible uses for SOFC application was determined in this research.

In conclusion, this work can provide a guideline for choosing the appropriate operations for the decomposition process. However, the decision for selecting the proper system for hydrogen production from the decomposition process needed more gathered information such as more realistic process by applying the kinetic model into the decomposition unit, consideration of the reaction performances and efficiency from the fuel cell application, and the economic analysis.

CHAPTER VI
CONCLUSIONS AND RECOMMENDATIONS

6.1 Conclusions

In this work, the study of hydrogen production for different fuel cells was investigated. It could be concluded into two sections i.e. comparative study of reaction performances between decomposition and steam reforming processes, and investigation of decomposition process fed by biogas. In addition, it can be proposed as the following summarization below.

6.1.1 Comparative Study of Reaction Performances between Decomposition and Steam Reforming Processes

The thermodynamic analyses of hydrogen production by the decomposition and the steam reforming under energy self-sustained condition were investigated. Several primary fuels such as light hydrocarbons (methane, ethane, and propane) and alcohols (methanol, ethanol, and glycerol) were considered. This section can be summarized as follows:

- The optimum value of hydrogen production for the steam reforming processes was obtained as a result of the occurrence of reverse water gas shift reaction at high temperature.
- The optimum value of hydrogen production for the decomposition processes was gained due to the reduction in feed fraction and gas product fraction.
- The process with splitting primary fuel gave higher hydrogen production than that with splitting gas product stream.
- Higher in carbon yield but lower in CO_2 emission from the burner were achieved in case of splitting product, compared to splitting feed case.

- Most of the steam reforming processes gave high hydrogen production; however, SR-C_3H_8 with splitting feed at 1050 K provided the highest hydrogen production.
- D-light hydrocarbons exhibited the highest carbon yield at high temperature.
- Among D-alcohols, the highest carbon yield was obtained from D-C_2H_5OH at high temperature.
- No carbon formation was observed at high temperature for the steam reforming processes.

Aim for PEMFC:

- The suitable process was D-light hydrocarbon.
- D-alcohols and SR-all primary fuels could not employ with this fuel cell since high reaction performance could be obtained from the process with CO concentration higher than 10 ppm.

Under the criteria of the highest hydrogen production:

- D-C_3H_8 with splitting feed operated at 1275 K was selected.

Under the criteria of environmental concern (carbon capture and CO_2 emission):

- D-CH_4 with splitting product at 1100 K was preferred.

Aim for SOFC:

- The products from D-light hydrocarbons and D-alcohols could be supplied to this fuel cell.
- The steam reforming processes could also equipped with this fuel cell. However, less hydrogen and carbon monoxide concentrations were achieved might lead to producing lower power density from SOFC.

Under the criteria of the highest hydrogen production:

- D-C_3H_8 with splitting feed operated at 1275 K was selected.

Under the criteria of environmental concern (carbon capture and CO_2 emission):

- D-CH_4 with splitting product at 1100 K was preferred.
- D-C_2H_5OH with splitting product at 1175 K providing high H_2/CO product ratio and carbon yield could be used. However, D-CH_3OH and D-$C_3H_8O_3$ at 1225 K giving lower H_2/CO ratio could be also used.

6.1.2 Investigation of Decomposition Process Fed by Biogas

From this section, it focuses on the decomposition process fed by biogas. Therefore, the conclusion can be drawn as listed below.

- Methane in methane-containing gas mixture such as CH_4/N_2 mixture could improve the equilibrium conversion of methane by reducing the methane content in feed stream.
- The CO/H_2 product ratio could be estimated from the CO_2/CH_4 feed ratio.
- At low temperature, the equilibrium methane conversion and carbon yield increased with increasing CO_2/CH_4 ratio, while the former showed slightly different but the latter exhibited the opposite trend at high temperature.

Aim for PEMFC:

- It needed to separate CO_2 before supplying to the decomposition unit in order to gain CO concentration below 10 ppm with high reaction performances.

Aim for SOFC:

- The operating temperature of SOFC (T_{SOFC}) was considered in the range of 900-1300 K

Under the criteria of no carbon formation at the SOFC inlet:

- At high CO_2/CH_4 ratio (0.67-1.00), the decomposition unit could be operated in case of $T_r < T_{SOFC}$.
- At low CO_2/CH_4 ratio (0.00001-0.11), the decomposition unit could be operated in case of $T_r > T_{SOFC}$.
- At the CO_2/CH_4 ratio of 0.25 acting as a transition state, it could be carried out in both ranges
- Since the reaction performances were limited at T_{SOFC}, it was necessary to separate CO_2 before feeding to the decomposition reactor until the CO_2/CH_4 ratio less than 0.25.

For the decomposition process fed by biogas with CO_2 capture:

- The reaction performances were maximized at 1600 K. There was no optimum point for this case.

Under the energy self-sustained operation:

- The insignificant difference in reaction performances was observed for T_{SOFC} in the range of 900-1300 K.

Aim for PEMFC:

- It could not be compatible with this fuel cell.

Aim for SOFC:

Under the criteria of the highest hydrogen and carbon monoxide production:

- The process with splitting feed at 1275 K could be operated with SOFC in the SOFC temperature range of 900-1200 K.

Under the criteria of environmental concern (carbon capture and CO_2 emission):

- The process with splitting product at 1300 K could be operated with SOFC in the SOFC temperature range of 900-1300 K

For this case, IT-SOFC was preferred to operate with the decomposition process.

6.2 Recommendations for Future Works

In order to achieve more reasonable selection of an appropriate process for different fuel cells, the following future works are suggested.

- In this work, thermodynamic analysis of hydrogen production was investigated without considering the catalyst used, the selective reactions occurred for each kind of catalyst, the reaction rate of the related reactions in the system, and other forms of carbon production such as carbon nanofiber and carbon nanotube. Therefore, this information was necessary to take into account in the calculation in order to precisely validate with the available experiment results.

For example, the simulation results obtained from hydrogen production via the decomposition of biogas with CO_2/CH_4 ratio of 1 at atmospheric pressure were validated with the experiment results from Khalesi *et al*. [117] and Jablonski *et al*. [118] in term of methane conversion with $Sr_{0.8}La_{0.2}Ni_{0.3}Al_{0.7}O_{2.6}$ and Pt/Na(0.3 wt.%)-Al_2O_3 as the catalyst used, respectively. In addition, this comparison is presented in Figure 6.1.

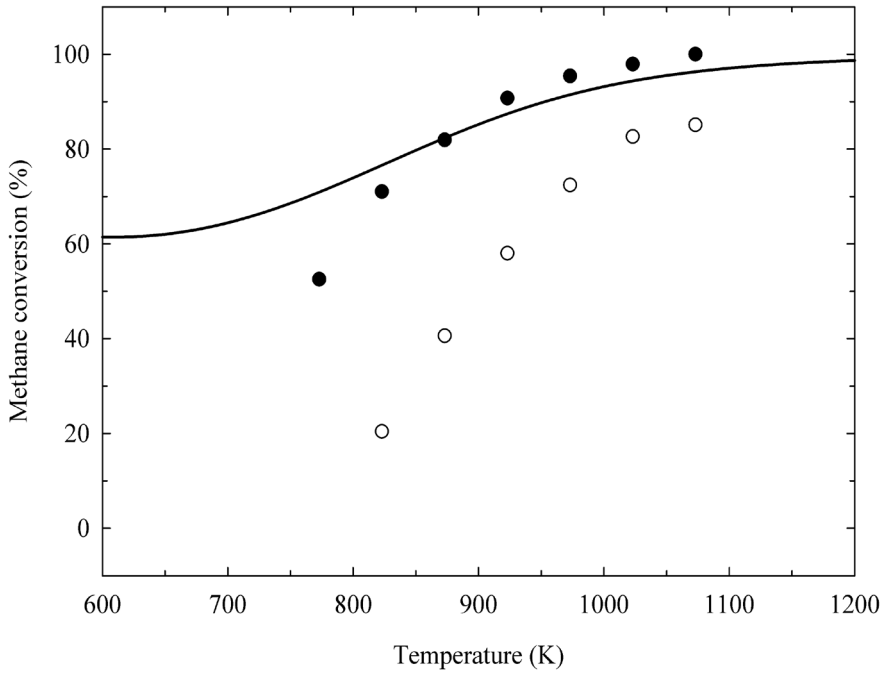

Figure 6.1 The simulation results (line) and experiment results of Khalesi *et al*. [117] (black circle) and Jablonski *et al*. [118] (white circle) obtained from the decomposition process fed by CH_4/CO_2 mixture with CO_2/CH_4 ratio of 1 at atmospheric pressure.

Even methane conversion increased with increasing the operating temperature for all systems in Figure 6.1, the different catalysts could provide the difference in methane conversion. It was revealed that the equilibrium conversion values from the simulation results are close to the published experimental results from Khalesi *et al*. [117]. However, at the reaction temperature higher than 923 K, the methane conversion from the experimental

results exhibited higher value, compared to the equilibrium conversion. It was presumably due to the effect of coke formation at high temperature. Moreover, graphitic carbon was assumed in the simulation without considering the deactivation rate of catalyst, while the different carbon forms could be generated in the experiment.

Hence, in order to validate with the experimental results from the different catalysts used, it was necessary to apply the kinetic model. However, the reaction rates should be obtained from the selected catalyst. In addition, the properties of other carbon forms including the deactivation rate of catalyst should be addressed.

- In case of liquid alcohol fed to the decomposition reactor, it was considered as it was entirely vaporized and then fed to the system. However, the carrier gas such as nitrogen might be required in the practical process. Therefore, the primary fuel mixed with inert gas should be additionally employed and further compared the reaction performances.

- In this work, only hydrogen production was studied. For comparing the obtained electricity between the decomposition process equipped with fuel cell and the conventional process, it was necessary to apply the fuel cell operation in the calculation. Moreover, the characteristics of and the reaction taken place in the fuel cell should be included in order to determine the overall reaction performances and the overall efficiency.

- In case of carbon-containing gas mixture for SOFC, the carbon formation should be corrected by considering the related reactions inside the SOFC for achieving the proper range of possible uses.

- More CO_2 capture methods such as adsorption by calcium looping cycle, pressure swing adsorption, and membrane separation with various CO_2 capture

efficiency should be considered in order to compare the reaction performances among all processes.

- Wider range of CO_2/CH_4 ratio should be studied for the process with CO_2 capture under energy self-sustained operation.

- The economic analysis should be applied.

REFERENCES

[1] Farrauto, R.J., and Bartholomew, C.H. Fundamentals of Industrial Catalytic Processes. 1st ed. London: Chapman & Hall, 1997.

[2] EG & G Technical Services Fuel Cell Handbook. 7th ed. Morgantown, WV: US DOE, 2004.

[3] Ledjeff-Hey, K., Roes, J., and Wolters, R. CO_2-scrubbing and methanation as purification system for PEFC. Journal of Power Sources 86 (2000): 556-561.

[4] Kordesch, K.V., and Simader, G.R. Fuel Cells and Their Applications. Weinheim, Germany: VCH Verlagsgesellschaft mbH, 1996.

[5] McHugh, K., Eisele, S., and Nestell, J. Hydrogen production methods. MPR-WP-0001 (2005).

[6] Spath, P.L., and Mann, M.K. Life cycle assessment of hydrogen production via natural gas steam reforming. NREL/TP-570-27637 (2001).

[7] Pinilla, J.L., et al. Production of hydrogen and carbon nanofibers by thermal decomposition of methane using metal catalysts in a fluidized bed reactor. International Journal of Hydrogen Energy 32 (2007): 4821-4829.

[8] Avdeeva, L.B., Kochubey, D.I., and Shaikhutdinov, S.K. Cobalt catalysts of methane decomposition: accumulation of the filamentous carbon. Applied Catalysis A: General 177 (1999): 43-51.

[9] Chai, S.-P., Zein, S.H.S., and Mohamed, A.R. CO_x-Free Hydrogen and Carbon Nanofibers Produced from Direct Decomposition of Methane on Nickel-Based Catalysts. Journal of Natural Gas Chemistry 15 (2006): 253-258.

[10] Zabidi, N.A.M., Zein, S., and Mohamed, A.R. Hydrogen production by catalytic decomposition of methane. Universiti Technologi Pertonas. Platform 3 (2003): 3-9.

[11] Shah, N., Ma, S., Wang, Y., and Huffman, G.P. Semi-continuous hydrogen production from catalytic methane decomposition using a fluidized-bed reactor. International Journal of Hydrogen Energy 32 (2007): 3315-3319.

[12] Qian, W., Liu, T., Wei, F., Wang, Z., and Li, Y. Enhanced production of carbon nanotubes: combination of catalyst reduction and methane decomposition. Applied Catalysis A: General 258 (2004): 121-124.

[13] Niu, C., Sichel, E.K., Hoch, R., Moy, D., and Tennent, H. High power electrochemical capacitors based on carbon nanotube electrodes. Applied Physics Letters 70 (1997): 1480-1482.

[14] Gadd, G.E., et al. The World's Smallest Gas Cylinders? Science 277 (1997): 933-936.

[15] Gao, R., Tan, C.D., and Baker, R.T.K. Ethylene hydroformylation on graphite nanofiber supported rhodium catalysts. Catalysis Today 65 (2001): 19-29.

[16] Chambers, A., Nemes, T., Rodriguez, N.M., and Baker, R.T.K. Catalytic Behavior of Graphite Nanofiber Supported Nickel Particles. 1. Comparison with Other Support Media. Journal of Physical Chemistry B 102 (1998): 2251-2258.

[17] Otsuka, K., Ogihara, H., and Takenaka, S. Decomposition of methane over Ni catalysts supported on carbon fibers formed from different hydrocarbons. Carbon 41 (2003): 223-233.

[18] Steinberg, M. Fossil fuel decarbonization technology for mitigating global warming. International Journal of Hydrogen Energy 24 (1999): 771-777.

[19] Dufour, J., Serrano, D.P., Gálvez, J.L., Moreno, J., and García, C. Life cycle assessment of processes for hydrogen production. Environmental feasibility and reduction of greenhouse gases emissions. International Journal of Hydrogen Energy 34 (2009): 1370-1376.

[20] Muradov, N. Thermocatalytic CO_2-free production of hydrogen from hydrocarbon fuels. Proceeding of the 2000 US DOE hydrogen program review. NREL/CP-570-28890.

[21] Muradov, N. Thermocatalytic CO_2-free production of hydrogen from hydrocarbon fuels. Proceeding of the 2002 US DOE hydrogen program review. NREL/CP-610-32405.

[22] Trimm, D.L. Coke formation and minimisation during steam reforming reactions. Catalysis Today 37 (1997): 233-238.

[23] Graf, P.O., Mojet, B.L., van Ommen, J.G., and Lefferts, L. Comparative study of steam reforming of methane, ethane and ethylene on Pt, Rh and Pd supported on yttrium-stabilized zirconia. Applied Catalysis A: General 332 (2007): 310-317.

[24] Schädel, B.T., Duisberg, M., and Deutschmann, O. Steam reforming of methane, ethane, propane, butane, and natural gas over a rhodium-based catalyst. Catalysis Today 142 (2009): 42-51.

[25] Rossi, C.C.R.S., Alonso, C.G., Antunes, O.A.C., Guirardello, R., and Cardozo-Filho, L. Thermodynamic analysis of steam reforming of ethanol and glycerine for hydrogen production. International Journal of Hydrogen Energy 34 (2009): 323-332.

[26] Faungnawakij, K., Kikuchi, R., and Eguchi, K. Thermodynamic evaluation of methanol steam reforming for hydrogen production. Journal of Power Sources 161 (2006): 87-94.

[27] Dunker, A.M., and Ortmann, J.P. Kinetic modeling of hydrogen production by thermal decomposition of methane. International Journal of Hydrogen Energy 31 (2006): 1989-1998.

[28] Konieczny, A., Mondal, K., Wiltowski, T., and Dydo, P. Catalyst development for thermocatalytic decomposition of methane to hydrogen. International Journal of Hydrogen Energy 33 (2008): 264-272.

[29] Ogihara, H., et al. Formation of highly concentrated hydrogen through methane decomposition over Pd-based alloy catalysts. Journal of Catalysis 238 (2006): 353-360.

[30] Shah, N., Panjala, D., and Huffman, G.P. Hydrogen Production by Catalytic Decomposition of Methane. Energy & Fuels 15 (2001): 1528-1534.

[31] Dayton, D.C. Fuel cell integration-a study of the impacts of gas quality and impurities. Milestone Completion Report. NREL/MP-510-30298 (2001).

[32] de Llobet, S., Pinilla, J.L., Lázaro, M.J., Moliner, R., and Suelves, I. Catalytic decomposition of biogas to produce H_2-rich fuel gas and carbon nanofibers. Parametric study and characterization. International Journal of Hydrogen Energy 37 (2012): 7067-7076.

[33] Nagayasu, Y., et al. Effect of carbon dioxide cofeed on decomposition of methane over Ni catalysts. Journal of Japan Petroleum Institute 49 (2006): 186-193.

[34] Asai, K., et al. Decomposition of methane in the presence of carbon dioxide over Ni catalysts. Chemical Engineering Science 63 (2008): 5083-5088.

[35] Nikoo, M.K., and Amin, N.A.S. Thermodynamic analysis of carbon dioxide reforming of methane in view of solid carbon formation. Fuel Processing Technology 92 (2011): 678-691.

[36] Cents, A.H.G., Brilman, D.W.F., and Versteeg, G.F. CO_2 absorption in carbonate/bicarbonate solutions: The Danckwerts-criterion revisited. Chemical Engineering Science 60 (2005): 5830-5835.

[37] Dong, F., Lou, H., Goto, M., and Hirose, T. A new PSA process as an extension of the Petlyuk distillation concept. Separation and Purification Technology 15 (1999): 31-40.

[38] Powell, C.E., and Qiao, G.G. Polymeric CO_2/N_2 gas separation membranes for the capture of carbon dioxide from power plant flue gases. Journal of Membrane Science 279 (2006): 1-49.

[39] Ammendola, P., Chirone, R., Lisi, L., Ruoppolo, G., and Russo, G. Copper catalysts for H_2 production via CH_4 decomposition. Journal of Molecular Catalysis A: Chemical 266 (2007): 31-39.

[40] EG & G Technical Services Fuel Cell Handbook. 6th ed. Morgantown, WV: US DOE, 2002.

[41] Kohl, A.L., and Nielsen, R.B. Gas purification. 5 ed. Houston, Texas: Gulf Publishing, 1997.

[42] IPCC IPCC Special Report on Carbon Dioxide Capture and Storage. Prepared by Working Group III of the Intergovernmental Panel on Climate Change: Cambridge University Press. Cambridge, United Kingdom and New York, NY, USA: Cambridge University Press, 2005.

[43] Mariz, C.L. Carbon dioxide recovery: Large scale design trends. Journal of Canadian Petroleum Technology 37 (1998): 42-47.

[44] Dicks, A.L. Hydrogen generation from natural gas for the fuel cell systems of tomorrow. Journal of Power Sources 61 (1996): 113-124.

[45] Dias, J.A.C., and Assaf, J.M. The advantages of air addition on the methane steam reforming over Ni/γ-Al_2O_3. Journal of Power Sources 137 (2004): 264-268.

[46] Laosiripojana, N., Sutthisripok, W., and Assabumrungrat, S. Synthesis gas production from dry reforming of methane over CeO_2 doped Ni/Al_2O_3: Influence of the doping ceria on the resistance toward carbon formation. Chemical Engineering Journal 112 (2005): 13-22.

[47] Takeguchi, T., et al. Study on steam reforming of CH_4 and C_2 hydrocarbons and carbon deposition on Ni-YSZ cermets. Journal of Power Sources 112 (2002): 588-595.

[48] Steinberg, M., and Cheng, H.C. Modern and prospective technologies for hydrogen production from fossil fuels. International Journal of Hydrogen Energy 14 (1989): 797-820.

[49] Alves, H.J., et al. Overview of hydrogen production technologies from biogas and the applications in fuel cells. International Journal of Hydrogen Energy 38 (2013): 5215-5225.

[50] Piao, L., Li, Y., Chen, J., Chang, L., and Lin, J.Y.S. Methane decomposition to carbon nanotubes and hydrogen on an alumina supported nickel aerogel catalyst. Catalysis Today 74 (2002): 145-155.

[51] Villacampa, J.I., et al. Catalytic decomposition of methane over Ni-Al_2O_3 coprecipitated catalysts: Reaction and regeneration studies. Applied Catalysis A: General 252 (2003): 363-383.

[52] Rahman, M., Croiset, E., and Hudgins, R. Catalytic Decomposition of Methane for Hydrogen Production. Topics in Catalysis 37 (2006): 137-145.

[53] Ermakova, M.A., Ermakov, D.Y., Chuvilin, A.L., and Kuvshinov, G.G. Decomposition of Methane over Iron Catalysts at the Range of Moderate Temperatures: The Influence of Structure of the Catalytic Systems and the Reaction Conditions on the Yield of Carbon and Morphology of Carbon Filaments. Journal of Catalysis 201 (2001): 183-197.

[54] Aiello, R., Fiscus, J.E., zur Loye, H.-C., and Amiridis, M.D. Hydrogen production via the direct cracking of methane over Ni/SiO_2: catalyst deactivation and regeneration. Applied Catalysis A: General 192 (2000): 227-234.

[55] Nuernberg, G.B., et al. Preparation and evaluation of Co/Al_2O_3 catalysts in the production of hydrogen from thermo-catalytic decomposition of methane: Influence of operating conditions on catalyst performance. Fuel 87 (2008): 1698-1704.

[56] Wang, H., and Baker, R.T.K. Decomposition of Methane over a Ni-Cu-MgO Catalyst to Produce Hydrogen and Carbon Nanofibers. The Journal of Physical Chemistry B 108 (2004): 20273-20277.

[57] Muradov, N., Smith, F., and T-Raissi, A. Catalytic activity of carbons for methane decomposition reaction. Catalysis Today 102-103 (2005): 225-233.

[58] Muradov, N., Chen, Z., and Smith, F. Fossil hydrogen with reduced CO_2 emission: Modeling thermocatalytic decomposition of methane in a fluidized bed of carbon particles. International Journal of Hydrogen Energy 30 (2005): 1149-1158.

[59] Bai, Z., Chen, H., Li, B., and Li, W. Catalytic decomposition of methane over activated carbon. Journal of Analytical and Applied Pyrolysis 73 (2005): 335-341.

[60] Lee, S.Y., Ryu, B.H., Han, G.Y., Lee, T.J., and Yoon, K.J. Catalytic characteristics of specialty carbon blacks in decomposition of methane for hydrogen production. Carbon 46 (2008): 1978-1986.

[61] Muradov, N.Z., and Veziroglu, T.N. From hydrocarbon to hydrogen-carbon to hydrogen economy. International Journal of Hydrogen Energy 30 (2005): 225-237.

[62] Serrano, D.P., Botas, J.A., and Guil-Lopez, R. H_2 production from methane pyrolysis over commercial carbon catalysts: Kinetic and deactivation study. International Journal of Hydrogen Energy 34 (2009): 4488-4494.

[63] Krzyzynski, S., and Kozlowski, M. Activated carbons as catalysts for hydrogen production via methane decomposition. International Journal of Hydrogen Energy 33 (2008): 6172-6177.

[64] Bai, Z., Chen, H., Li, B., and Li, W. Methane decomposition over Ni loaded activated carbon for hydrogen production and the formation of filamentous carbon. International Journal of Hydrogen Energy 32 (2007): 32-37.

[65] Grabke, H.J. The kinetics of decarburization and carburization of gamma-iron in methane-hydrogen mixtures. Physikalisch Chemische 69 (1965): 409-414.

[66] Fukada, S., Nakamura, N., Monden, J., and Nishikawa, M. Experimental study of cracking methane by Ni/SiO_2 catalyst. Journal of Nuclear Materials 329-333 (2004): 1365-1369.

[67] Catón, N., et al. Hydrogen production by catalytic cracking of methane using Ni-Al_2O_3 catalysts. Influence of the operating conditions. Studies in Surface Science and Catalysis 139 (2001): 391-398.

[68] Grabke, H. Evidence on the surface concentration of carbon on gamma iron from the kinetics of the carburization in CH_4–H_2. Metallurgical and Materials Transactions B 1 (1970): 2972-2975.

[69] Bernardo, C.A., Alstrup, I., and Rostrup-Nielsen, J.R. Carbon deposition and methane steam reforming on silica-supported Ni-Cu catalysts. Journal of Catalysis 96 (1985): 517-534.

[70] Demicheli, M.C., Ponzi, E.N., Ferretti, O.A., and Yeramian, A.A. Kinetics of carbon formation from CH_4-H_2 mixtures on nickel-alumina catalyst. Chemical Engineering Journal 46 (1991): 129-136.

[71] Snoeck, J.W., Froment, G.F., and Fowles, M. Kinetic Study of the Carbon Filament Formation by Methane Cracking on a Nickel Catalyst. Journal of Catalysis 169 (1997): 250-262.

[72] Kuvshinov, G.G., Mogilnykh, Y.I., and Kuvshinov, D.G. Kinetics of carbon formation from CH_4-H_2 mixtures over a nickel containing catalyst. Catalysis Today 42 (1998): 357-360.

[73] Alstrup, I., and Teresa Tavares, M. The kinetics of carbon formation from CH_4 + H_2 on a silica-supported nickel catalyst. Journal of Catalysis 135 (1992): 147-155.

[74] Zavarukhin, S.G., and Kuvshinov, G.G. The kinetic model of formation of nanofibrous carbon from CH_4-H_2 mixture over a high-loaded nickel catalyst with consideration for the catalyst deactivation. Applied Catalysis A: General 272 (2004): 219-227.

[75] Hazra, M., Croiset, E., Hudgins, R.R., Silveston, P.L., and Elkamel, A. Experimental investigation of the catalytic cracking of methane over a supported Ni catalyst. The Canadian Journal of Chemical Engineering 87 (2009): 99-105.

[76] Borghei, M., Karimzadeh, R., Rashidi, A., and Izadi, N. Kinetics of methane decomposition to CO_x-free hydrogen and carbon nanofiber over Ni-Cu/MgO catalyst. International Journal of Hydrogen Energy 35 (2010): 9479-9488.

[77] Romeo, L.M., Escosa, J., and Bolea, I. Postcombustion CO_2 sequestration. Universidad de Zaragoza, Zaragoza, spain, 2006.

[78] Çengel, Y.A., and Boles, M. Thermodynamics: An Engineering Approach 6ed. New York, USA: McGraw-Hill, 2008.

[79] Tondeur, D., and Teng, F., Chapter 18 - Carbon Capture and Storage for Greenhouse Effect Mitigation. In *Future Energy*, Trevor, M. L., Ed. Elsevier: Oxford, 2008; pp 303-331.

[80] Muñoz, M.R. Viabilidad de un proceso para la eliminación conjunta de H_2S y NH_3 contenido en efluentes gaseosos. Doctoral dissertation, Universidad de Cádiz, Cádiz, spain, 2007.

[81] Ryckebosch, E., Drouillon, M., and Vervaeren, H. Techniques for transformation of biogas to biomethane. Biomass and Bioenergy 35 (2011): 1633-1645.

[82] Göttlicher, G., and Pruschek, R. Comparison of CO_2 removal systems for fossil-fuelled power plant processes. Energy Conversion and Management 38 (1997): S173-S178.

[83] Riemer, P. Greenhouse gas mitigation technologies, an overview of the CO_2 capture, storage and future activities of the IEA Greenhouse Gas R&D programme. Energy Conversion and Management 37 (1996): 665-670.

[84] Bracht, M., et al. Water gas shift membrane reactor CO_2 control in IGCC systems: techno-economic feasibility study In ICCDR-3, pp. 1-5, Boston, 1996.

[85] Lee, D.K., Hyun Baek, II, and Lai Yoon, W. A simulation study for the hybrid reaction of methane steam reforming and in situ CO_2 removal in a moving bed reactor of a catalyst admixed with a CaO-based CO_2 acceptor for H_2 production. International Journal of Hydrogen Energy 31 (2006): 649-657.

[86] Herzog, H.J. The economics of CO_2 capture. In Eliasson, B.; Reimer, P.; Wokaum, A., (eds.) Proceedings of the 4th International Conference on Greenhouse Gas Control Technologies, pp. 101-106, Interlaken, Switzerland: Elsevier Science Ltd., 1999.

[87] Koornneef, J., van Keulen, T., Faaij, A., and Turkenburg, W. Life cycle assessment of a pulverized coal power plant with post-combustion capture, transport and storage of CO_2. International Journal of Greenhouse Gas Control 2 (2008): 448-467.

[88] Bolland, O., and Undrum, H. Removal of CO_2 from gas turbine power plants: Evaluation of pre- and postcombustion methods. In Proceedings of the 4th International Conference on Greenhouse Gas Control Technologies, Interlaken, Switzerland, 1998.

[89] House, K.Z., Harvey, C.F., Aziz, M.J., and Schrag, D.P. The energy penalty of post-combustion CO_2 capture & storage and its implications for retrofitting the U.S. installed base. Energy & Environmental Science 2 (2009): 193-205.

[90] Freguia, S., and Rochelle, G.T. Modeling of CO_2 capture by aqueous monoethanolamine. AIChE Journal 49 (2003): 1676-1686.

[91] Singh, B., Strømman, A.H., and Hertwich, E. Life cycle assessment of natural gas combined cycle power plant with post-combustion carbon capture, transport and storage. International Journal of Greenhouse Gas Control 5 (2011): 457-466.

[92] Chakma, A. An energy efficient mixed solvent for the separation of CO_2. Energy Conversion and Management 36 (1995): 427-430.

[93] Chapel, D.G., Mariz, C.L., and Ernest, J. Recovery of CO_2 from Flue Gases: Commercial Trends. In Proceedings of the Canadian Society of Chemical Engineers annual meeting Saskatoon, Saskatchewan, Canada, 1999.

[94] Rao, A.B., Rubin, E.S., Keith, D.W., and Granger Morgan, M. Evaluation of potential cost reductions from improved amine-based CO_2 capture systems. Energy Policy 34 (2006): 3765-3772.

[95] Knudsen, J.N., Vilhelmsen, P.J., Biede, O., and Jensen, J.N. CASTOR 1 t/h CO_2 absorption pilot plant at the Elsam Kraft A/S Esbjerg power plant–First year operation experience. In Proceedings of the Greenhouse Gas Control Technologies, Trondheim, Norway, 2006.

[96] Gibbins, J., and Chalmers, H. Carbon capture and storage. Energy Policy 36 (2008): 4317-4322.

[97] Alie, C., Backham, L., Croiset, E., and Douglas, P.L. Simulation of CO_2 capture using MEA scrubbing: a flowsheet decomposition method. Energy Conversion and Management 46 (2005): 475-487.

[98] Abu-Zahra, M.R.M., Schneiders, L.H.J., Niederer, J.P.M., Feron, P.H.M., and Versteeg, G.F. CO_2 capture from power plants: Part I. A parametric study of the technical performance based on monoethanolamine. International Journal of Greenhouse Gas Control 1 (2007): 37-46.

[99] Assabumrungrat, S., Laosiripojana, N., and Piroonlerkgul, P. Determination of the boundary of carbon formation for dry reforming of methane in a solid oxide fuel cell. Journal of Power Sources 159 (2006): 1274-1282.

[100] Sangtongkitcharoen, W., Assabumrungrat, S., Pavarajarn, V., Laosiripojana, N., and Praserthdam, P. Comparison of carbon formation boundary in different modes of solid oxide fuel cells fueled by methane. Journal of Power Sources 142 (2005): 75-80.

[101] Tsiakaras, P., and Demin, A. Thermodynamic analysis of a solid oxide fuel cell system fuelled by ethanol. Journal of Power Sources 102 (2001): 210-217.

[102] Wang, X., et al. Thermodynamic analysis of glycerol dry reforming for hydrogen and synthesis gas production. Fuel 88 (2009): 2148-2153.

[103] Kale, G.R., and Kulkarni, B.D. Thermodynamic analysis of dry autothermal reforming of glycerol. Fuel Processing Technology 91 (2010): 520-530.

[104] Wang, W., and Wang, Y. Thermodynamic analysis of hydrogen production via partial oxidation of ethanol. International Journal of Hydrogen Energy 33 (2008): 5035-5044.

[105] Parmar, R.D., Kundu, A., and Karan, K. Thermodynamic analysis of diesel reforming process: Mapping of carbon formation boundary and representative independent reactions. Journal of Power Sources 194 (2009): 1007-1020.

[106] Adhikari, S., et al. A thermodynamic analysis of hydrogen production by steam reforming of glycerol. International Journal of Hydrogen Energy 32 (2007): 2875-2880.

[107] García, E.Y., and Laborde, M.A. Hydrogen production by the steam reforming of ethanol: Thermodynamic analysis. International Journal of Hydrogen Energy 16 (1991): 307-312.

[108] Wang, X., Li, S., Wang, H., Liu, B., and Ma, X. Thermodynamic Analysis of Glycerin Steam Reforming. Energy & Fuels 22 (2008): 4285-4291.

[109] Peng, D.-Y., and Robinson, D.B. A New Two-Constant Equation of State. Industrial & Engineering Chemistry Fundamentals 15 (1976): 59-64.

[110] Belohlav, Z., Zamostny, P., and Herink, T. The kinetic model of thermal cracking for olefins production. Chemical Engineering and Processing 42 (2003): 461-473.

[111] Lwin, Y., Daud, W.R.W., Mohamad, A.B., and Yaakob, Z. Hydrogen production from steam-methanol reforming: thermodynamic analysis. International Journal of Hydrogen Energy 25 (2000): 47-53.

[112] Lima da Silva, A., Malfatti, C.d.F., and Müller, I.L. Thermodynamic analysis of ethanol steam reforming using Gibbs energy minimization method: A detailed study of the conditions of carbon deposition. International Journal of Hydrogen Energy 34 (2009): 4321-4330.

[113] Seo, Y.S., Shirley, A., and Kolaczkowski, S.T. Evaluation of thermodynamically favourable operating conditions for production of hydrogen in three different reforming technologies. Journal of Power Sources 108 (2002): 213-225.

[114] Bartholomew, C.H., and Farrauto, R.J. Fundamentals of Industrial Catalytic Processes. 2 ed. Hoboken, New Jersey: John Wiley & Sons, 2006.

[115] Huijsmans, J.P.P., van Berkel, F.P.F., and Christie, G.M. Intermediate temperature SOFC – a promise for the 21st century. Journal of Power Sources 71 (1998): 107-110.

[116] Yentekakis, I.V. Open- and closed-circuit study of an intermediate temperature SOFC directly fueled with simulated biogas mixtures. Journal of Power Sources 160 (2006): 422-425.

[117] Khalesi, A., Arandiyan, H.R., and Parvari, M. Effects of Lanthanum Substitution by Strontium and Calcium in La-Ni-Al Perovskite Oxides in Dry Reforming of Methane. Chinese Journal of Catalysis 29 (2008): 960-968.

[118] Jablonski, E.L., Schmidhalter, I., de Miguel, S.R., Scelza, O.A., and Castro, A.A. Dry reforming of methane on Pt/Al_2O_3–alkaline metal catalysts. In 2nd Mercosur Congress on Chemical Engineering, pp. 1–13, Rio de Janeiro, 2005.

APPENDICES

APPENDIX A
THERMODYNAMIC DATA OF SELECTED COMPONENT

In order to determine heat of reaction or heat of the system, the thermodynamic data from Aspen Plus such as heat of formation of various components at the studied operating temperature are applied as listed in the following table.

Table A.1 Heat of formation $\left(H_{\mathrm{f}}^{0}\right)$ of selected component at 1 bar for the temperature in the range of 400-1600 K.

Temperature (K)	Heat of formation (kJ mol^{-1})				
	$CH_{4(g)}$	$CO_{(g)}$	$CO_{2(g)}$	$H_2O_{(g)}$	$H_{2(g)}$
298	-74.5	-110.5	-393.6	-241.9	0
400	-70.7	-107.6	-389.5	-238.4	3.0
500	-66.3	-104.6	-385.2	-234.9	5.9
600	-61.3	-101.6	-380.6	-231.3	8.8
700	-55.8	-98.5	-375.7	-227.6	11.8
800	-49.7	-95.4	-370.7	-223.8	14.7
900	-43.1	-92.1	-365.5	-219.9	17.7
1000	-36.1	-88.8	-360.2	-215.8	20.7
1100	-28.6	-85.5	-354.7	-211.6	23.7
1200	-20.7	-82.1	-349.1	-207.3	26.8
1300	-12.5	-78.7	-343.4	-202.9	29.9
1400	-4.0	-75.2	-337.6	-198.3	33.1
1500	4.8	-71.7	-331.8	-193.7	36.3
1600	13.8	-68.1	-325.9	-188.9	39.5

APPENDIX B
CALCULATION OF FEED FRACTION AND GAS PRODUCT FRACTION

Referred to the system presented in Figure 5.4, feed fraction to reactor (f_d) and gas product fraction (g_d) were needed to determine in case of the system operated under energy self-sustained condition. For this operation, net heat of the system (Q_{net}) are shown in the equation below.

$$Q_{net} = Q_r + Q_c = 0 \quad \text{(B-1)}$$

$$f_d Q_{r,0} + \Delta H_1(1-f_d) = 0 \quad \text{and} \quad Q_{r,0} + \Delta H_2(1-g_d) = 0 \quad \text{(B-2)}$$

$$\text{Thus,} \quad f_d = \frac{-\Delta H_1}{Q_{r,0} - \Delta H_1} \quad \text{and} \quad g_d = \frac{Q_{r,0} + \Delta H_2}{\Delta H_2} \quad \text{(B-3)}$$

where $Q_{r,0}$ is heat of reaction at the decomposition unit in case of the system without splitting feed or gas product stream

ΔH_1 is heat generation at the burner, considering each mole of gas at the burner inlet equal to that from the inlet of decomposition process

ΔH_2 is heat generation at the burner, considering each mole of gas at the burner inlet equal to that from the outlet of decomposition unit

Like the calculation above, the decomposition process with CO_2 capture under energy self-sustained operation as shown the system configurations in Figure 5.30 could be determined by the similar way as follows:

$$Q_{net} = Q_1 + Q_2 + Q_r + Q_c = 0 \quad \text{(B-4)}$$

$$Q_1 + \Delta H_3(f_d) + f_d Q_{r,0} + \Delta H_4(1-f_d) = 0 \quad \text{(B-5)}$$

$$f_d = \frac{-(Q_1 + \Delta H_4)}{Q_{r,0} + \Delta H_3 - \Delta H_4} \quad \text{(B-6)}$$

where Q_1 is heat consumption by CO_2 capture as expressed in Section 3.5

ΔH_3 is heat generation/consumption at the SOFC inlet, considering each mole of gas at the SOFC inlet equal to that from the outlet of decomposition unit in case of without splitting feed

ΔH_4 is heat generation at the burner, considering each mole of gas at the burner inlet equal to that from the outlet of CO_2 capture unit

In case of gas product fraction, equation (B-4) could be expressed as the following equation.

$$Q_1 + \Delta H_5(g_d) + Q_{r,0} + \Delta H_6(1-g_d) = 0 \quad \text{(B-7)}$$

$$g_d = \frac{Q_1 + Q_{r,0} + \Delta H_6}{\Delta H_6 - \Delta H_5} \quad \text{(B-8)}$$

where ΔH_5 is heat generation/consumption at the SOFC inlet, considering each mole of gas at the SOFC inlet equal to that from the outlet of decomposition unit in case of without splitting product

ΔH_6 is heat generation at the burner, considering each mole of gas at the burner inlet equal to that from the outlet of decomposition unit

APPENDIX C
LIST OF PUBLICATION

International Publication

Khaodee, W., Wongsakulphasatch, S., Kiatkittipong, W., Arpornwichanop, A., Laosiripojana, N., and Assabumrungrat, S. Selection of appropriate primary fuel for hydrogen production for different fuel cell types: Comparison between decomposition and steam reforming. International Journal of Hydrogen Energy 36 (2011): 7696-7706.

VITA

Mr. Watcharapong Khaodee was born in May 5, 1982 in Trang, Thailand. He finished high school from Surasakmontri School, Bangkok in 2000. He received his Bachelor's and Master's Degrees in Chemical Engineering from the Department of Chemical Engineering, Chulalongkorn University in 2004 and 2006, respectively. Afterward, he continued studying Doctoral degree of Chemical Engineering, Chulalongkorn University since June 2006. During his Master's and Doctoral degrees, he received the Chulalongkorn University Graduate Scholarship commemoratory the 72nd Anniversary of H.M. Rama IX.